

# EVALUATION OF THE UBC3D-PLM CONSTITUTIVE MODEL FOR PREDICTION OF EARTHQUAKE INDUCED LIQUEFACTION ON EMBANKMENT DAMS

---



**Msc Graduation Thesis**

**Antonia Makra**

**February 2013**

# EVALUATION OF THE UBC3D-PLM CONSTITUTIVE MODEL FOR PREDICTION OF EARTHQUAKE INDUCED LIQUEFACTION ON EMBANKMENT DAMS

---

Master Graduation Thesis

Antonia Makra

Student number: 4116712

Graduation Committee:

Prof. dr. M.A. Hicks      TU Delft CITG

Dr. ir. R.B.J. Brinkgreve      TU Delft CITG

Dr. ir. K.J. Bakker      TU Delft CITG

Dr. Richard Witasse      PLAXIS B.V.

## ABSTRACT

---

The following graduation project is concerned with the response of embankment dams subjected to earthquake loading. The scope of the project was to determine the applicability of UBC3D-PLM constitutive model implemented in PLAXIS 2D for prediction of the onset of liquefaction in embankments.

The project consists of three discrete parts: a) Calibration and evaluation of the effect of critical parameters on the performance of the model through simulation of laboratory tests; b) Simulation of dynamic centrifuge tests on sloping ground and c) the case history of the Upper San Fernando Dam.

Through this process, correlations for the model parameters with measured SPT blow-counts were suggested and validated. The effects of the state of the soil, lateral earth pressure coefficient, the damping ratio and static shear were evaluated. And the model was validated in the case of controlled conditions like the ones in the centrifuge and in the field with the case study.

In general it has been observed that the model has certain limitations especially when anisotropic initial loading conditions are encountered, but with proper calibration it can provide a good prediction of the pore pressure generation in the embankment.

## ACKNOWLEDGEMENTS

---

I would like to thank my graduation committee for their guidance. Their comments and suggestions were invaluable for the completion of this project. Especially I would like to thank Ronald Brinkgreve and Richard Witasse for their daily supervision, openness to my questions and very constructive advice without which this work would not be possible.

I also want to thank PLAXIS B.V. for all their help and support and for giving me all the necessary access to their software and facilities. It has been a pleasure to work with them. Here I should add a special thanks to Vahid Galavi and Alexandros Petalas for sharing their insight about UBC3D-PLM and PLAXIS 2D dynamics.

And last but not least, I would like to thank my good friends and colleagues Katerina Ziotopoulou and Panagiota Tasiopoulou for their precious comments. Their experience on earthquake engineering and modelling offered me a better perspective of the problem.

# CONTENTS

---

CONTENTS .....	4
1 INTRODUCTION AND PROJECT DESCRIPTION .....	7
1.1 Introduction.....	7
1.2 Project description and objectives .....	8
2 LITERATURE REVIEW.....	10
2.1 Embankment dams.....	10
2.2 Failure modes of embankment dams.....	11
2.3 Seismic hazards .....	12
2.4 Historical overview of methods.....	12
2.5 Modelling the earthquake response of embankment dams.....	14
2.6 Input ground motion .....	16
2.7 Earthquake induced liquefaction .....	16
2.7.1 Liquefaction assessment .....	18
2.7.2 Liquefaction susceptibility .....	18
2.7.3 Parameters that affect the cyclic resistance of sands.....	20
2.7.4 Liquefaction Triggering.....	21
2.7.5 Consequences of liquefaction .....	22
2.8 Constitutive models for liquefaction.....	22
2.9 Types of constitutive models for advanced seismic analysis of embankment dams....	24
2.10 UBC3D-PLM constitutive model .....	26
2.11 Summary and conclusions .....	29
3 MATERIAL PROPERTIES AND MODEL CALIBRATION.....	31
3.1 UBCSAND parameters-SPT correlations .....	32
3.2 Soil tests.....	33
3.3 Cyclic strength curve .....	43
3.4 Material properties selection .....	45
3.5 Critical parameters and their effect on soil tests .....	47
3.5.1 The effect of state .....	47

3.5.2	Effect of $K_0$ .....	50
3.5.3	Material damping .....	51
3.5.4	Static shear stress effect.....	53
3.6	Summary and conclusions .....	58
4	CENTRIFUGE TESTS ON SLOPING GROUND.....	60
4.1	Centrifuge tests: scaling, geometry and boundary conditions.....	60
4.2	Input ground motion .....	61
4.3	Numerical modelling of centrifuge tests .....	62
4.4	Parameter selection .....	64
4.5	Finite element analysis .....	65
4.6	Finite element analysis assuming the initial static shear affects all the loose layer .....	75
4.7	Summary and Conclusions .....	83
5	CASE STUDY: UPPER SAN FERNANDO DAM .....	85
5.1	Upper San Fernando Dam .....	85
5.1.1	Response to the 1971 San Fernando Earthquake .....	86
5.1.2	Site investigation .....	88
5.2	Numerical modelling .....	90
5.2.1	Input ground motion .....	90
5.2.2	Material models.....	91
5.2.3	Material Properties.....	93
5.2.4	Geometry and Mesh.....	96
5.2.5	Boundary Conditions .....	96
5.2.6	Static analysis .....	97
5.2.7	Dynamic analysis .....	99
5.2.8	Free field boundaries.....	99
5.2.9	Tied degrees of freedom .....	101
5.3	Comparison between the two analyses and the measured displacements of the dam 104	
5.4	Comparison with other finite element analyses of the case history of the Upper San Fernando Dam.....	105

5.5	Summary and conclusions .....	106
6	CONCLUSIONS AND DISCUSSION .....	107
6.1	Conclusions.....	107
6.2	Recommendations and fields that require further research .....	109
7	REFERENCES.....	110

# 1 INTRODUCTION AND PROJECT DESCRIPTION

---

## 1.1 Introduction

Earthquakes have always been a significant factor in the design and target safety of dams, since they pose multiple hazards for the structure itself, its foundation, the surrounding structures and the reservoir. Taking also into account the high risk associated to the failure of dams; design against earthquakes has been incorporated in their construction since the 1930s, which is long before it was implemented in other conventional structures such as buildings, roads and bridges. Indicative of the aforementioned is the fact that the design earthquake for large dams has a return period of 10,000 years while buildings and bridges are usually designed for an earthquake with a return period of 475 years (ICOLD, 2010).

Embankment dams are by far the most usual type of dam representing the 83% of the existing large dams, according to the International Commission of Large Dams (ICOLD, 1998). For embankment dams and particularly for earthfill dams, one of the most critical aspects concerning seismic response is earthquake induced liquefaction either of the soils of the foundation or of a certain zone within the embankment (ICOLD, Bulletin 120, 2001). There has been extensive research on this topic during the past 40 years, especially after the San Fernando earthquake in 1971 which led to the catastrophic failure of the Lower San Fernando dam and to serious deformations of the Upper dam (Seed et al 1973, 1976, 1988 Castro et al 1985, Vasquez-Herrera and Dobry 1989, Olsen and Stark 2001).

The aforementioned research has led to a much better understanding of the liquefaction phenomenon and especially of flow failures that are a big threat in the case of earth dams. This has led to a significant improvement of dam design. However, there are still aspects of the phenomenon that remain uncertain and controversial, especially concerning the deformations connected with liquefaction and the residual strength of the soils after seismic loading.

Despite these uncertainties, a general framework for the assessment of liquefaction has been drawn by the NCEER/NSF workshops in 1996 and 1998, which is mainly based on empirical solutions and field observations from case histories. This framework provides the basic guidelines for assessment of liquefaction hazards and it is continuously improved as new cases of liquefaction arise.

Lately, sophisticated constitutive models such as bounding surface and multi-surface plasticity models have been used to predict liquefaction in embankment dams. Unfortunately, the complexity of these models and the very large number of parameters involved does not allow their use in everyday practice yet.

For practical applications in general but also specifically for earth dams, accuracy is compromised via several assumptions and approximations so as to obtain an economically efficient but still reasonably representative estimation of the actual response that is expected in the case of an earthquake. This is done with the use of more usable and simpler constitutive models, which might not be able to describe the liquefaction phenomenon in its entity, but they are able to give reliable predictions that can be directly used in dam design or remediation.

In this project, the use of one of these practical models, UBC3D, is evaluated for its ability to predict liquefaction triggering in earthfill dams.

In the following, the term liquefaction will be used to describe earthquake induced liquefaction, since this project is not concerned with static liquefaction.

## 1.2 Project description and objectives

In this project an attempt is made to evaluate the performance of UBC3D-PLM constitutive model as implemented in the finite element software PLAXIS for triggering of earthquake induced liquefaction in earthfill dams. UBC3D-PLM (Petalas and Galavi, 2012) has shown a great potential for predicting the onset of liquefaction in element tests with accuracy. However, a full scale problem presents significant differences, since the conditions are not controlled anymore and the parameters affecting the problem are numerous and frequently unknown.

The main objectives of this project are the following:

- Assess the applicability of UBC3D-PLM for earthquake induced liquefaction in earthfill dams;
- Determine suitable correlations of the material properties used in UBC3D with in situ test results;
- Determine the critical parameters that affect the problem and the sensitivity of the accuracy of the acquired results to them;
- Evaluate the effect of the initial conditions;
- Determine the effects of the interaction between zones with different properties;
- Compare the acquired results with test results, recordings and other analytical and numerical analyses;
- Provide recommendations for better use of UBC3D for dynamic analyses of embankment dams;
- Determine the potentials and limitations of UBC3D for the geotechnical problem under discussion;
- Suggest possible improvements and fields that require further research.

The project is divided in three distinct parts: element simulations, centrifuge tests on sloping ground and finally the case study of the performance of the Upper San Fernando Dam during the 1971 San Fernando earthquake.

The element tests that are performed initially aim at aiding the calibration of the model for the stress paths that are pertinent to the case of the dam and to evaluate the existing correlations between UBC3D-PLM parameters and in situ test measurements for the version of the model that is implemented in PLAXIS. Moreover, with the use of element tests, the individual effect of each of the critical parameters that affect the soil behaviour under dynamic loading can be observed and documented, which is very important for the interpretation of the results of the embankment analysis.

The second step is to perform dynamic analyses on a simple geometry similar to the one of an embankment dam. This is done by simulating centrifuge tests on sloping ground. The results are compared with the centrifuge tests performed for the project “Earthquake Induced Damage Mitigation from Soil Liquefaction” directed by Prof. Peter M. Byrne at the university British Columbia. Through this process a first assessment of the applicability of the model is done in a model where the soil properties, the saturation and the boundary conditions are controlled and known.

Taking into account the results of the previous processes, the case history is modelled. Initially some basic assumptions and simplifications of the actual situation are necessary. A typical cross section and a representative ground motion are selected. The susceptibility to liquefaction of the dam materials is assessed. The material properties are determined from existing documentation of the case study and using the correlations that were evaluated before.

Finally, a general assessment of the constitutive model for earthquake-induced liquefaction will be done, uncertainties will be determined and, if possible, improvements for the model will be suggested.

## 2 LITERATURE REVIEW

### 2.1 Embankment dams

Embankment dams are made of natural materials excavated or obtained in the surrounding area without any binding. They can be homogeneous but the most usual structures consist of distinct zones of materials with different characteristics.

There are two main types of embankment dams: earthfill and rockfill dams depending on the materials used on the embankment.

An embankment dam can be characterized as an earthfill dam if compacted soils account for over 50% of the placed volume of material. An earthfill dam is constructed primarily of selected engineering soils compacted uniformly and intensively in relatively thin layers and at a controlled moisture content. They, usually, consist of an impermeable core made of clayey soils, filters and drains usually made of sandy and gravelly soil to prevent the core from being washed out and two shells made of variable soils to ensure the stability of the structure and the suitable weight to withstand the water load. The shells are usually protected by thin external zones of coarser soil or rock (Novak et al, 2007). A typical cross-section of this type of dam is shown in Figure 1.

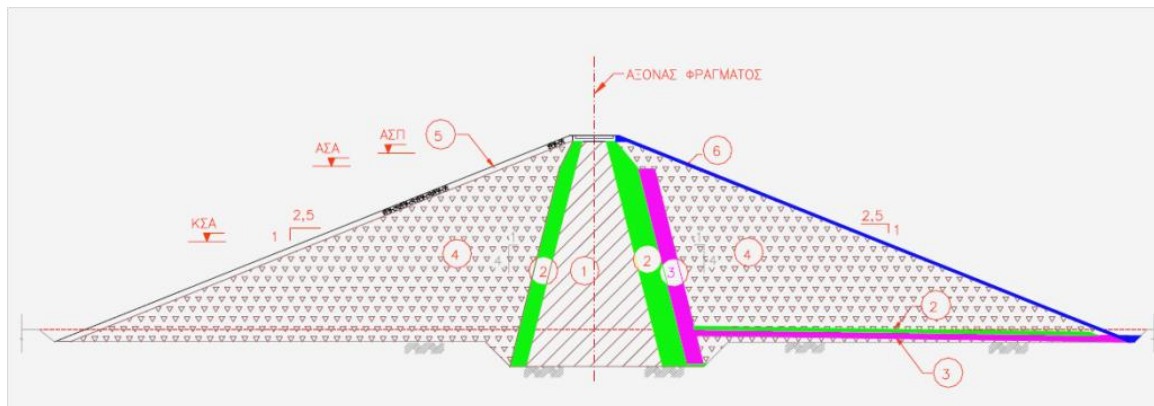


**Figure 2.1: typical cross section of an earthfill dam. Zone 1 is the impermeable core, zones 2 and 3 are the filters and drainage, zone 4 is the shell and zones 5 and 6 are the upstream and downstream protection layers respectively**

Due to this kind of zoning and to the very strict regulations concerning material properties and compaction specifications amongst others, earthfill dams have performed very well in earthquake loading over the years. The earth dams that have sustained significant damage from seismic loads are mainly old earth dams constructed with tailings and hydraulic fill dams. This is also the case for the Upper San Fernando dam. Although this construction technique has been abandoned, there are several operational dams that have been constructed this way and whose safety against earthquake needs to be re-evaluated (ICOLD, Bulletin 120, 2001).

Moreover, since there is little experience with large earthquakes affecting large earthfill dams, it is difficult to predict the actual response that they will have under earthquake loading. In daily practice, mainly quasi-static and linear elastic models are suggested by ICOLD (Bulletin 72, 1989) to simulate earthquake response, while more sophisticated non-linear methods are only used in

very high risk and high budget constructions. However, the use of non-linear elasto-plastic models can lead to a safer and more cost-efficient design without increasing significantly the expenses for site investigation and material testing.

## 2.2 Failure modes of embankment dams

The most common modes of failure of embankment dams can be separated in three main categories: hydraulic, seepage and structural failures. Some of these mechanisms are depicted in Figure 2.2.

### Hydraulic failures:

- a) Overtopping: when the free board of the dam or the capacity of the spillway is insufficient the flood water will pass beyond the crest of the dam and cause erosion of the crest and the downstream side (Figure 2.2a).
- b) Erosion of the downstream toe: This is due to heavy cross current from the spillway or tail water.
- c) Erosion of the upstream face: This mode of failure is caused by waves on the surface of the reservoir (Figure 2.2b).
- d) Erosion of the downstream face: This failure is caused by weathering of the face due to heavy rain or due to animals and plants (Figure 2.2c).

### Seepage failures:

- a) Piping through dam body: During seepage small channels can be formed which transport material downstream and gradually increase (Figure 2.2d).
- b) Piping trough foundation: If in the dam foundation there are highly permeable cavities, fissures or strata, concentrated seepage at a high rate occurs. This leads to erosion and flow of water and soil in the foundation (Figure 2.2e).
- c) Sloughing of the downstream side of dam: The downstream toe of the dam becomes saturated and starts eroding causing small slump or slide of the dam which can gradually progress and lead to failure.

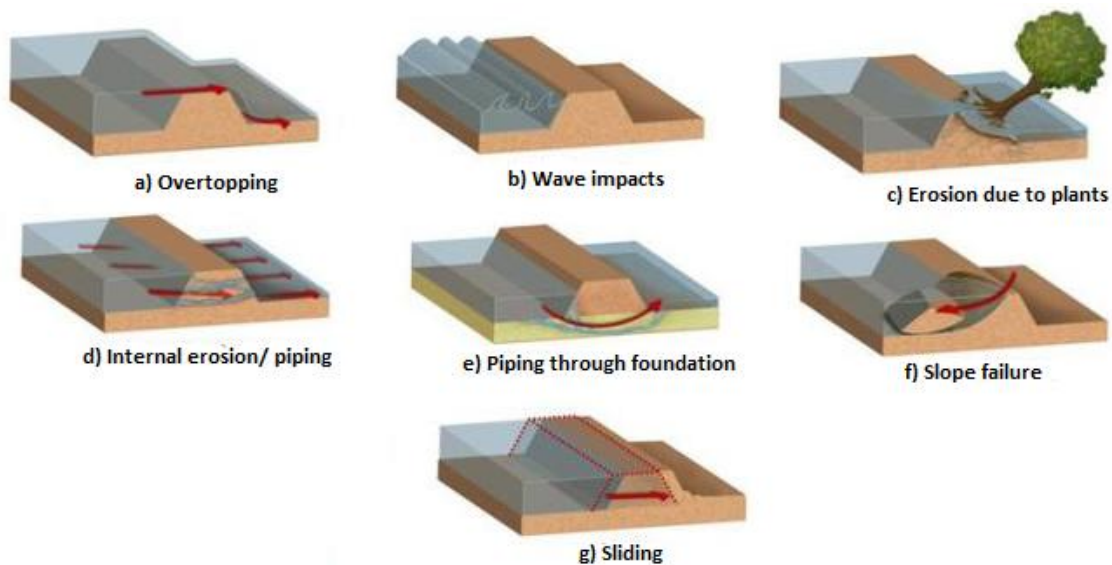


Figure 2.2: Modes of failure of embankment dams (by Ziha Deretsky,NSF)

### Structural failures:

- a) Slide in embankment: If either of the slopes of the embankment is too steep it can slide. For the upstream slope this is usually triggered by a sudden drawdown (Figure 2.2f).
- b) Foundation slide: This mode of failure occurs if the foundation is composed by soft soil and can lead to the whole dam sliding due to water thrust (Figure 2.2g).
- c) Earthquake failure: Earthquake loading can lead to failure of the dam itself but also of the foundation and the appurtenant structures (spillways, water intakes etc). The hazards that an earthquake represents for an embankment dam are presented in the following section.

## 2.3 Seismic hazards

ICOLD in their position paper of 2010 suggest that earthquakes represent multiple hazards for all types of storage dams, the most important of which are the following:

- Ground shaking causes vibrations and structural distortions in dams, appurtenant structures and equipment and their foundations
- Fault movements or discontinuities in the dam foundation near major faults can be activated causing structural distortions
- Fault displacement in the reservoir bottom may cause water waves in the reservoir or loss of freeboard
- Rockfalls and landslides may cause damage to gates, spillway piers retaining walls surface powerhouses, electromechanical equipment etc
- Mass movements in the reservoir can cause impulse waves in the reservoir
- Mass movements blocking rivers and forming landslide dams whose failure may lead to overtopping of run of river power plants or inundation of powerhouses with equipment and damage downstream
- Ground movements and settlements due to liquefaction, densification of soil and rockfill, causing distortions in dams
- Abutment movements causing sliding of the dam or distortions

These hazards refer to the whole dam-lake-appurtenant structures system. When it comes to the seismic hazards faced by the body of an embankment dam itself, the most important effects are the following (Gazetas, 1987):

- a) slope instabilities,
- b) liquefaction flow failures due to excess pore pressure generation,
- c) longitudinal cracks occurring near the crest due to shear sliding deformations and large tensile strains during lateral oscillations,
- d) differential crest settlements and loss of freeboard possibly resulting from lateral sliding deformations or soil densification,
- e) transverse cracks caused by tensile strains from longitudinal oscillations or by different lateral response near the abutments and near the central crest zone and
- f) piping failures through cracks in cohesive soil zones.

## 2.4 Historical overview of methods

Over the years several approaches have been used for evaluating the seismic response of embankment dams. The first method used for this problem has been the pseudo-static

approach, which is often used even in current practice with certain improvements. The pseudo static approach would treat the dam as a rigid body experiencing a uniform acceleration equal to the ground acceleration. This way the earthquake would be implemented in the analysis as a horizontal inertia-like force acting in one direction and a static slope stability analysis would be performed to obtain the factor of safety of the slope. With increasing experience of the effects of seismic loading on large dams, the drawbacks of this method became apparent over the years. Namely, the perception of the dam as a rigid body was proved erroneous. Also, the assumption of horizontal force acting on one direction could not simulate the actual effects of the rapid fluctuations of seismic loading. Finally, the loss of strength and stiffness of the soil during shaking was not taken into account.

To deal with the problem of the change of direction, Newmark (1965) presented a new method based on the assessment of deformations of the embankment rather than on a factor of safety against slope failure. His method assumed rigid plastic behaviour of the embankment and a known time history of the earthquake. Therefore, he idealized the sliding mass as a rigid block on an inclined plane which would slide every time that the shearing resistance of the contact became smaller than the inertia force due to shaking. Newmark's method is also still used in practice to predict deformations of slopes and has proved to perform well in cases where the yield resistance of the soil can be reliably determined and does not experience significant decrease with time during earthquake loading (Gazetas, 1987).

A very important step in the seismic analysis of embankment dams was done through the 'shear beam' model, initially introduced by Mononobe (1936) but formed into a complete engineering theory much later in the 1960s by Hatanaka and Ambraseys. They demonstrated that bending-type rocking deformations are negligible compared to those in simple shear. Thus, they assumed the soil as a viscoelastic material and treated the dams as "stacked" one-dimensional or two dimensional shear beams and proposed a design method using seismic coefficients which varied through the body of the dam. This model led to a better understanding of the propagation of the earthquake motion through the body of the dam.

A major step in the seismic analyses of embankment dams was taken through the use of finite element methods, initially by Clough and Chopra (1966). These methods became popular very fast for two main reasons: (a) their capability of handling any number of zones and (b) their capability of reproducing rationally the 2D dynamic stress and displacement field during shaking (Gazetas, 1987). The initial constitutive models used for finite element analyses were viscoelastic and therefore incapable of modelling pore pressure generation and permanent deformations. To overcome this problem Finn (1967) suggested a procedure to interpret the effects of the computed dynamic stresses through cyclic tests in the laboratory.

The following large step came from Seed and the University of California at Berkeley, who developed an analysis procedure for the assessment of the seismic stability of dams. In 1972, this group introduced the equivalent linear method of analysis for approximating nonlinear behaviour. This method was implemented in several 1D and 2D finite element programs such as SHAKE and QUAD 4 and was able to account for the strain dependence of damping and shear modulus. This gave the possibility of much more realistic analyses, although the model was still elastic and thus direct computation of permanent deformations was not possible (Finn and Marcuson, 1995).

Along with the new constitutive models, empirical methods for liquefaction assessment were developed, initially by Seed and his co-workers, based mainly on laboratory and in situ testing.

As the liquefaction hazard has been determined as critical for the behaviour of embankment dams under earthquake loading, these empirical methods used to determine cyclic resistance of soils have been used in combination with finite element analysis for the evaluation of seismic safety of dams. These methods have improved over the years and constitute the most common process for liquefaction triggering assessment currently.

In 1971 the failure of the Upper and Lower San Fernando Dams lead to extensive research on the earthquake safety of earth dams. The analyses done with the existing methods made obvious that in order to acquire more reliable results, the nonlinearity of the ground response and the pore pressure generation need to be taken into account directly. The Martin-Finn-Seed (MSF) model, published in 1975, for generating pore pressures paved the way for effective stress analysis and direct estimation of displacements.

Since then, several constitutive models based mainly on plasticity theory and Biot's consolidation equation have been used in finite element and finite difference programs for dynamic analyses of embankment dams. These are presented in more detail in the following sections, since they correspond to the models used for liquefaction assessment.

## 2.5 Modelling the earthquake response of embankment dams

There can be several variations in the procedure followed to evaluate the liquefaction potential and the general dynamic response of an earth dam. However, the process presented in the following includes all the necessary steps needed for such an analysis, as described by Seed and Harder (1990). This process is based on the suggestions of Seed, but it has been improved over the years with the evolution of analysis methods. It is the most common process used in practice and its sophistication depends highly on the models used for the static and dynamic analyses. The resistance of the soil is determined by empirical methods based on in situ testing. The analysis process consists of the following steps:

- Selection of a representative cross section of the dam to be used for analysis.
- Determination of the maximum time history of base excitation to which the dam and its foundation might be subjected.
- Determination of the initial static stresses and water conditions existing in the embankment before earthquake loading. This is preferably done by using finite element analysis.
- Determination through laboratory and in situ testing of the dynamic properties of the embankment and foundation materials along with their dependency on strain, since the material characteristics are non-linear.
- Computation using appropriate finite element analysis of the accelerations and/or stresses induced in the embankment and its foundation by the selected earthquake motion.
- Evaluate the resistance of potentially liquefiable soil types within the dam and foundation to pore pressure generation under cyclic loading. This can be generally done by laboratory and in situ testing. In current practice, it is common to evaluate liquefaction resistance through Standard Penetration Test (SPT) and Cone Penetration Test (CPT) data.
- Based on the results of the dynamic analysis and the resistance, the pore pressure generation or cyclic strain accumulation within the dam and foundation is evaluated. This determines the potential of liquefaction triggering.

- If there pore pressures increase significantly, the residual undrained strength of the dam and foundation needs to be determined. In this case also, common practice depends on correlations based on SPT and CPT data.
- If from the previous analysis the dam and foundation are found to be safe for liquefaction triggering and post triggering major slide movements or deformations, then the magnitude of the deformations caused by the combined effects of static and dynamic loading need to be evaluated and their effect on the dam stability and performance is assessed.

In every step of this process several simplifications are made so that the analysis can be performed. This means that engineering judgement and use of examples of other case histories is necessary for a final assessment of the probable performance of the embankment dam.

In this project not all of these steps will be used in the analysis, since certain aspects such as the input ground motion and the laboratory testing will be taken from existing documentation on the case history.

Also, the post liquefaction analysis of embankment is beyond the scope of this project and will not be taken into consideration in the analysis. The main concern is the determination of the conditions during loading and mainly of the assessment of liquefaction triggering.

In an earthquake response analysis, there are certain characteristics that differentiate embankment dams from other earth structures or natural soil deposits. First of all, every dam is unique. Due to the restrictions posed by the topography of the construction area, the available materials, the size and hydrologic data of the valley etc, there are large variations in the zoning, the inclinations of the slopes and the properties of the construction materials between dams. For this reason, contrary to other engineering structures, it has been very difficult to form a set of technical specifications for design against earthquake that can apply globally. Even the specifications suggested by ICOLD have the form of general guidelines which depending on the specific case should be followed or not. This also means that any analysis of embankments has to take into account the particularities of the specific case.

Furthermore, the geometry of the structure with an upstream and a downstream slope makes it completely different from a typical ground level soil deposit for which most existing liquefaction correlations are created. Beneath dams and slopes the soil elements have two characteristics in terms of stress: an initial static shear stress on the horizontal planes and a low confining stress. Cyclic simple shear tests for these conditions have shown that it results in accumulated large displacements, rather than zero effective stress (Park and Byrne, 2004).

Moreover, the structure is made out of distinct zones of materials with completely different properties and behaviour. This means that for the modelling of each one of these zones their special characteristics need to be taken into consideration and the most suitable model for each case needs to be determined. Also, the interaction between these zones is another topic that requires attention and investigation in dynamic response analysis.

The topography of the area at which the dam is constructed is also affecting the dynamic response. Generally for large valleys a 2D analysis of a typical cross-section of the dam is adequate, while in narrow valleys, where the crest length over dam height ratio is less than 3:1, the 3D effects are such that they have to be taken into consideration (Seed and Harder, 1990).

In addition, every embankment dam consists of saturated and unsaturated soil materials, whose degree of saturation varies dependent on the elevation of the lake. Also, independent of how watertight is the impermeable core there is a certain degree of seepage from the upstream to the downstream side. These particularities complicate the determination of the water conditions, inside the body of the dam and also in the foundation layers, before the earthquake.

## 2.6 Input ground motion

The earthquake ground motion is one of the largest unknowns in any dynamic analysis. In general, an acceleration time history of the dam site is needed at either bedrock or rock outcrop. All the potential earthquake sources in the area of the dam need to be identified along with the greatest earthquake each source can produce and time histories representing the resulting attenuated ground motions at the dam site. It is not always obvious which is the most critical ground motion, so analyses with multiple earthquakes is often necessary.

For the determination of the input motion either deterministic or probabilistic methods can be used. Probabilistic seismic hazard analysis has become popular recently and it is useful for estimating structural response (Marcuson, 2007).

According to ICOLD (2010) to prevent uncontrolled rapid release of water from the reservoir of a storage dam, it should be able to withstand an extreme earthquake which is referred to as the Safety Evaluation Earthquake (SEE) or the Maximum Credible Earthquake (MCE). If a probabilistic approach is used for the determination of the MCE then a reasonable return period of this event is 10,000 years which means that there is a possibility of 1% for this event to be exceeded in 100 years.

In this project, the input ground motion will be considered a given by the documentation of the case study, although even in this case that the earthquake has already happened and its effects are known, the reliability of the measured accelerations is doubtful.

## 2.7 Earthquake induced liquefaction

Loose cohesionless soils tend to contract during cyclic loading, which can transfer normal stress from the soil skeleton to pore water, if the soil is saturated and largely unable to drain during shaking. The result is a reduction in effective confining stress within the soil and an associated loss of strength and stiffness that contributes to deformations of the soil deposit (Idriss and Boulanger, 2008). This loss of strength and stiffness due to increasing pore pressures is called liquefaction and can have devastating effects.

Although the previous definition gives a qualitative description of the liquefaction phenomenon, there is not one single definition to determine the exact conditions at which liquefaction occurs. This is mainly because, depending on the initial conditions before earthquake, the mechanisms that lead to failure are different. Liquefaction can be divided in two main groups of phenomena: flow liquefaction and cyclic mobility.

Flow liquefaction concerns slopes and it can lead to very large displacements (Figure 2.3). In the case of flow liquefaction, the shear strength of the soil decreases up to a point that the shear stresses required for equilibrium exceed it. This leads to flow failure whose driving force is the static shear stress.



**Figure 2.3: Liquefaction flow failure at the Lower San Fernando Dam due to the 1971 San Fernando earthquake, after lowering the reservoir**

In contrast to flow liquefaction, for cyclic mobility the deformations that lead to failure are produced incrementally during shaking and are due to the combined effect of static and cyclic loading. One type of cyclic mobility is lateral spreading which can occur in gently sloping ground or on virtually flat ground adjacent to bodies of water. Although in this case the deformations are significantly smaller than in the case of flow failures, still, if there are structures present in the area, the damages can be large. This kind of phenomenon can extend in very large areas (Figure 2.4).

Another type of cyclic mobility is level-ground liquefaction. In this case there is no static shear stress. During earthquake loading large chaotic movement of the soil can occur, but the permanent lateral deformation of the soil is small. This type of liquefaction causes failures due to excessive settlements connected with the dissipation of the excess pore pressures after shaking stops (Kramer, 1996).

Generally cyclic mobility leads to larger generation of excess pore pressures that eventually can equal the initial effective stress, while in the case of flow liquefaction failure occurs before this point is reached.

Despite the differences of the failure mechanisms, flow liquefaction and cyclic mobility are not separate phenomena. Their difference occurs due to the initial conditions before liquefaction, but the mechanics behind pore pressure generation, softening and loss of shear strength are the same. For this reason, in constitutive modelling there is no distinction between them (Been and Jefferies, 2006)

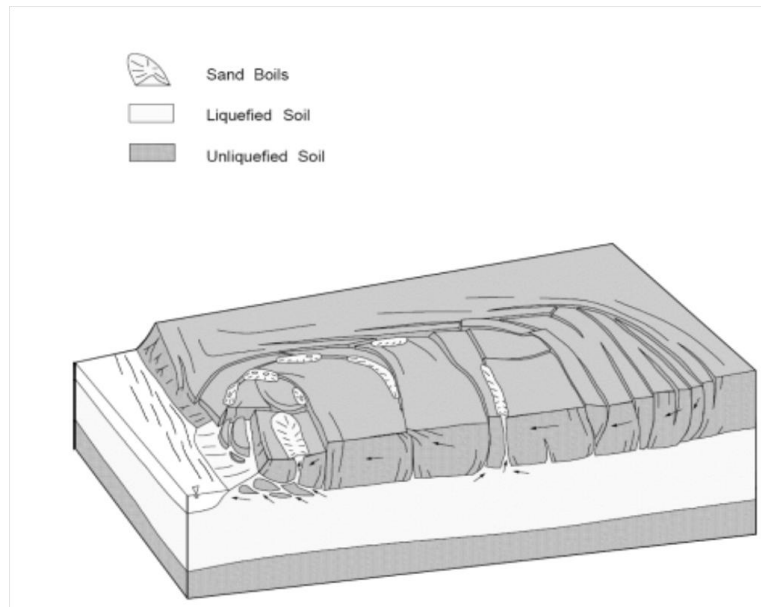


**Figure 2.4: Complex deformation patterns due to lateral spreading**

### 2.7.1 Liquefaction assessment

To assess the liquefaction hazard at a specific site three main questions need to be answered (Kramer, 1996):

- Are the soils susceptible to liquefaction?
- Will liquefaction be triggered by the earthquake ground motion under consideration?
- If liquefaction is triggered, what are the potential consequences?

In current practice, usually these three questions are treated separately. First the susceptibility of the soil to liquefaction is assessed, then a triggering analysis is performed and finally the consequences are evaluated by a flow slide analysis or a displacement analysis (if a flow slide does not occur).

### 2.7.2 Liquefaction susceptibility

Not all soil deposits are susceptible to liquefaction. To evaluate the susceptibility of a soil to liquefaction several criteria are used and can be summarised in the following categories: historical, geologic, compositional and state criteria (Kramer, 1996).

#### **Historical criteria:**

Liquefaction often recurs at the same location when soil and groundwater conditions remain unchanged. (Youd, 1984a). This way, case histories of previous earthquakes can be used to determine specific sites that are susceptible to liquefaction and also more general site conditions.

Moreover there seems to be a specific distance from the epicentre of the earthquake within which liquefaction can occur. This distance depends strongly on the magnitude of the earthquake. Although it is not safe to assume that liquefaction cannot occur in larger distances it can be helpful for evaluation of regional liquefaction hazards.

**Geological criteria:**

The depositional environment, hydrological environment and age of soil deposits all contribute to its liquefaction susceptibility. The most susceptible sediments are fills and alluvial, fluvial, marine, deltaic and wind-blown deposits. Moreover, recently deposited sediments are more susceptible than older ones.

Concerning man-made deposits well compacted fills are much more unlikely to liquefy compared to loose fills like hydraulic fill dams and mine tailings piles in which soil particles are deposited by settling through water.

**Compositional criteria:**

Since liquefaction is connected with the generation of excess pore pressures the compositional characteristics that influence liquefaction susceptibility are the ones affecting the volume change behaviour, including particle shape, size and gradation.

Liquefaction concerns cohesionless soils ranging from non-plastic coarse silts to gravel. Cohesive soils can also develop significant strains and deformations during earthquake loading. This phenomenon is described as cyclic softening and since cohesive soils have significantly different shear strength characteristics from cohesionless, it is not evaluated by the same engineering procedures.

As far as the gradation is concerned well graded soils are less susceptible to liquefaction than poorly graded ones because they have lower volume change potential. Moreover, soils with rounded grains are known to densify more easily than soils with angular grains which makes them generally more susceptible to liquefaction.

For fine grained soils the Chinese criteria (Wang, 1979) can be applied to evaluate liquefaction susceptibility:

- Fraction finer than 0,005mm  $\leq$  15%
- Liquid limit LL  $\leq$  35%
- Natural water content  $\geq$  0.9LL
- Liquidity index  $\leq$  0.75

**State criteria:**

Even if all the previously described criteria are met the triggering or not of liquefaction will be determined by the initial state of the soil. The state of the soil is determined with respect to its critical state. A measure of the state of the soil is the state parameter introduced by Been and Jefferies (1985) which is defined as the difference between the current void ratio ( $e$ ) and the void ratio at the critical state ( $e_{cs}$ ). The state parameter gives a description of the combined effects of the relative density and the confining stress. The critical state refers to the conditions that exist in the soil when it is sheared continuously and no further change in stress and volume is occurring (Idriss and Boulanger, 2008). For a specific type of sand and a type of laboratory test the cyclic resistance of the soil is a function of the state parameter. Generally, in sand that is denser than in the critical state flow failure cannot occur, so if liquefaction is triggered, it will lead to the limited deformations connected with cyclic mobility.

In more detail, at a given confining stress, the cyclic resistance increases with increasing relative density ( $D_r$ ). Moreover, the effect of the confining stress on cyclic resistance reflects its effect on the tendency of the soil to contract or dilate. Cyclic strength increases with increasing

consolidation stress for all values of  $D_r$  although the relationship varies from practically linear in lower densities to more concave in larger ones (Figure 2.5a).

### 2.7.3 Parameters that affect the cyclic resistance of sands

For liquefaction assessment, the cyclic stress is usually expressed in terms of the cyclic stress ratio (CSR) which is the induced horizontal cyclic stresses normalized by the vertical effective consolidation stress. While the liquefaction resistance is described by the cyclic resistance ratio (CRR) which is the CSR required to reach liquefaction at a specified number of loading cycles.

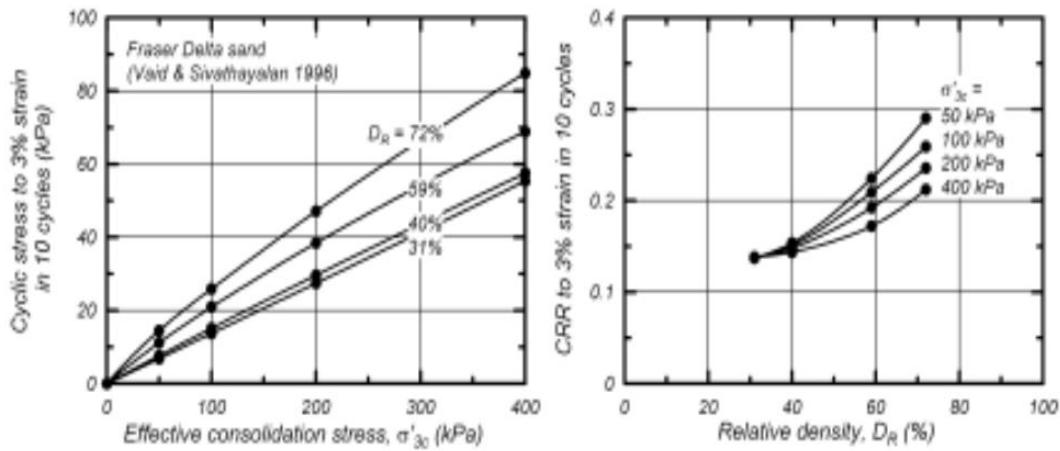


**Figure 2.5: Cyclic triaxial test results for clean Fraser delta sand showing the cyclic stress and CRR cause 3% shear strain in 10 cycles for  $D_r$  values of 31-72% and effective consolidation stresses of 50-400kPa. (Idriss and Boulanger, 2008)**

Except from the effect of the state that is described in the previous paragraph, there several other parameters that affect the liquefaction resistance of sand. One such parameter that is of importance is the lateral earth pressure coefficient at rest ( $K_0$ ). Ishihara et al (1985) have shown that the cyclic resistance ratio of anisotropically consolidated specimens can be related with the CRR of isotropically consolidated ones by the following approximation:

$$CRR_{K_0 \neq 1} = \frac{1 + 2K_0}{3} CRR_{K_0 = 1} \quad (2.1)$$

Another significant parameter is the aforementioned static shear stress, which is usually expressed in terms of the static shear stress ratio ( $\alpha$ ) defined as the initial shear normalized by the initial vertical effective stress. The effect of  $\alpha$  on the CRR of the soil is described by the factor  $K_\alpha$  which is the ratio of the CRR with initial static shear over the CRR without static shear. This effect for different relative densities and SPT normalized values ( $(N_1)_{60}$ ) is shown in Figure 2.6.

In addition, the generation of pore pressure and shear strains during undrained cyclic loading of saturated sand is affected by the rotation of principal stresses. This has been a difficult process to implement in constitutive models for liquefaction.

Finally other parameters that affect the cyclic resistance are the depositional method, the fabric, the stress strain history, age, cementation and over-consolidation. The effect of over-consolidation seems to exceed the effect caused by the increase of  $K_0$ .

### 2.7.4 Liquefaction Triggering

Over the years several approaches have been used for the assessment of liquefaction triggering. The most commonly used is the stress based approach that compares the earthquake induced cyclic stress with the cyclic resistance of the soil.

For laboratory tests liquefaction can be determined as a specific percentile increase in pore water pressure ratio or shear strain (e.g.  $r_u=100\%$  or  $\gamma=3\%$ ) where the pore pressure ratio is defined as:

$$r_u = \frac{\Delta u}{\sigma'_{vc}} \quad (2.2)$$

for cyclic simple shear tests, where  $\Delta u$  is the excess pore pressure and  $\sigma'_{vc}$  is the vertical effective consolidation stress. However, in the field liquefaction refers to observations, mainly from ground surface, which can be interpreted by the generation of excess pore pressures and significant shear or volumetric strains (Idriss and Boulanger, 2008).

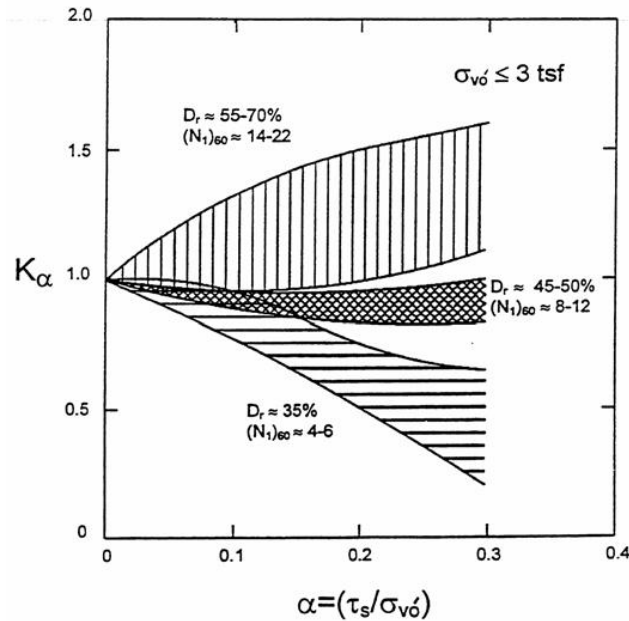


Figure 2.6: Static shear stress correction coefficient  $K_\alpha$  (Harder and Boulanger, 1997)

In practice, as described by the NCEER workshop report (2001), the earthquake induced shear stresses (i.e. the CSR) are commonly estimated by the Seed-Idriss simplified procedure (1971). Alternatively, the calculation of the static and dynamic stresses is done with the use of finite element analyses. The liquefaction resistance (CRR) is usually estimated empirically using existing correlations with in situ tests, such as standard and cone penetration tests. The cyclic resistance estimated with this method refers to earthquakes of magnitude  $M=7.5$ , at a reference confining stress of 100kPa and for ground-level conditions. So, to represent the actual

conditions on site and for the expected earthquake loading correction factors for the magnitude of the earthquake, the overburden load and the effect of static shear are used. All these factors are based on observations from case histories and from laboratory testing.

### 2.7.5 Consequences of liquefaction

Liquefaction can lead to a large range of consequences depending on the site conditions the seismic loading characteristics and the nature of the structures on the site. Three of the most important consequences that involve all the main concerns that are connected to liquefaction are the following (Idriss and Boulanger,2008):

- Loss of shear strength leading to instability of slopes or embankments
- Lateral spreading of mildly sloping ground
- Settlement caused by reconsolidation of the liquefied soils

As it was mentioned earlier these consequences are directly related to the phenomena of flow liquefaction and cyclic mobility.

Liquefaction induced deformations depend not only on the soil characteristics and the earthquake ground motion but also on the site stratigraphy and topography and on several other complicating phenomena such as three dimensional effects and ground cracking. Current analyses cannot account for the full effect of all the factors affecting liquefaction induced deformations. Generally liquefaction analyses for both triggering and deformations are based on several approximations and assumptions. Especially when it comes to post-liquefaction residual strength, although there is extensive research on the topic, there is not a commonly accepted framework for analysis.

## 2.8 Constitutive models for liquefaction

Although empirical methods have helped significantly in the improvement of design against liquefaction and generally in the decision-making process concerning the problem under consideration, there are two important drawbacks in the approach. First, empirical approaches lead to the widely known issue that different researchers come up with completely different conclusions and interpretations, even when they process the same case studies with the same data. Second, full-scale experiments are not a viable option in civil engineering, so the databases that lead to and support the empirical solutions are limited. An attempt to face these problems can be made by explicitly considering liquefaction as a constitutive behaviour of soil and trying to explain and model the mechanics behind it. In this framework, several constitutive models have been produced trying not only to predict liquefaction triggering but also to determine permanent deformations and post-liquefaction behaviour. However, solely relying on mechanics is not enough, since there are factors such as time, scale effects, pore pressure migration etc. that are usually neglected in theories and models, but might be very important in certain cases (Been and Jefferies, 2006).

Advanced constitutive models for liquefaction are based on critical state theory. Soil behaviour is highly dependent on soil density and confinement. The general idea is that dense soils are strong and dilatant and loose soils are weak and contractive. Critical state theory provides the framework that can explain why a particular density behaves in a particular way, by categorizing the soil properties according to state parameters. Evidently, liquefaction phenomenon is closely

dependent on the soil state. Therefore, soil models based on critical state soil mechanics are the most appropriate for liquefaction analysis.

There is a very large variety of soil constitutive models ranging from descriptive to idealized. Descriptive models are based on test data and are calibrated by curve fitting which means that they can provide very good results if the stress paths in the problem are similar to the test conditions. On the other hand, idealised models start from postulated mechanisms from which behaviours are then derived. In these models, consistent and known physics are considered more important than accuracy in a particular problem (Been and Jefferies, 2006).

In the case of earth dams, the evolution of the models used to evaluate their seismic response has been significant over the years. Initial approaches were pseudo-static, simulating the seismic loading as a horizontal force. Later on, viscoelastic models were introduced. A breakthrough, in this process, was the equivalent linear method for approximating non-linear behaviour, developed by H.B. Seed, the University of California at Berkeley. As previously mentioned, the main failure mechanism of earth dams under seismic loading is caused by liquefaction of either the dam body or the foundation soil. However, all these models were total stress models, so they were not capable of capturing the pore pressure generation. Also, despite the strain dependence of damping and shear modulus implemented in the equivalent linear model, the model is still elastic so the direct prediction of permanent deformations is not possible. Nevertheless, the equivalent linear method is still widely used in practice (Finn et al, 1995). Especially after the San Fernando failures, which gave a boost to the research for seismic response of embankment dams by emphasizing the shortcomings of the previously used models, the main concern was to create constitutive models able to simulate the pore pressure generation and the nonlinearity of the soil. This way the interest of the research has turned to effective stress concept and nonlinear elasto-plastic constitutive models. Thus, in the framework of these following models, soil is generally treated as a two phase material using partially or fully coupled equations for the soil and the water phases. The most complex of these models, which are state of the art today, are non-linear elastic plastic constitutive models based on kinematic hardening theory using either multi-yield surfaces or a boundary surface theory with a hardening law giving the evolution of the plastic modulus (Marcuson, 2007).

A common problem of this sophisticated advanced models is that the number of parameters, required for calculation, is large and often, these parameters cannot be directly measured in laboratory tests. Also although they have a theoretical generality, validation of these models has shown a strong stress path dependency (Marcuson 2007, Idriss and Boulanger 2008).

All available constitutive models have strengths and weaknesses. According to Beaty and Perlea (2011), the requirements that need to be met by a constitutive model for an advanced dynamic analysis of an embankment dam are the following:

- The formulation of the constitutive model should adequately address the key features of the soil behaviour. These may include the relationship between shear stiffness and strain, stress level dependence, generation of pore pressures and strain softening;
- It should have a sound theoretical basis;
- It should reasonably model the stress strain and pore pressure generation in monotonic and cyclic laboratory tests. Direct comparison between numerical simulation and laboratory data should be available;
- It should reasonably capture the behaviour described by empirical relationships for liquefaction triggering and post liquefaction effects;

- The selection of input parameters should be reasonably transparent particularly when direct calibration from laboratory data is not possible;
- Successful use of the model should be documented through back analysis of case history response.

Given these requirements and the specifics of the problem at hand, a proper selection amongst a wide variety of constitutive models needs to be done for advanced analysis of embankment dams. The level of sophistication of the chosen model or models needs to correspond firstly to the kind of structure analysed and how critical this structure is, as well as the detail and reliability of the site investigation and laboratory data.

In general, nonlinear dynamic analyses, using finite element or finite difference methods can be invaluable for addressing complex problems (like the modelling of embankment dams under consideration) and is more and more used on large projects. However, this kind of analysis requires high level of expertise with computational methods. In addition, the accuracy of such an analysis depends strongly on the site characterisation, the necessary simplifications/assumptions that are made, the details of the selected constitutive model and its numerical implementation, the importance of the potential phenomena that cannot be captured by the given numerical model and the selection of input ground motions. For all these reasons, the level of sophistication of a constitutive model is not analogous to the accuracy of the predicted behaviour (Idriss and Boulanger, 2008).

## 2.9 Types of constitutive models for advanced seismic analysis of embankment dams

A constitutive model is basically a law that connects stress and strain increments. There is a large variety of models that can be used for advanced analysis of embankments. Each one of these models can be potentially used in the analysis depending on the anticipated material behaviour of each zone or foundation layer and the objective of the analysis. The following three categories concern mainly the non-liquefiable layers of the embankment:

**Linear elastic models:** Simple linear elastic models impose a constant proportional relationship between stress increments and strain increments. This model is extremely simple and its results are path independent, but it has the disadvantage that it over simplifies soil behaviour. There is no yielding and permanent shear strains cannot be modelled directly. It can be used though for rock-like zones where shear failure or significant nonlinearities are unlikely.

**Elastic-perfectly plastic models:** In these models, there is a fixed yield surface and upon yielding the plastic strains can grow without bound given that no further change in stress occurs and no outside constraints are present. These models are useful for competent materials, such as compacted embankment shell, impervious core, unsaturated materials when material yielding is possible but effects related to pore pressure generation or cyclic degradation are not significant. Mohr-Coulomb model is a common example of this category.

**Non-linear elasto-plastic models with work hardening plasticity:** Elastic and elastic perfectly plastic models can be used for certain materials within the dam and its foundation. However, modelling of nonlinearities and stress dependency plays a significant role in seismic response. Thus, elasto-plastic models, using work hardening plasticity, can produce better results.

In contrast to perfect plasticity, work hardening implies that the yield surface changes in a certain way after initial yielding has occurred. The way the yield surface changes depends on the

plastic strain or the accumulated plastic work. In these models, changes of the yield surface are determined by a hardening rule. The yield surface can either expand (isotropic hardening) or move (kinematic hardening) in the stress space.

For the liquefiable materials of the embankment and foundation, there are three general types of constitutive models that can be used. These models are also based on elasto-plastic soil behaviour. The reason that they are described separately is just that since liquefaction is of concern, the coupling of the two phases of the soil skeleton (soil and water) and the subsequent pore pressure generation are a main concern.

**Total stress models:** These models simulate the softening of the liquefiable elements at the time of triggering. Timing and distribution of liquefaction can be manually controlled by cycle counters based on laboratory data and theoretical formulations to predict the evolution of liquefaction. The pore pressures are not directly predicted and the strengths in the saturated elements are specified as undrained values with a friction angle of zero. The advantage of these models is that they are relatively simple but still incorporate critical aspects of liquefaction in the analysis.

**Loosely coupled effective stress models:** The element response is a function of the evolving effective stress state. They use an independent pore pressure generator instead of calculating volumetric strains directly. They evaluate the predicted cycles of shear stress or shear strain to estimate the corresponding change in the pore pressure and then adjust the pore pressures at the end of each cycle or half-cycle. Loosely coupled models can be extensions of elastic perfectly plastic models or non-linear models.

Some examples of loosely coupled models are the TARA models developed by Finn and the Finn-Byrne-Itasca model. The TARA models have been the first ones to be used for advanced analysis of embankments.

**Fully coupled effective stress models:** This is the most sophisticated class of constitutive models for liquefaction. They predict the soil's tendency to dilate or contract in response to each load increment. The volumetric strains are resisted by the stiffness of the pore fluid in the saturated elements and thus, pore pressure generation can be estimated. Often, the effects due to pore water flow can also be considered, although in these cases the analysis becomes extremely complex.

The stiffness and pore pressure response of this type of models depends on the accurate prediction of volumetric strains. For this reason the calibration and verification becomes difficult as their appropriateness for critical structures needs to be demonstrated through laboratory tests, case histories, centrifuge comparative analysis and critical evaluation of predicted element response. However, fully coupled, effective stress models simulate better the soil behaviour seen in laboratory tests.

Examples of this kind of models include DYNFLOW by Prevost, DYNARD by Moriwaki et al, UBCSAND by Byrne et al, DYSAC2 by Muraaleetharan et al and more (Marcuson,2007). These models have significant differences between them and different levels of sophistication. For example, DYNFLOW is a fully coupled dynamic analysis procedure whose constitutive model is based on multi yield surface plasticity. DYNARD and DYSAC2 are both based on bounding surface plasticity. UBCSAND is probably the simplest of these models and the one that is most commonly used in practice, since it is based on classical plasticity.

## 2.10 UBC3D-PLM constitutive model

As mentioned in the project description, this report is concerned with the applicability of the UBC3D-PLM constitutive model for dynamic analysis of embankment dams. The model is based on the UBCSAND model developed by Puebla et al (1997) and Beaty and Byrne (1998). In general, UBCSAND is one of the most commonly used constitutive models for liquefaction problems in practice. Even though it is an advanced model, it is relatively simple to apply, since it has a reasonable number of parameters that can be extracted from laboratory or in situ tests. The model was initially developed for sand-like soils having the potential for liquefaction under seismic loading.

Similarly to the original UBCSAND model, UBC3D-PLM is an effective stress model based on classical plasticity theory with a hyperbolic hardening rule (Figure 2.8). The hardening rule relates the mobilized friction angle to the plastic shear strain at a given stress. The main difference with UBCSAND is that UBC3D-PLM uses Mohr-Coulomb yield criterion (Figure 2.7) in 3-D instead of 2-D principal stress space. UBC3D-PLM has a modified non-associated plastic potential function based on Drucker-Prager's criterion. Furthermore, in its current version, it includes a soil densification rule to better predict the evolution of pore pressures during cyclic loading.

For undrained behaviour, the volumetric strains that would occur for drained loading are compensated by the generation of excess pore pressures. In this sense the model is coupled although it does not account for groundwater flow.

The elastic behaviour is assumed isotropic and is expressed in terms of elastic bulk and shear moduli as described by the following equations:

$$K_B^e = k_B^e \cdot P_A \cdot \left( \frac{p'}{P_A} \right)^{m_e} \quad (2.3)$$

$$K_G^e = k_G^e \cdot P_A \cdot \left( \frac{p'}{P_A} \right)^{n_e} \quad (2.4)$$

where  $K_B^e$  is the elastic bulk modulus,  $K_G^e$  is the elastic shear modulus,  $p'$  is the mean effective stress,  $P_A$  is the reference stress (usually equal to 100kPa),  $k_B^e$  and  $k_G^e$  are the bulk and shear modulus numbers respectively and,  $m_e$  and  $n_e$  are the elastic exponents which define the rate dependency of stiffness.

The aforementioned Mohr-Coulomb yield function is used and the critical yield surface is given by the following equation:

$$f_m = \frac{\sigma'_{\max} - \sigma'_{\min}}{2} - \left( \frac{\sigma'_{\max} - \sigma'_{\min}}{2} + c' \cot \varphi'_p \right) \sin \varphi_{mob} \quad (2.5)$$

where  $\sigma'_{\max}$  and  $\sigma'_{\min}$  are the maximum and minimum principal stresses,  $\varphi'_p$  and  $\varphi_{mob}$  are the peak and mobilized friction angles respectively and  $c'$  is the cohesion.

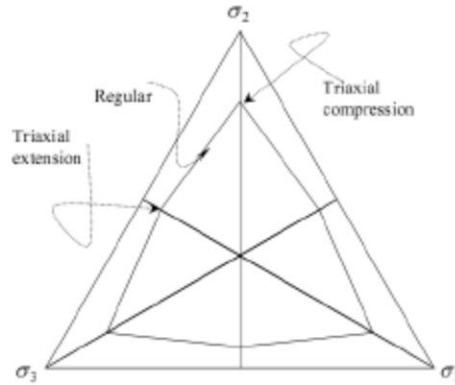


**Figure 2.7: Projection of the Mohr Coulomb yield surface on the deviatoric plane**

Once the yield surface is reached, if loading continues, the soil deforms plastically and plastic hardening occurs which is described by the hyperbolic hardening rule (Beatty and Byrne, 1998) which relates the plastic shear strain increment with the mobilized friction angle increment:

$$\delta\gamma^p = \frac{1}{G^*} \delta \sin\phi_{mob} \quad (2.6)$$

where:

$$G^* = k_G^p \cdot \left(\frac{p'}{P_A}\right)^{np} \left\{ \left(1 - \frac{\sin\phi_{mob}}{\sin\phi'_p}\right) R_f \right\}^2 \quad (2.7)$$

where  $k_G^p$  is the plastic shear modulus number,  $np$  is the plastic shear modulus exponent and  $R_f$  is the failure ratio  $n_f/n_{ult}$  while  $n_f$  is the stress ratio at failure and  $n_{ult}$  is the asymptotic stress

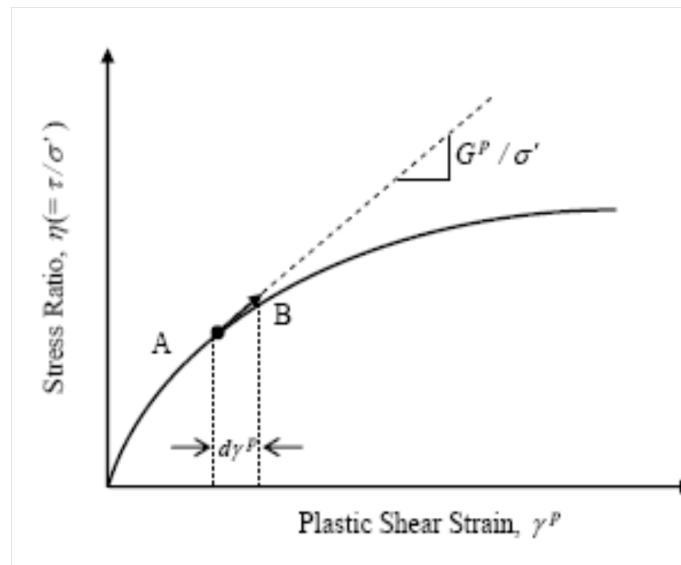


**Figure 2.8: Hyperbolic hardening rule in UBCSAND (Beatty and Byrne, 1998)**

The plastic potential function is based on Drucker Prager and is formulated as:

$$g = q - \alpha(p' + c \cot\varphi_p) \quad (2.8)$$

where:

$$\alpha = \frac{\sqrt{3} \sin\psi_m}{\cos\theta + \frac{\sin\theta \sin\psi}{\sqrt{3}}} \quad (2.9)$$

Where  $\psi$  is the dilatancy angle and  $\theta$  is the Lode angle equal to  $30^\circ$  because the Drucker Prager surface is fixed in the compression point.

The flow rule is given by the following equation:

$$d\varepsilon_v = \sin\psi_m d\gamma_p \quad (2.10)$$

where

$$\sin\psi_m = \sin\varphi_m - \sin\varphi_p \quad (2.11)$$

The densification rule is implemented in UBC3D by a secondary yield surface for which a simplified kinematic hardening rule is used. For secondary loading the plastic shear modulus is increased after each loading cycle according to the following densification rule:

$$K_G^p = K_G^p \left( 4 + \frac{n_{\text{cross}}}{2} \right) \text{hard fac}_{\text{hard}} \quad (2.12)$$

where  $n_{\text{cross}}$  is the number of half cycles generated from the beginning of the test,  $\text{hard}$  is a factor which is correcting the densification rule for loose soils and  $\text{fac}_{\text{hard}}$  is a multiplier to adjust the densification rule.

UBC3D-PLM is a descriptive model, so its parameters are derived by curve fitting from laboratory tests on the same material. The calibration of the suitable stress path is of great significance, in order to obtain an accurate solution. In this case the most suitable tests are drained simple shear tests. However, DSS test results for the same materials are not always possible to find. In this case, there are several correlations for the acquisition of the input parameters, either from triaxial test results or from SPT results.

The input parameters of UBC3D-PLM are summarized in Table 2-1.

$\phi_{cv}$	the constant volume friction angle
$\phi_p$	the peak friction angle
c	the cohesion of the soil
$K_B^e$	the elastic bulk modulus of the soil at the reference level $P_A = 100\text{kPa}$
$K_G^e$	the elastic shear modulus at the reference level $P_A = 100\text{kPa}$
$K_G^p$	the drained plastic shear modulus
$k_B^e, k_G^e, k_G^p$	the modulus numbers corresponding to the elastic shear and bulk moduli and the plastic shear modulus respectively
me	the elastic bulk modulus exponent
ne	the elastic shear modulus exponent
np	the plastic shear modulus exponent
$R_f$	the failure ratio
$fa_{hard}$	the densification factor
$(N_1)_{60}$	the corrected SPT value
$fa_{post}$	a factor that determines the minimum value of the shear modulus during stiffness degradation
$P_A$	the reference stress which is equal to the atmospheric pressure

**Table 2-1: UBC3D-PLM parameters**

## 2.11 Summary and conclusions

Dynamic analysis of embankment dams is a problem that has concerned numerous researchers for over 50 years. The most important problem connected with seismic loading in embankment dams is liquefaction either of the dam body or of the foundation layers, which is one of the most controversial topics in geotechnical engineering.

The state of practice dictates separate treatment of the triggering mechanisms for liquefaction and deformation analysis. The state of the art, effective stress, dynamic analyses generate pore pressures under earthquake motion while soil stiffness and strength are degraded accordingly during shaking.

In general, besides the very large variety of methods and constitutive models, there is not yet a commonly accepted way to perform dynamic analysis in earth dams. This is not only attributed to the occurrence of liquefaction, which is a complex mechanism to capture, but also to the particularities that this kind of structures presents. Another reason is that even in well-known case histories the documentation is poor.

The development of sophisticated models has provided a much better understanding of the liquefaction problem and the general dynamic response of dams, but they are still too complex and difficult to use in daily practice. For this reason, in everyday practice, either quasi-static or equivalent linear methods are used, although their drawbacks have been observed in detail over the years.

However, nonlinear analyses are increasingly used for embankment dams, especially in large projects. Special care needs to be taken in these cases, so that the models are calibrated for the suitable stress path and that the necessary simplifications and assumptions are reasonable.

Given these observations, in the following chapters a dynamic analysis using the effective stress model UBC3D-PLM will be performed in an attempt to evaluate the performance of the model, observe its possibilities and limitations and assess the applicability of the model for dynamic analyses in earth dams.

### 3 MATERIAL PROPERTIES AND MODEL CALIBRATION

In any kind of finite element analysis, using the simplest or the most sophisticated constitutive model, the first step is to determine the model parameters for the specific soil type and loading conditions. As it was mentioned earlier, this step can be complicated when liquefaction constitutive models are used, since they often involve parameters that cannot be determined directly from laboratory testing and also most of them are stress path dependent and demand calibration before applied in any project.

Many different types of laboratory tests have been used for calibration of liquefaction models. Due to the dependency of the models on the stress path, it is recommended by several researchers (Finn et al 1995, Marcuson 2007, Beaty and Perlea 2011) that calibration of elasto-plastic models used for dynamic analysis should be done using cyclic loading tests such as triaxial torsional shear or simple shear tests. It is critical for the accuracy of the analysis to determine the parameters using suitable laboratory tests that fit properly the loading conditions existing in the field. An example of the suitable tests for lateral spreading and flow failure caused by liquefaction is shown in Figure 3.1.

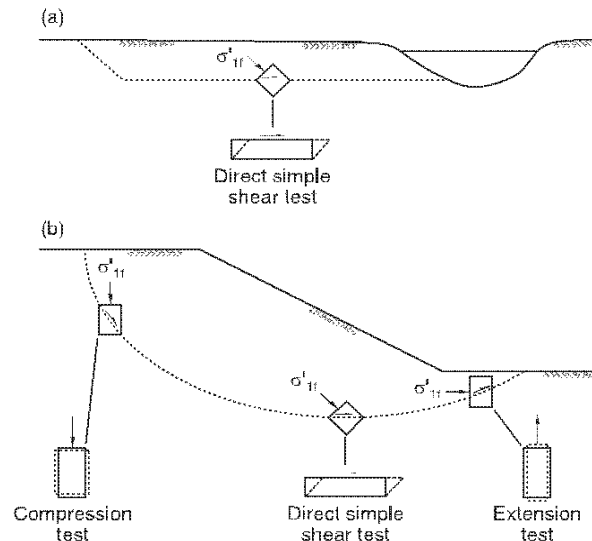


**Figure 3.1: Relevance of laboratory shear tests to modes of shearing on potential surfaces of sliding in the field (a) lateral spreading (b) flow failure**

However the determination of the soil properties and especially of the volume-change characteristics of cohesionless materials is not a simple process since the acquisition of undisturbed samples of sandy soils is very difficult. For this reason, as an additional check of the model performance, it is advisable (Finn et al 1995, Marcuson 2007, Beaty and Byrne 2011) to use the model to reproduce the field cyclic strength curve which correlates the cyclic resistance ratio (CRR) with the corrected clean sand SPT blow-count ( $(N_1)_{60}$ ) (Seed et al, 1986). This curve is also suggested by the 1997 NCEER/NSF workshop (Youd et al, 2001) for prediction of liquefaction.

In this chapter, the main objectives are:

- to find a method, as general as possible, to determine suitable parameters for use in UBC3D-PLM using in situ and laboratory test results;
- to evaluate the performance of the suggested calibration;
- to determine the effect of the critical parameters affecting liquefaction triggering on the model performance.

To achieve these goals, initially undrained cyclic direct simple shear tests (DSS) are reproduced by means of the soil test facility of PLAXIS 2D, using existing correlations and reasonable assumptions for the model parameters, from the UBCSAND model and other laboratory observations. The laboratory tests that have been used for the comparison have been performed for the project “Earthquake Induced Damage Mitigation from Soil Liquefaction” directed by Prof. Peter M. Byrne at the university British Columbia. The test results are acquired from the UBC database (<http://www.civil.ubc.ca/liquefaction/>). After an initial curve fitting process for these tests, an attempt to determine a more general calibration that is able to fit the aforementioned cyclic strength curve is done. After acquiring the more general correlations, the initial tests are once again run with the new calibration and the initial assumptions are revised to determine final parameters that will be used in the centrifuge test simulation that will be performed in the next section.

For the assessment of the effects of the critical parameters, again direct simple shear tests will be performed in PLAXIS under suitable conditions so that the results can be compared with existing laboratory and empirical observations concerning the same parameters. This way a general evaluation of the effect of each individual parameter can be made.

### 3.1 UBCSAND parameters-SPT correlations

Alike most liquefaction models UBC3D-PLM is a descriptive model and the model parameters are determined by curve fitting, preferably from cyclic undrained direct simple shear (DSS) tests. However in many cases these tests are not available and data from in situ tests such as Standard Penetration (SPT) or Cone Penetration (CPT) tests exist. For this reason for the UBCSAND model, Beaty and Byrne (2011) have proposed certain correlations connecting the model parameters (Table 2.1) with the corrected clean sand equivalent SPT blow-count measurements  $((N_1)_{60})$ .

These correlations are the following:

$$k_G^e = 21.7 \cdot 20.0 \cdot (N_1)_{60}^{0.333} \quad (3.1)$$

$$k_B^e = k_G^e \cdot 0.7 \quad (3.2)$$

$$k_G^p = k_G^e \cdot (N_1)_{60}^2 \cdot 0.003 + 100.0 \quad (3.3)$$

$$\varphi_{pi} = \varphi_{cv} + (N_1)_{60}/10.0 \quad (3.4)$$

where  $\varphi_{pi}$  is the peak friction angle for  $(N_1)_{60}$  values lower than 15 while for larger an additional increase is suggested as described by relation (3.5):

$$\varphi_p = \varphi_{pi} + \max \left( 0.0, \frac{(N_1)_{60} - 15}{5} \right) \quad (3.5)$$

The values on  $m_e$  and  $n_e$  are considered equal to 0,5 and the value of  $n_p$  equal to 0.4 by default. For the failure ratio the following correlation applies:

$$R_f = 1.1 \cdot (N_1)_{60}^{-0.15} \quad (3.6)$$

as long as the occurring value is smaller than 0.99 otherwise a value of 0.99 is used. Concerning the densification factor ( $f_{ac_{hard}}$ ), the suggested value for UBCSAND is 1.0.

From equation (3.2) a direct relation between elastic shear and bulk modulus is derived which corresponds to a Poisson's ratio of 0,02 from the theory of elasticity. This ratio is very low for static calculations and would lead to unrealistic results. However, it has been shown (Hardin 1978, Negusse, 1984) that Poisson's ratio varies with strain and that for small strains its value can range between 0.0-0.2. For this reason, for dynamic calculations a much lower Poisson's ratio can be used, the same way the small strain shear modulus is used. Still the assumption is on the low side, since the usual assumption for sands is around 0.1 (Byrne et al, 1987). To address the problems that might occur in the static analyses, it is suggested to either use a different calibration of the model or a different constitutive model for those.

Although there are significant similarities between the UBCSAND model and UBC3D-PLM, the models are not identical and these correlations cannot be used directly for UBC3D-PLM without validation. Nonetheless, they constitute a very good starting point to determine suitable correlations for UBC3D-PLM.

## 3.2 Soil tests

The undrained cyclic DSS tests have been performed on Fraser River Sand. The index properties of the sand, determined for tests performed in UBC, are shown in Table 3-1. In the literature there are several values for the constant volume friction angle ( $\phi_{cv}$ ) of clean Fraser River sand (Thomas 1992, Chirillage et al 1997, Vaid et al 2001), the range of the values is from 30° to 34°. The value of  $\phi_{cv}$  that was used for the simulations is 33°.

The simple shear apparatus used in UBC for the undrained cyclic tests is of Norwegian Geotechnical Institute (NGI)-type and allows the testing of a specimen of ≈70mm height and ≈20-25mm diameter. The diameter of the specimen is constrained against lateral strain by a steel-wire-reinforced rubber membrane. The testing apparatus and the assumed boundary conditions are shown in Figure 3.2.

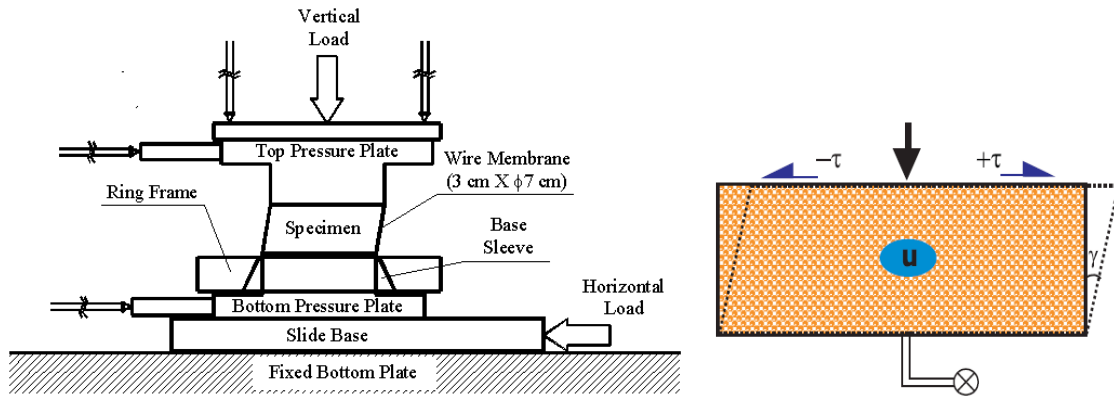


**Figure 3.2: NGI-type Direct Simple Shear test apparatus and boundary conditions for undrained cyclic test**

Specific gravity ( $G_s$ )	2.71
Medium grain size ( $D_{50}$ , mm)	0.26
Minimum void ratio ( $e_{min}$ )	0.62
Maximum void ratio ( $e_{max}$ )	0.94
Porosity ( $n$ ) at $D_r=40\%$	0.45
Porosity ( $n$ ) at $D_r=80\%$	0.41

**Table 3-1: Index properties of Fraser River Sand**

The laboratory tests have been performed at two different relative densities:  $D_r=40\%$  and  $D_r=80\%$ . All of the tests were executed at an initial vertical effective stress ( $\sigma_{v0}'$ ) of 100kPa. The tests were stress controlled and for each of the densities three tests were performed at the three cyclic stress ratios shown in Table 3-2.

Relative density ( $D_r$ )	40%	80%
Cyclic stress ratio (CSR)	0.08	0.25
	0.10	0.30
	0.12	0.35

**Table 3-2: CSR of undrained cyclic DSS tests**

To make an initial assumption for the  $(N_1)_{60}$  value the following common correlation between relative density and penetration resistance is used:

$$D_r = \sqrt{\frac{(N_1)_{60}}{C_d}} \quad (3.7)$$

where  $D_r$  is a ratio and  $C_d$  is a calibration factor. The equation was initially used by Meyerhof (1957) who suggested a  $C_d$  value of 41. However, over the year several values of  $C_d$  have been suggested by different researchers.  $C_d$  depends on several parameters such as the type of sand, the grain size, the percentage of fines, the over-consolidation ratio, whether the deposit is

natural or manmade and more. The range of  $C_d$  is between 36 and 60. Idriss and Boulanger (2003) have used a value of 46 to evaluate the consistency of SPT- and CPT-based liquefaction triggering correlations. This value is considered a reasonable assumption and it was used for the estimation of the initial  $(N_1)_{60}$  values of the laboratory tests.

The parameters that occurred from the previously described correlations are shown in Table 3-3 along with the changes that were made to the densification factor ( $fa_{c_{hard}}$ ) and the post liquefaction factor ( $fa_{c_{post}}$ ) to obtain a fit of the laboratory measurements with the PLAXIS calculations.

Model Parameters	Loose (Dr=40%)	Dense (Dr=80%)
$(N_1)_{60}$	7.4	29.5
$\phi_{cv}$ (°)	33.0	33.0
$\phi_p$ (°)	33.7	38.9
$k_g^e$	845.2	1339.5
$k_b^e$	591.6	937.6
$k_g^p$	238.8	3597.1
$R_f$	0.81	0.66
$fa_{c_{hard}}$	0.45	0.45
$fa_{c_{post}}$	0.02	0.02

**Table 3-3:UBC3D-PLM parameters after calibration by undrained cyclic DSS tests**

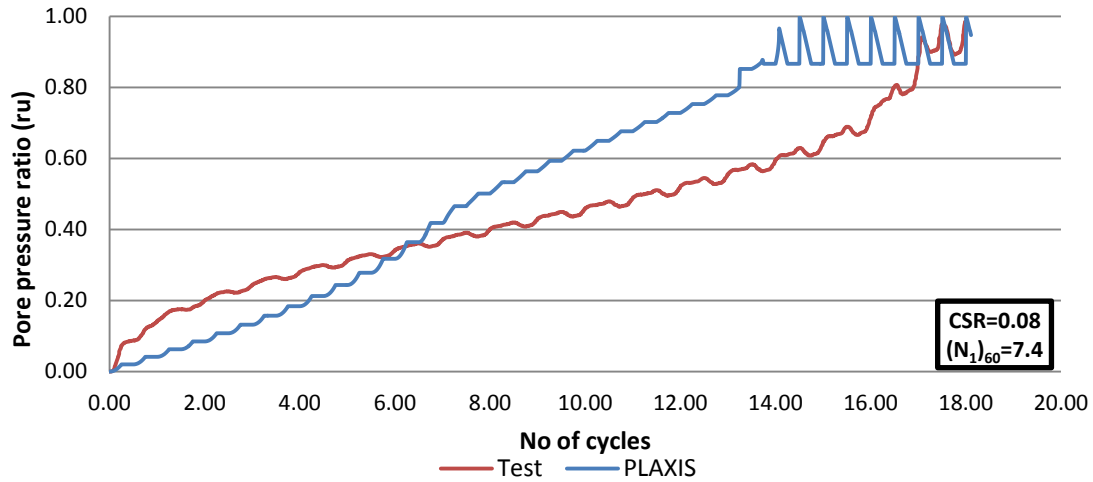
Some general observations can be made from the test results presented in Figure 3.3-Figure 3.8. In the stress-strain behaviour of the model, there are differences compared to the laboratory tests. In the laboratory the behaviour of the specimen seems to start softer, then it densifies until it starts softening again due to the excess pore pressures. In the model this behaviour cannot be completely captured. An important reason why this problem occurs is due to the anisotropic initial loading. According to Jaky's formula the  $K_0$  that as used for this soil was 0.46 and thus the lateral stresses were 46kPa with an initial vertical effective stress of 100kPa. From the stress path it can be seen that in the initial cycles a stiffer behaviour with practically constant stiffness is predicted and instead of densification the moment the isotropic axis is approached a softer cycle occurs. After that the densification rule is activated and the behaviour becomes stiffer. However, if this limitation is taken into account for the calibration the onset of liquefaction can be closely predicted for the test.

In both sets of tests (loose and dense sand) the calibration was done so that the best fit would be achieved for the medium stress ratio, with the assumption that, since the initial conditions are the same, if the model is calibrated for a certain cyclic stress ratio (CSR) then it should predict accurately the onset of liquefaction at any other CSR. However, from the presented test results, it can be observed that for lower CSR the model predicts liquefaction earlier than it occurs in the laboratory and for larger CSR it predicts liquefaction later. This behaviour can be attributed to the previously observed limitation about stiffness and densification. In larger cyclic

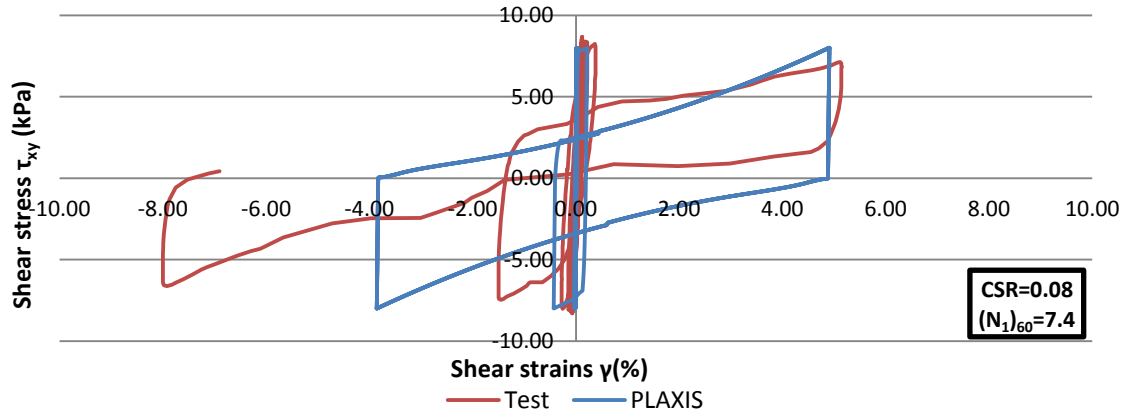
stress ratios the test liquefies earlier than the model suggests because the initial cycles are stiffer than in reality and they cause less pore pressure generation. Furthermore, if the densification rule is set so that the test with CSR=0.10 is fitted, to compensate for the initial stiffer cycles the densification factor is set to a lower value than it would be if isotropic initial conditions were assumed. So, in the smaller CSR where the number of cycles until liquefaction is larger, the effect of these initial stiffer cycles is less and this lower  $fac_{hard}$  causes the soil not to densify enough and liquefaction occurs earlier than in the test. To minimize this limitation, for dynamic response analyses of large scale problems, it would be advisable to calibrate the model based on DSS tests performed on similar CS ratios to the ones expected to occur in the field.

Concerning the shear strains in the laboratory tests, the effect of cyclic mobility can be observed. Cyclic mobility is the accumulation of limited strains after the pore pressure ratio ( $ru$ ) becomes 100%. This condition of  $ru=100\%$  is temporary and occurs only under isotropic states of stress. This happens due to the specimens incrementally dilative tendencies during shear loading and incrementally contractive during unloading. During dilation the vertical effective stress ( $\sigma_{v0}'$ ) increases, which leads to an increase of tangent stiffness and during contraction,  $\sigma_{v0}'$  decreases and causes a decrease in stiffness. If the laboratory test was to be continued the amount of shear strains would keep increasing. Cyclic mobility cannot be properly simulated by UBC3D-PLM because after a pore pressure ratio near 100% is approached the model does not allow for further softening of the soil behaviour and as it can be seen for the stress strain curves the model keeps repeating the same loop. The post-liquefaction behaviour of the soil is not included in the model.

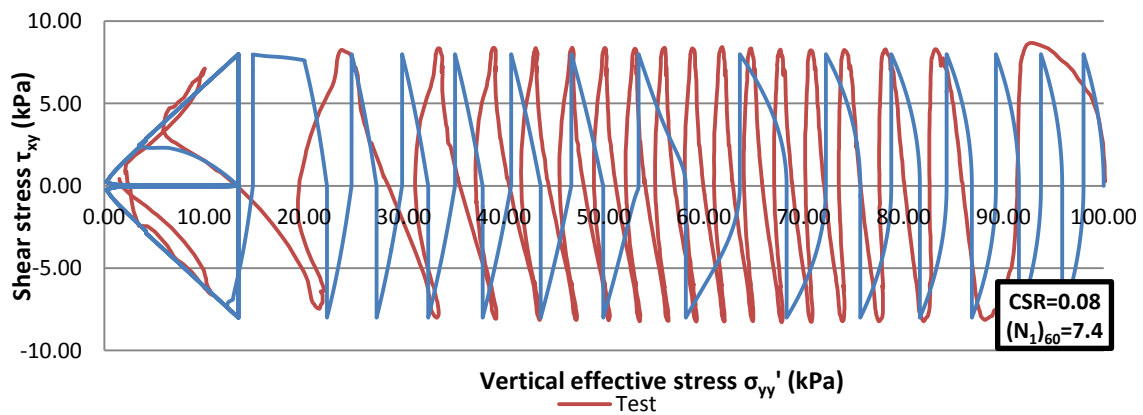
In general this behaviour in UBC3D-PLM is determined by the post liquefaction factor ( $fac_{post}$ ) which is implemented to account for the softening that occurs after the peak yield surface is reached. Reaching this yield surface does not mean that the soil is liquefied. In the latest version of the model  $fac_{post}$  determines the minimum shear stiffness of the soil. After the peak yield surface is reached the shear modulus is decreased in every loading cycle until it reaches this minimum value. To be able to get to a pore pressure ratio close to 100%, the post liquefaction factor needs to be very low (in an order of magnitude of  $10^{-2}$ ), otherwise after the minimum shear modulus is reached the new loading cycles will not produce any increase in pore pressures and liquefaction will not be reached. In loose soils the effect of the post liquefaction factor is less significant because high values of pore pressure ratio are reached and the soil is practically liquefied before the peak yield surface. For this reason the shear strains that have been observed in the laboratory tests in sand with relative density of 40% are better approximated by UBC3D-PLM than the shear strains in the samples with 80% relative density.



a) Rate of pore pressure generation

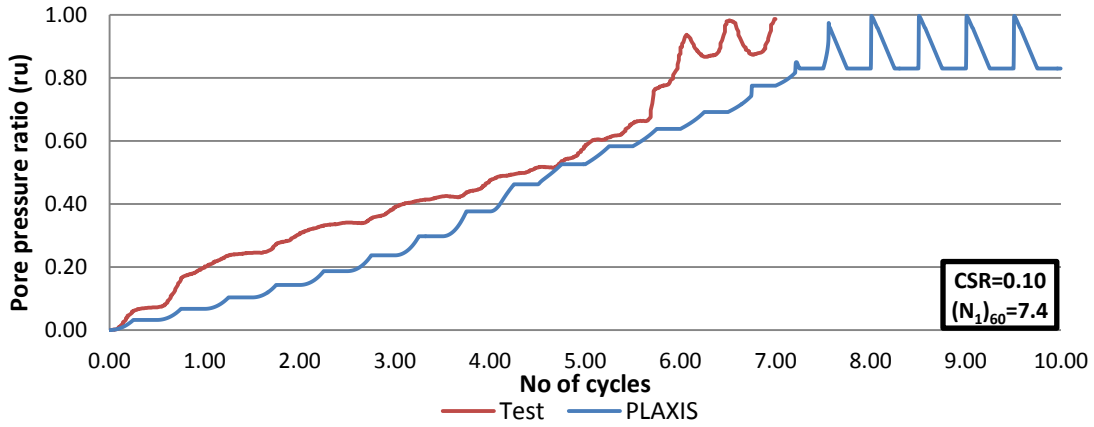


b) Stress strain behavior

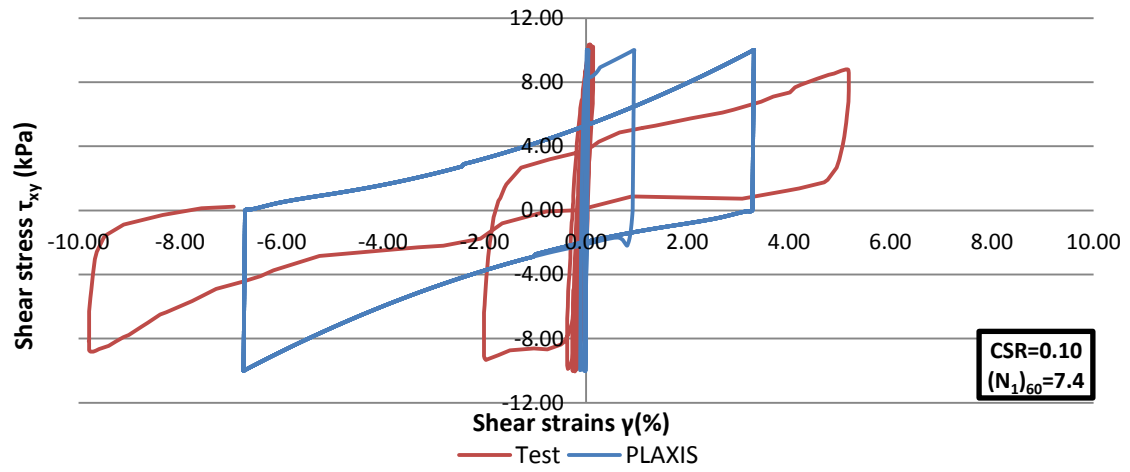


c) Stress path

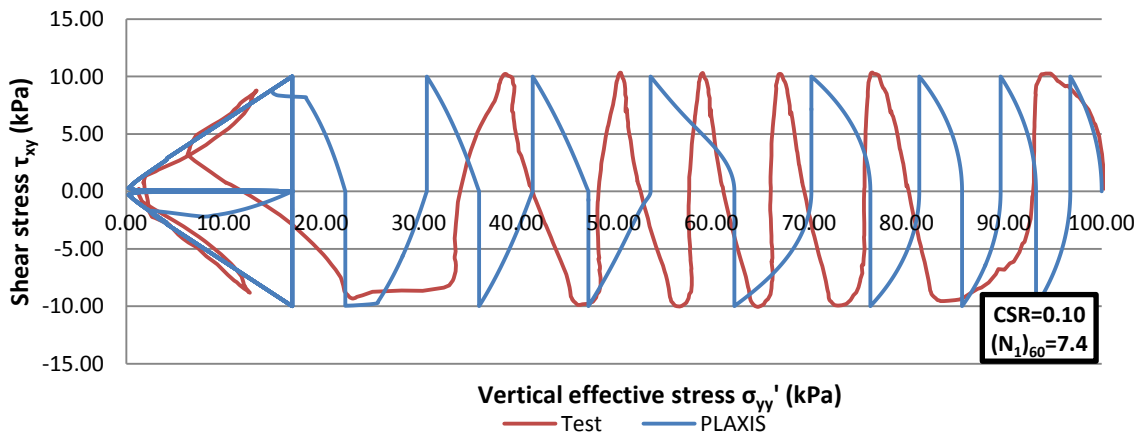
Figure 3.3: Cyclic undrained laboratory DSS test and PLAXIS simulation at  $Dr=40\%$ ,  $CSR=0.08$  and  $K_0=0.46$



a) Rate of pore pressure generation

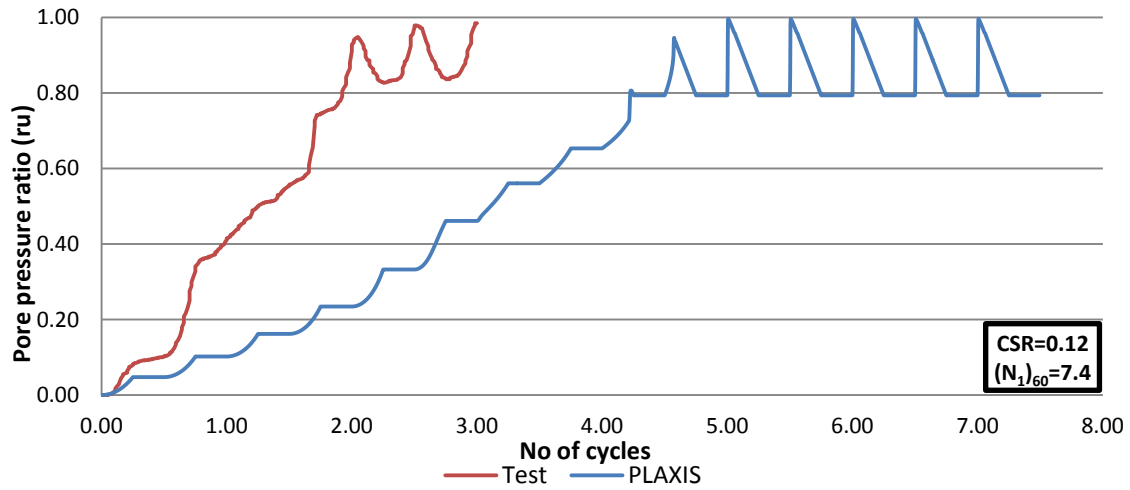


b) Stress strain behavior

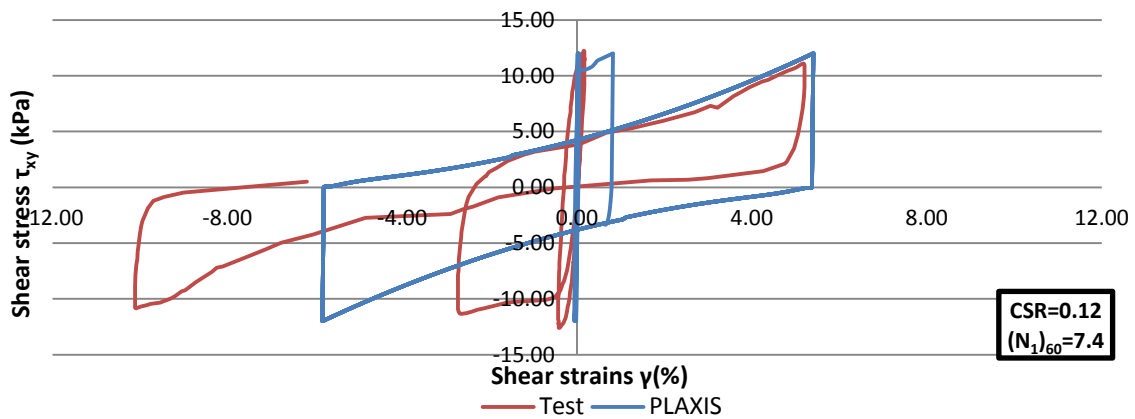


c) Stress path

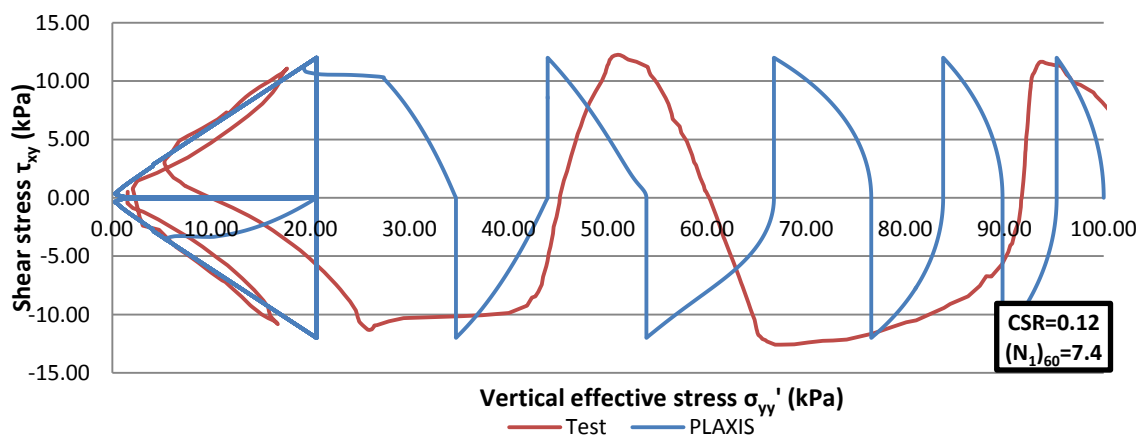
Figure 3.4: Cyclic undrained laboratory DSS test and PLAXIS simulation at  $D_r=40\%$ ,  $CSR=0.10$  and  $K_0=0.46$



a) Rate of pore pressure generation

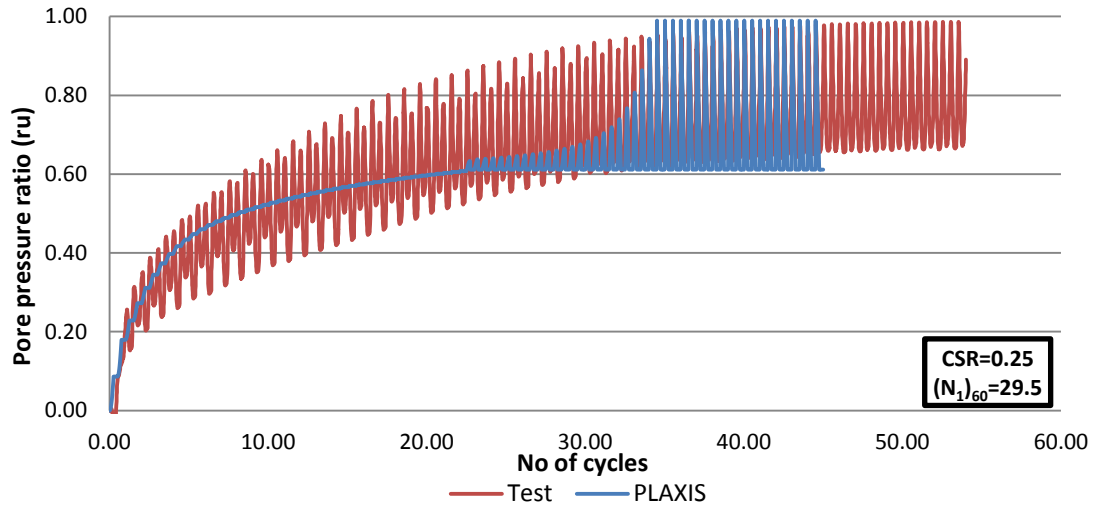


b) Stress strain behavior

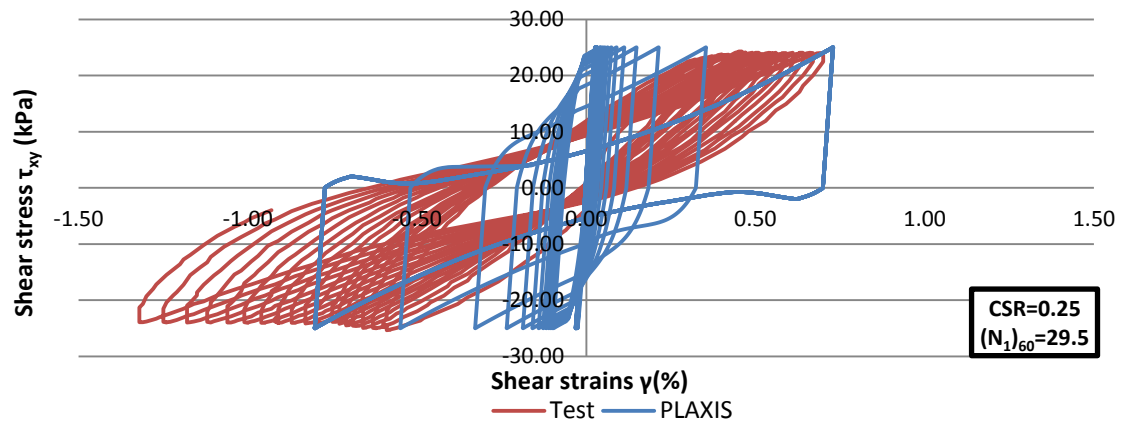


c) Stress path

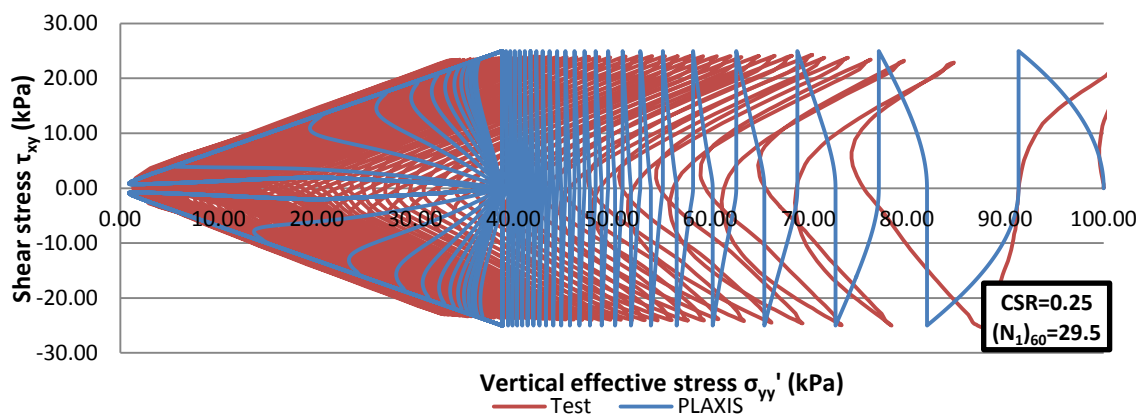
Figure 3.5: Cyclic undrained laboratory DSS test and PLAXIS simulation at  $D_r=40\%$ ,  $CSR=0.12$  and  $K_0=0.46$



a) Rate of pore pressure generation

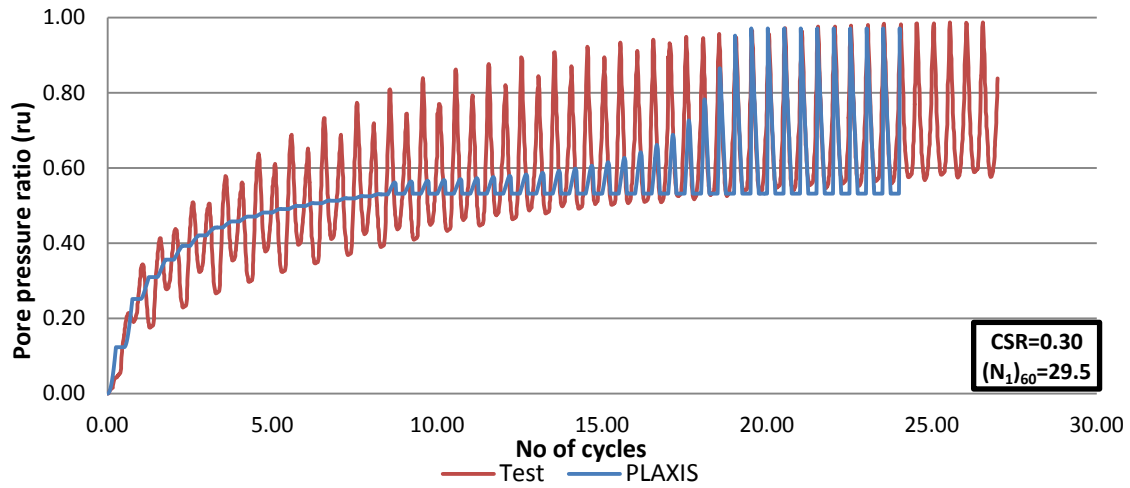


b) Stress strain behavior

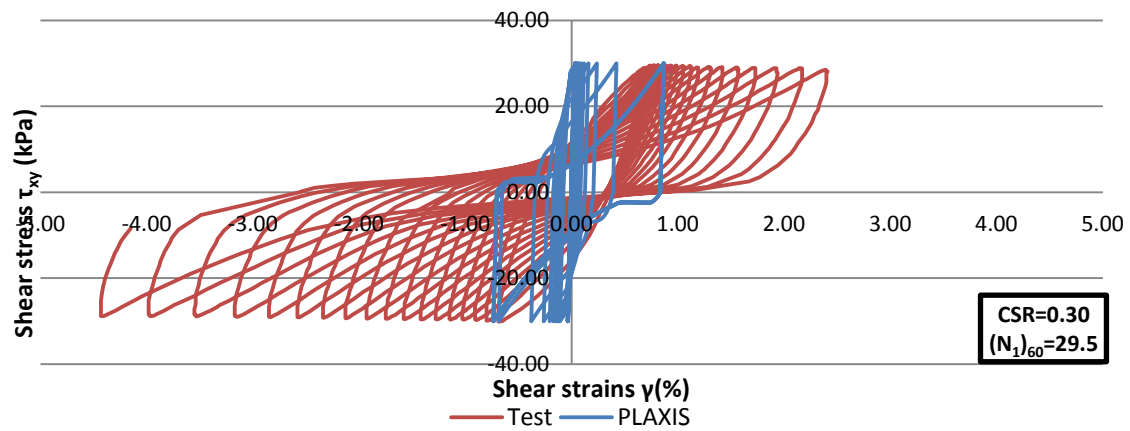


c) Stress path

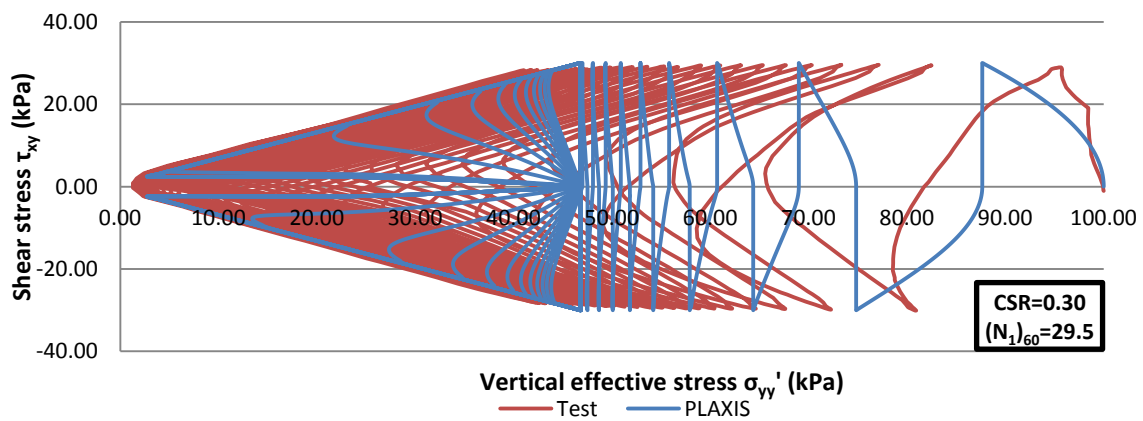
Figure 3.6: Cyclic undrained laboratory DSS test and PLAXIS simulation at  $D_r=80\%$ ,  $CSR=0.25$  and  $K_0=0.46$



a) Rate of pore pressure generation



b) Stress strain behavior



c) Stress path

Figure 3.7: Cyclic undrained laboratory DSS test and PLAXIS simulation at  $D_r=80\%$ ,  $CSR=0.30$  and  $K_0=0.46$

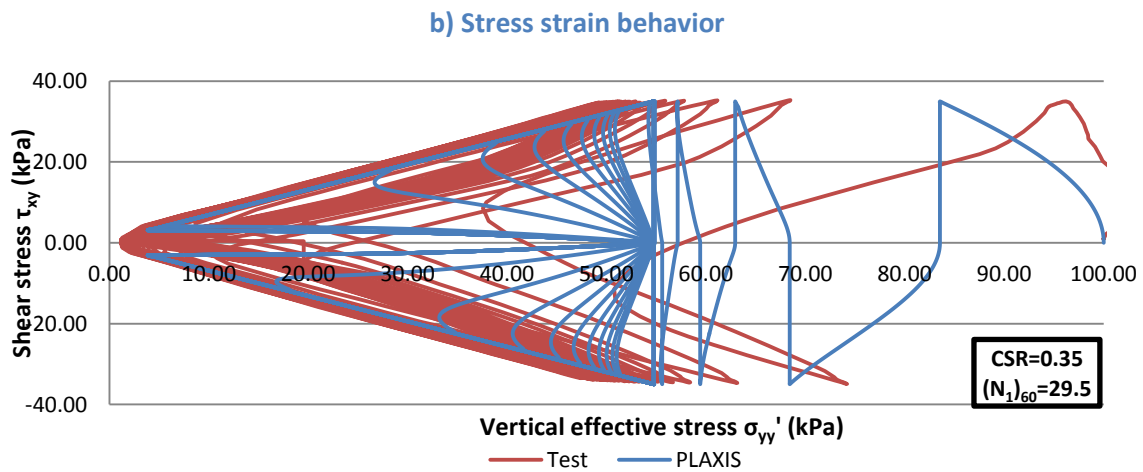
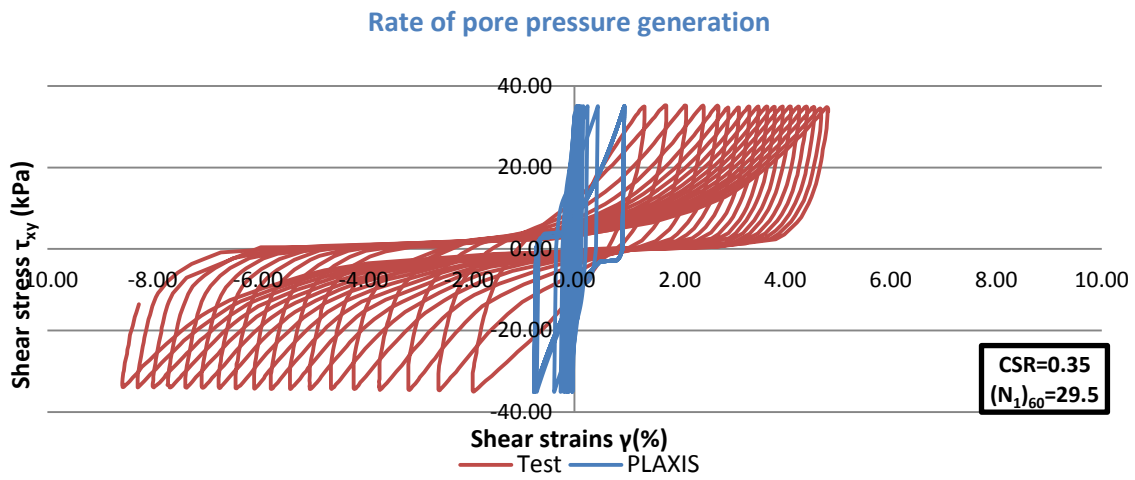
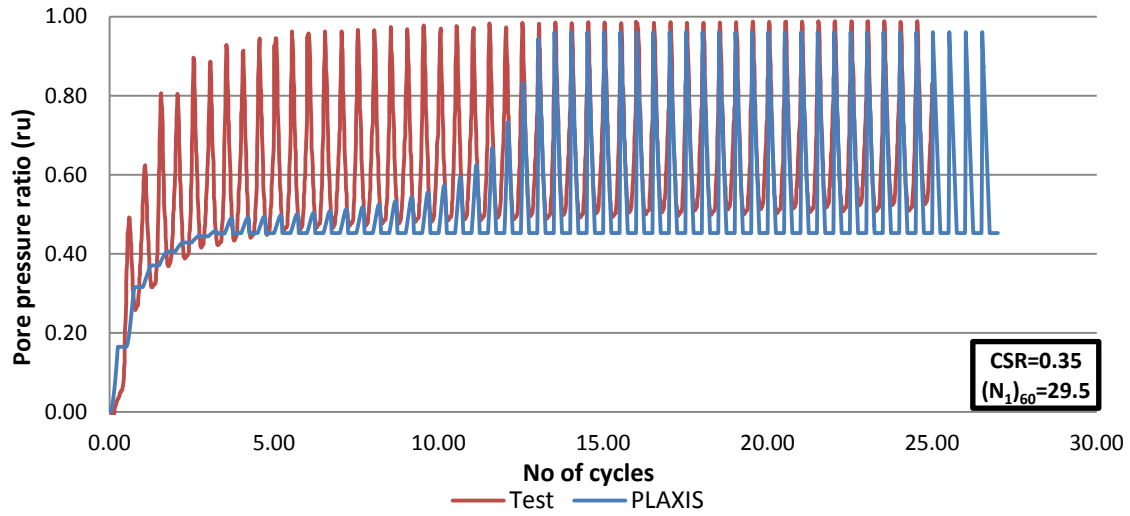


Figure 3.8: Cyclic undrained laboratory DSS test and PLAXIS simulation at  $D_r=80\%$ ,  $CSR=0.35$  and  $K_0=0.46$

### 3.3 Cyclic strength curve

It was mentioned earlier that the suggested way to validate the calibration of the constitutive model is to try and reproduce the cyclic strength curve which connects the cyclic resistance with the corrected clean sand SPT blow count. The CRR curve separates data from areas where there has been liquefaction from areas where no liquefaction has occurred (Figure 3.9). The blow count  $(N_1)_{60}$  has been normalized for an overburden stress of 100kPa and for a hammer efficiency of 60%. There are different curves depending on the percentage of fines existing in the sand. However, it is very common to use the curve that refers to less than 5% of fines and make a correction on the SPT measurement to get the value that corresponds to clean sand. In this case, since the sand is clean no such correction is needed.

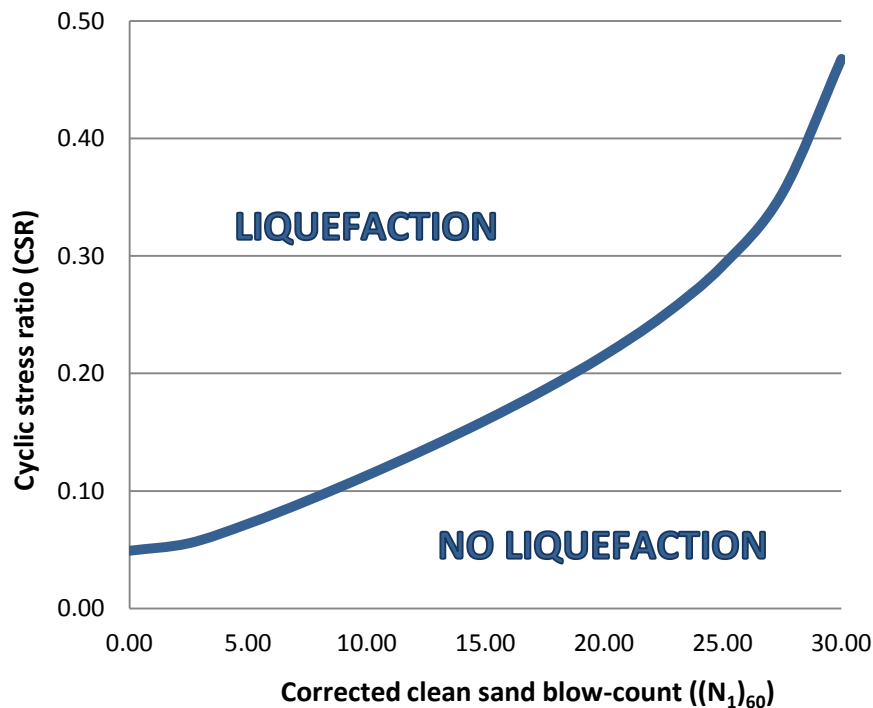
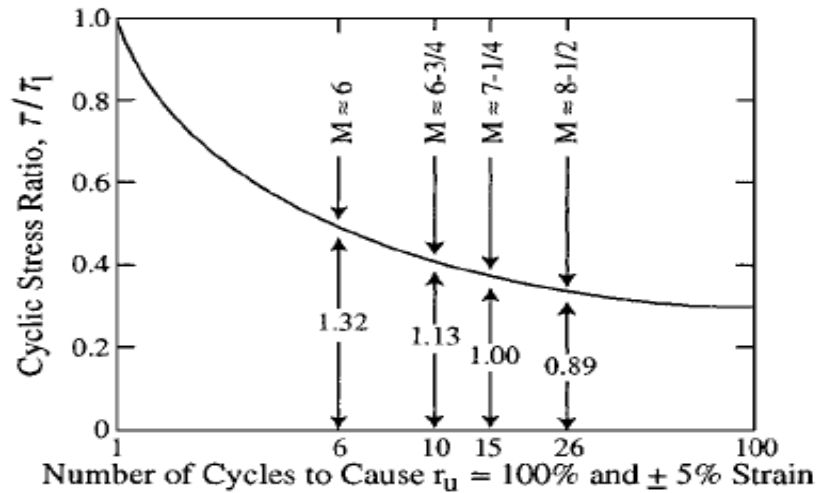


Figure 3.9: Cyclic strength curve (Seed et al, 1985)

Due to the limited database from which the initial curve was developed, it refers only to earthquakes of magnitude  $M_w=7.5$ . For other magnitudes a correction factor needs to be applied. Seed and Idriss (1982) have suggested values for the correction factor based on an average number of loading cycles for various earthquake magnitudes and laboratory test results. In Figure 3.10 a representative curve by Seed and Idriss is shown. This curve determines the number of cycles needed to reach liquefaction at a certain cyclic stress ratio (CSR) and the earthquake magnitude that corresponds to this number of cycles.



**Figure 3.10: Representative relationship between CSR and number of cycles to cause liquefaction (Seed et al, 1985)**

From this figure a magnitude 7.5 earthquake corresponds to 15 uniform loading cycles. So to reproduce the cyclic strength curve, the DSS tests in PLAXIS will be performed with variable  $(N_1)_{60}$  values to determine at which CSR each of these sands liquefies at 15 loading cycles. The acquired CSR will be the cyclic resistance ratio (CRR) of the sand for a  $M_w=7.5$  earthquake, which is comparable with the empirical curve. For the simulations with UBC3D-PLM, the onset of liquefaction was assumed at 85% pore pressure ratio. This is considered a reasonable assumption, because the comparison is done with empirical observations of liquefaction and such a ratio leads to an important loss of the shear strength of the soil which would lead to significant displacements in the field.

It was found after several tests that the value of the post liquefaction factor does not affect the onset of liquefaction in loose soils. Using the initial correlations from Beaty and Byrne (2011) and only changing the densification factor to 0.45 and the post liquefaction factor to 0.02 a good approximation of the post liquefaction curve can be achieved. Because the empirical curves have been produced from data provided by case studies, it was considered preferable to calibrate the model so that the acquired fitting is better for  $K_0=0.5$  because in sand, initial isotropic loading is not a reasonable assumption for field conditions. After the NCEER/NSF workshop several adjustments were suggested and other researchers have proposed different versions for the curve. In Figure 3.11 the cyclic strength curves acquired by DSS tests in PLAXIS is plotted against the most commonly used empirical curves by Seed et al 1985, Idriss and Boulanger 2003, Cetin et al 2004. The cyclic strength curve for  $K_0=0.5$  gives cyclic resistance ratios within the required values as predicted by the theoretical curves, while for  $K_0=1.0$  for very loose soils ( $(N_1)_{60} < 10$ ) the resistance is under-predicted and for a range of densities between  $17 < (N_1)_{60} < 27$  it is over-predicted.

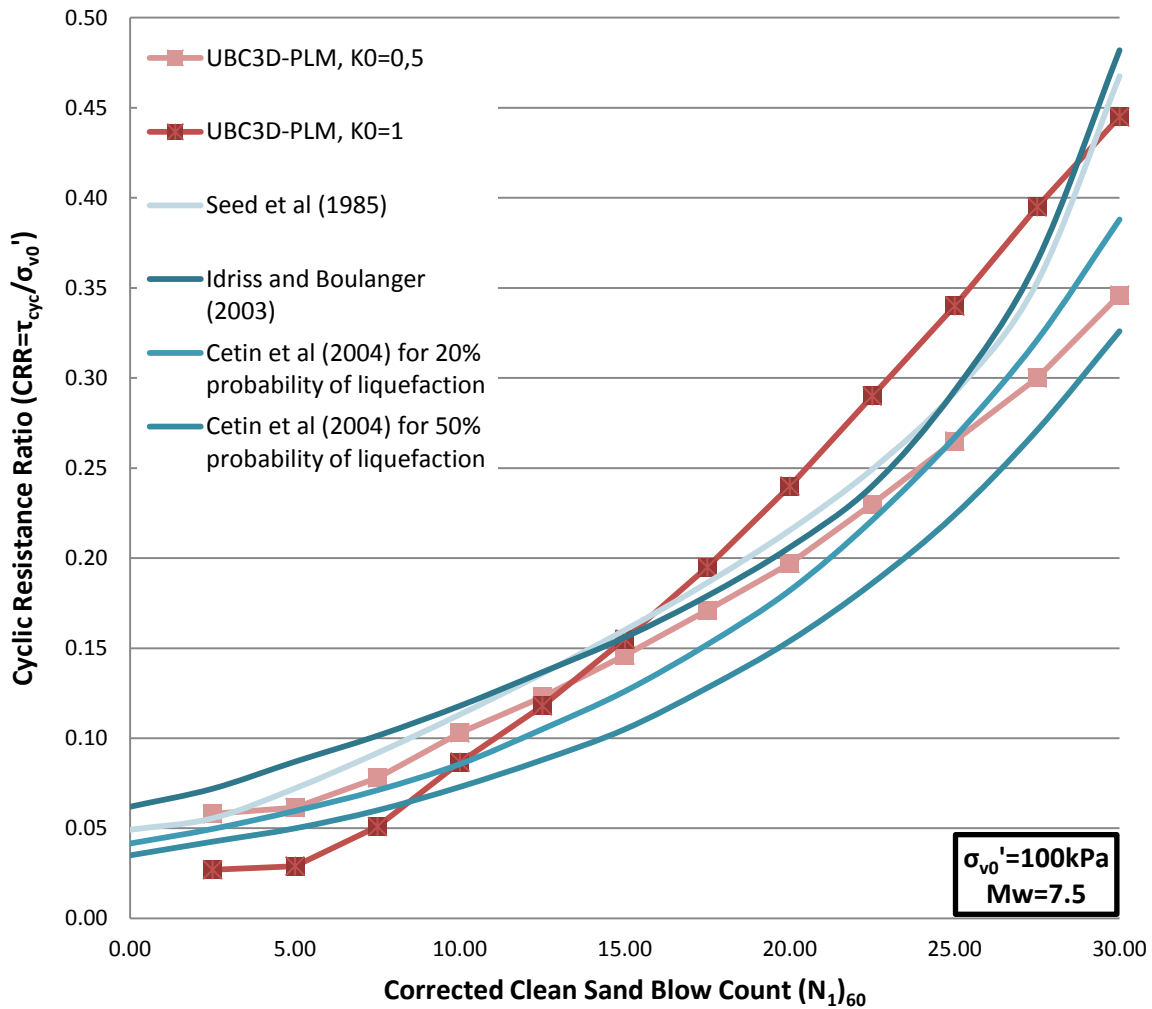


Figure 3.11: Cyclic strength curve from UBC3D-PLM in comparison with empirical curves

### 3.4 Material properties selection

After the satisfactory reproduction of the cyclic strength curve using the suggested correlations, it can be assumed that at least for this type of sand they offer a suitable calibration for use in the model. This calibration started with the soil tests presented in paragraph 3.2, under an initial assumption for the clean sand SPT blow-count.

Now that the calibration is done it is time to reconsider this initial assumption and try to reproduce the tests, for the dense and the loose samples, with different values of  $(N_1)_{60}$ . The final values of  $(N_1)_{60}$  that were found to fit the laboratory tests the best were:  $(N_1)_{60}=6.5$  for  $Dr=40\%$  and  $(N_1)_{60}=24.5$  for  $Dr=80\%$ . The results of the rate of pore pressure generation are shown in Figure 3.12 and Figure 3.13. If these results are compared with the initial tests shown in Figure 3.3 to Figure 3.8, it is apparent that a better fit is achieved.

Looking back to equation 3.7, the new calibration leads to a  $C_d$  value of  $\approx 40$  which is within the expected range. The parameters that were used are shown in Table 3-4.

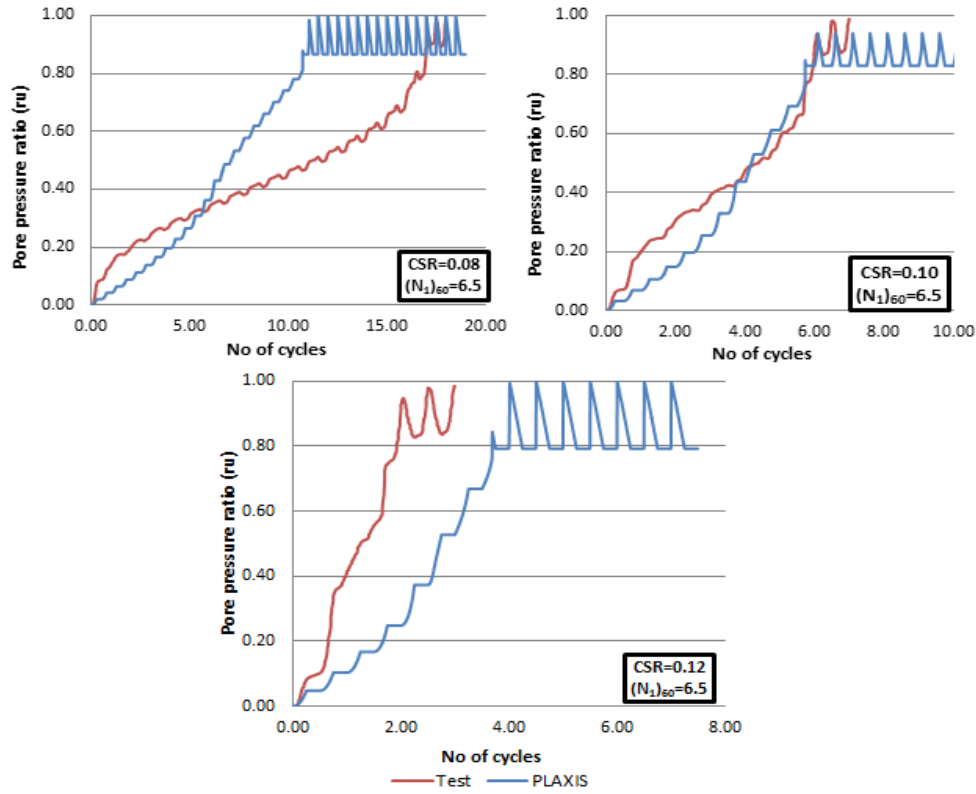


Figure 3.12: Rate of pore pressure generation for different cyclic stress ratios at  $Dr=40\%$

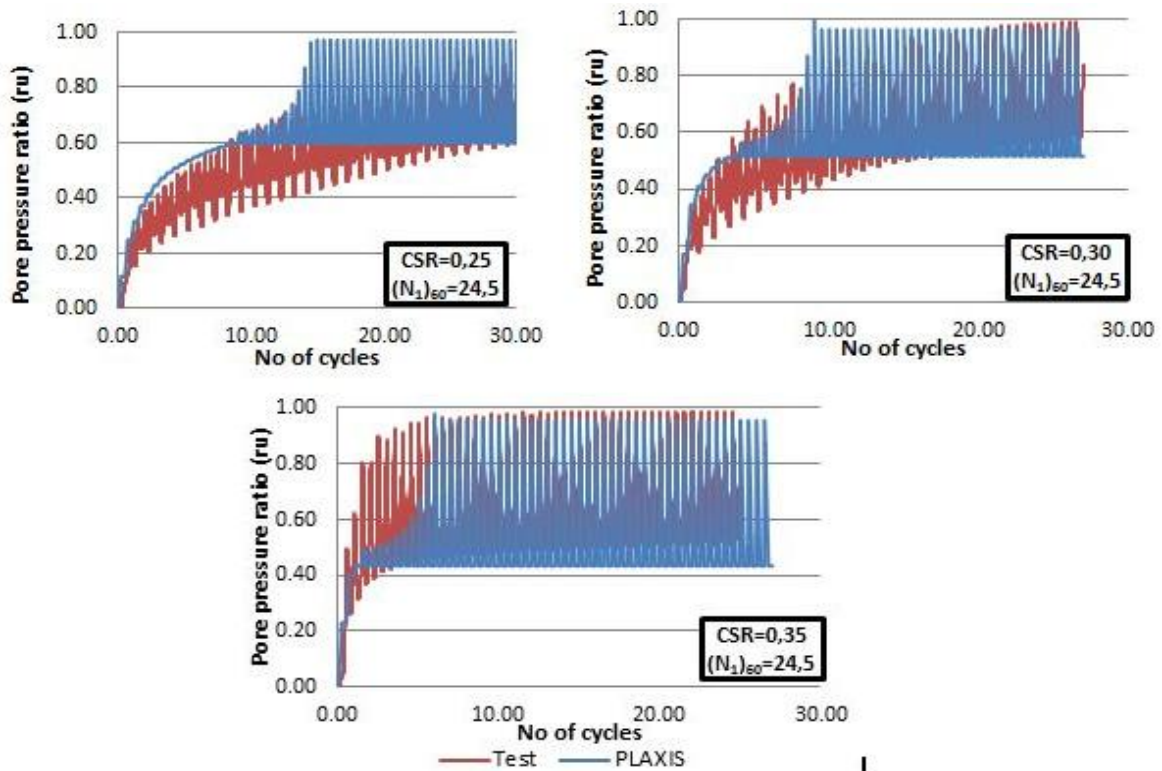


Figure 3.13: Rate of pore pressure generation for different cyclic stress ratios at  $Dr=80\%$

Model Parameters	Loose (Dr=40%)	Dense (Dr=80%)
$(N_1)_{60}$	6.50	24.50
$\phi_{cv}$ (°)	33.00	33.00
$\phi_p$ (°)	33.65	37.35
$k_g^e$	809.45	1259.2
$k_b^e$	566.61	881.4
$k_g^p$	202.60	2387.4
$R_f$	0.83	0.68
$fac_{hard}$	0.45	0.45
$fac_{post}$	0.02	0.02

**Table 3-4: Selected parameters for UBC3D-PLM for the DSS laboratory tests**

### 3.5 Critical parameters and their effect on soil tests

The parameters that affect the onset of liquefaction were described in the previous chapter and the most important ones are summarized below:

- the state of the sand ( $D_r$  and  $\sigma_{v0}'$ );
- the lateral earth pressure coefficient at rest ( $K_0$ );
- the static shear stress ratio ( $\alpha = \tau_{stat} / \sigma_{v0}'$ ).

For these parameters undrained cyclic DSS tests have been performed in PLAXIS and the results have been compared with theoretical and empirical solutions to evaluate their effect on the model performance. In addition to these parameters, an assessment of the damping properties of the model is done compared to empirical solutions for sand, because its effect is considered critical for the project.

#### 3.5.1 The effect of state

The state of the sand is determined by its relative density ( $D_r$ ) and the stress conditions as expressed by the vertical effective stress ( $\sigma_{v0}'$ ). The effect of the relative density can be shown by the cyclic strength curve if the correlation between  $(N_1)_{60}$  and  $D_r$  is used (equation 3.7). The occurring graph is shown in Figure 3.14. It is shown from the plot that as the relative density increases the cyclic resistance at a certain overburden stress also increases in an increasing rate.

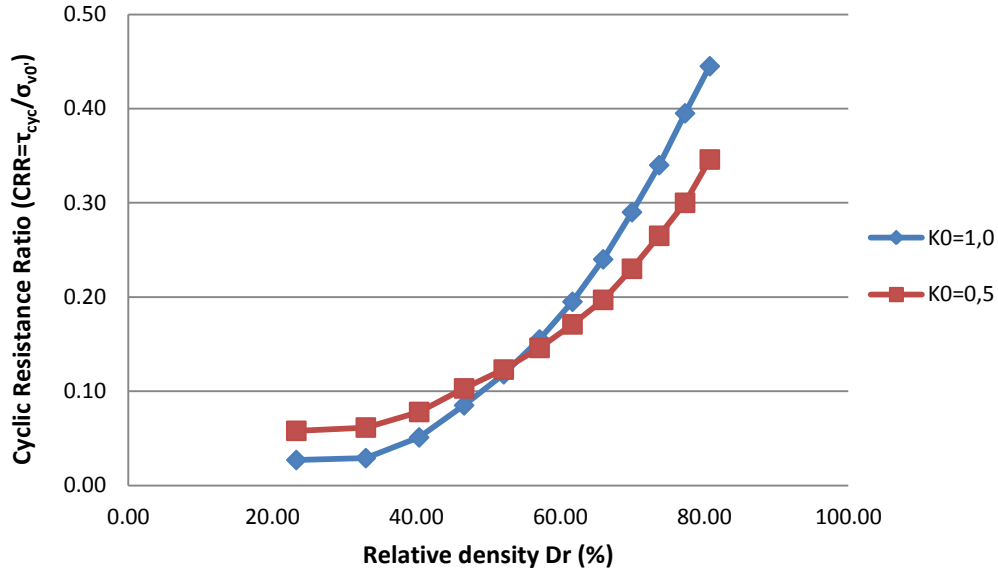


**Figure 3.14: Cyclic resistance ratio versus relative density for K0=1,0 and 0,5 from UBC3D-PLM**

It was mentioned before that a reference stress of 100kPa (1atm) is used. Obviously the stress dependent soil properties are not linearly connected to the stress level. The general observation is that the cyclic resistance ratio (CRR) of the soil decreases with increasing initial vertical effective stress. For this reason to make an assessment of the liquefaction resistance at different overburden stresses, in the simplified empirical procedure, a correction factor  $K_{\sigma}$  is used as initially introduced by Seed (1983) and is defined as:

$$K_{\sigma} = \frac{CRR_{\sigma_{vc}'}}{CRR_{\sigma_{vc}'=1}} \quad (3.8)$$

where  $CRR_{\sigma_{vc}'}$  is the cyclic resistance ratio at the given vertical effective stress and  $CRR_{\sigma_{vc}'=1}$  at the reference vertical effective stress of 1atm.

There are several different suggestions for suitable values of  $K_{\sigma}$ , based mainly on laboratory tests, but also on theoretical considerations and regression against field case histories. There is a large scatter in the suggested values by different researchers, which can be explained partly by the differences in cyclic resistance ratio of reconstituted samples and samples acquired in the field through different techniques.

The  $K_{\sigma}$  relation that is used in this case is from Boulanger (2003b):

$$K_{\sigma} = 1 - C_{\sigma} \ln \left( \frac{\sigma_{vc}'}{P_a} \right) \leq 1.1 \quad (3.9)$$

where  $C_{\sigma}$  is a coefficient that can be expressed in terms of relative density or penetration resistance normalized at the reference stress ( $P_a$ ).

Since for all the previous correlations the SPT penetration resistance is used, the value of  $C_\sigma$  will be also calculated from the following equation:

$$C_\sigma = \frac{1}{18.9 - 2.55\sqrt{(N_1)_{60}}} \leq 0.3 \quad (3.10)$$

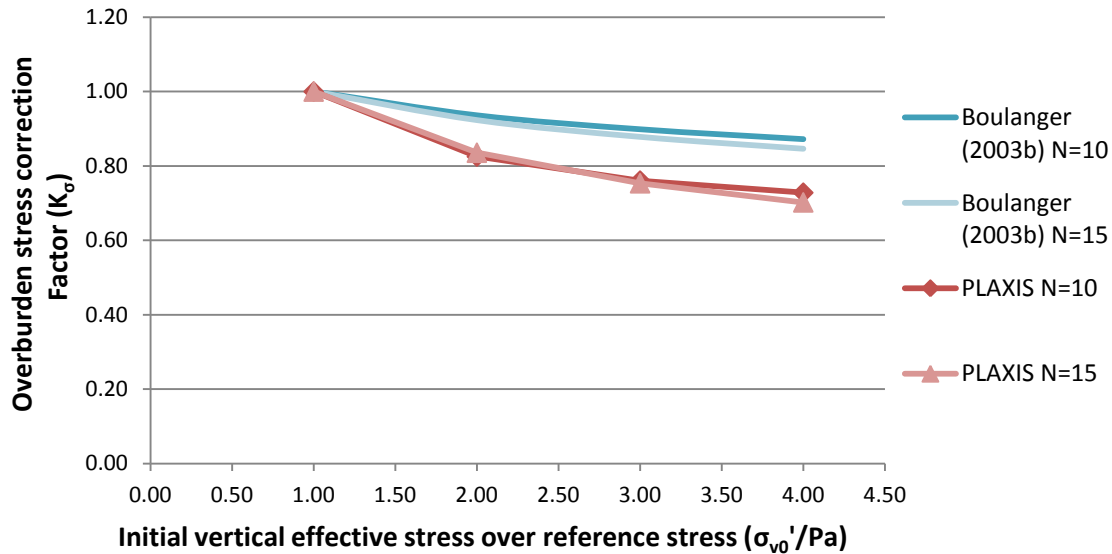


**Figure 3.15: Overburden stress correction factor at different stress levels from UBC3D-PLM compared with theoretical values from Boulanger (2003b)**

To determine the effect of the overburden stress in UBC3D-PLM, undrained cyclic DSS tests were performed at different stress levels. In all tests the assumption of a  $K_0=0.5$  was kept. The tests were performed at two different SPT penetration values  $(N_1)_{60} = 10$  ( $Dr \approx 46\%$ ) and  $(N_1)_{60} = 15$  ( $Dr \approx 57\%$ ). In Figure 3.15 the  $K_0$  values at different stress levels are plotted against the theoretical values by Boulanger. It is obvious from the results that with the previously described calibration of the model the decrease of CRR with  $\sigma_{v0}'$  is significantly larger in the model than in the theoretical solution. This could lead to an underestimation of the strength of the soil at higher overburden pressures. However, this problem can be solved by increasing accordingly the densification factor ( $fac_{hard}$ ) as the overburden stress increases. In Figure 3.16 suitable values for the  $fac_{hard}$  parameter are shown to achieve liquefaction at 15 cycles at the CSR suggested by the theoretical  $K_0$  values.

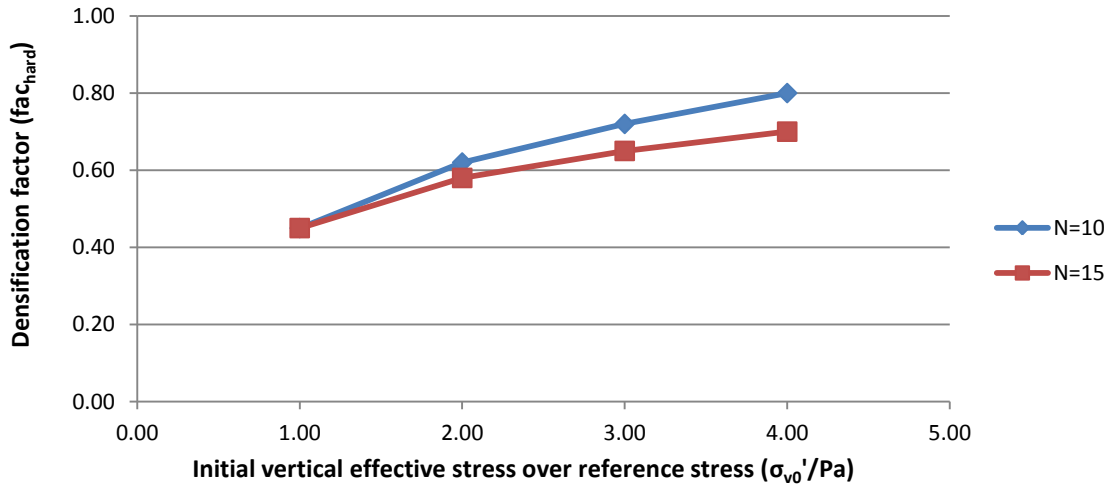


Figure 3.16: Suggested densification factors for initial effective stress over 100kPa for  $(N_1)_{60}$  equal to 10 and 15

### 3.5.2 Effect of $K_0$

As it was described in Chapter 2 the effect of the lateral earth pressure coefficient at rest is significant and it is usually expressed by the equation (2.1) by Ishihara. From this equation it is shown that the cyclic resistance ratio decreases with decreasing  $K_0$  at all densities. This is a reasonable observation, since at the same relative density and overburden stress, if the confining stress increases it becomes more difficult for the soil to liquefy. In this calibration of UBC3D-PLM this trend is not followed. From the cyclic strength curves obtained by UBC3D-PLM for  $K_0=1.0$  and  $K_0=0.5$ , the CRR for  $K_0=1.0$  is smaller than for  $K_0=0.5$  for loose sands ( $(N_1)_{60} < 10$ ) and larger in dense sands. The curves are shown again in Figure 3.17 along with the CRR over  $(N_1)_{60}$  values that would be acquired for  $K_0=0.5$  from equation (2.1). For comparison as initial CRR values for isotropic conditions the curve from PLAXIS for  $K_0=1.0$  was assumed.

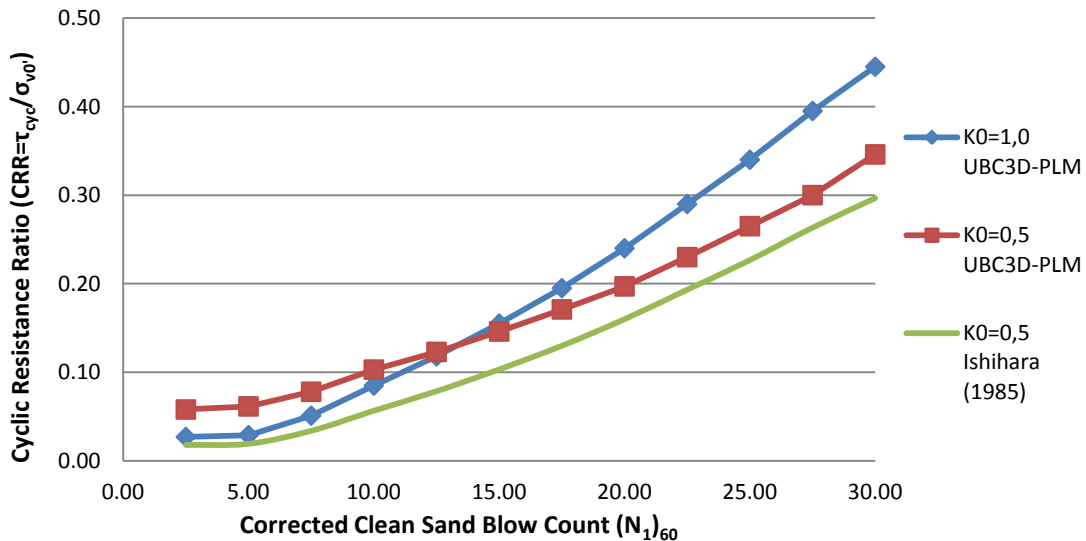


Figure 3.17: Predicted cyclic resistance ratio for  $K_0=0,5$  from UBC3D-PLM and Ishihara (1985)

### 3.5.3 Material damping

The dissipation of energy in soils and structures is connected with several mechanisms such as friction, heat generation and plastic yielding. However, the way these mechanisms operate is not sufficiently understood, so they cannot be modelled explicitly. For this reason, the effect of these mechanisms is usually modelled using convenient damping mechanisms. In the stress-strain curve of a cyclically loaded soil, the dissipated energy is shown by the hysteretic loop ( $\Delta w$ ). While the maximum stored energy ( $W$ ) is defined as the area of the triangle created between the maximum shear stress and strain and the beginning of the axes (see Figure 3.18). The energy dissipation is quantified by the damping ratio ( $\xi$ ) which is defined as:

$$\xi = \frac{\Delta w}{4\pi W} \quad (3.11)$$

and it can be calculated graphically from the hysteresis loop, as shown in Figure 3.18.

Generally the damping ratio at shear strains larger than  $10^{-5}$  is not constant and depends on the shear strain. For sands Idriss (1999) has suggested an empirical curve which determines the damping ratio of sand at different shear strain levels. To evaluate the damping produced by UBC3D-PLM strain controlled drained cyclic DSS tests are performed in PLAXIS at different maximum shear strains. The sand is subjected to four loading cycles and the damping ratio is calculated at the fourth cycle with the previously described process. In Figure 3.19 the hysteretic loops produced by UBC3D-PLM from cyclic drained DSS tests in PLAXIS at a maximum strain of  $10^{-3}$  are plotted. The results from these analyses are shown in Figure 3.20 against the theoretical Seed and Idriss curve. From this curve, it is apparent that the model shows an over-damped response compared to real soil behaviour. This behaviour was expected since the unloading in UBC3D-PLM is elastic. Moreover, the curves produced by UBC3D-PLM do not show significant variations for different  $K_0$  values. Differences occur only at strains smaller than  $10^{-3}$ . For the lower density ( $(N_1)_{60}=10$ ) the damping ratio is larger at strains smaller than  $10^{-2}$  and smaller for larger strains, compared to the denser sand.

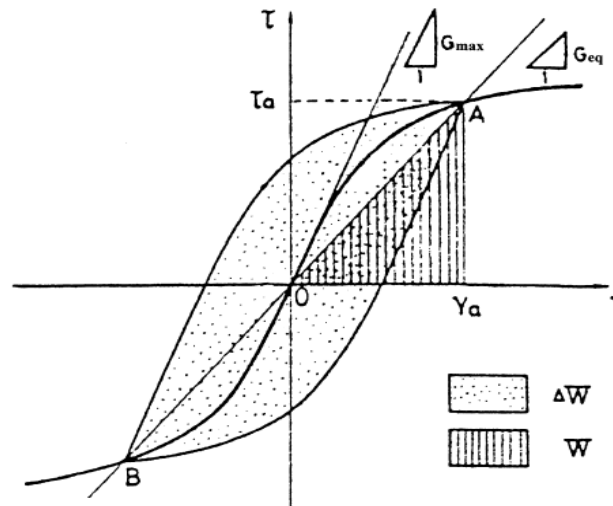


Figure 3.18: Graphical evaluation of damping ratio from measured hysteresis loop

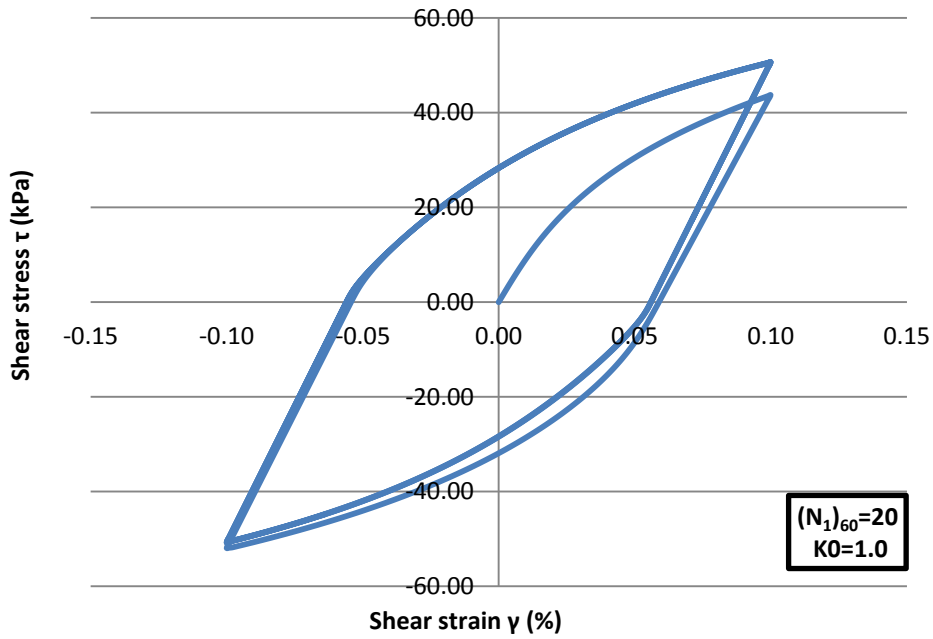


Figure 3.19: Hysteretic loop from simulation of strain controlled DSS test with UBC3D-PLM

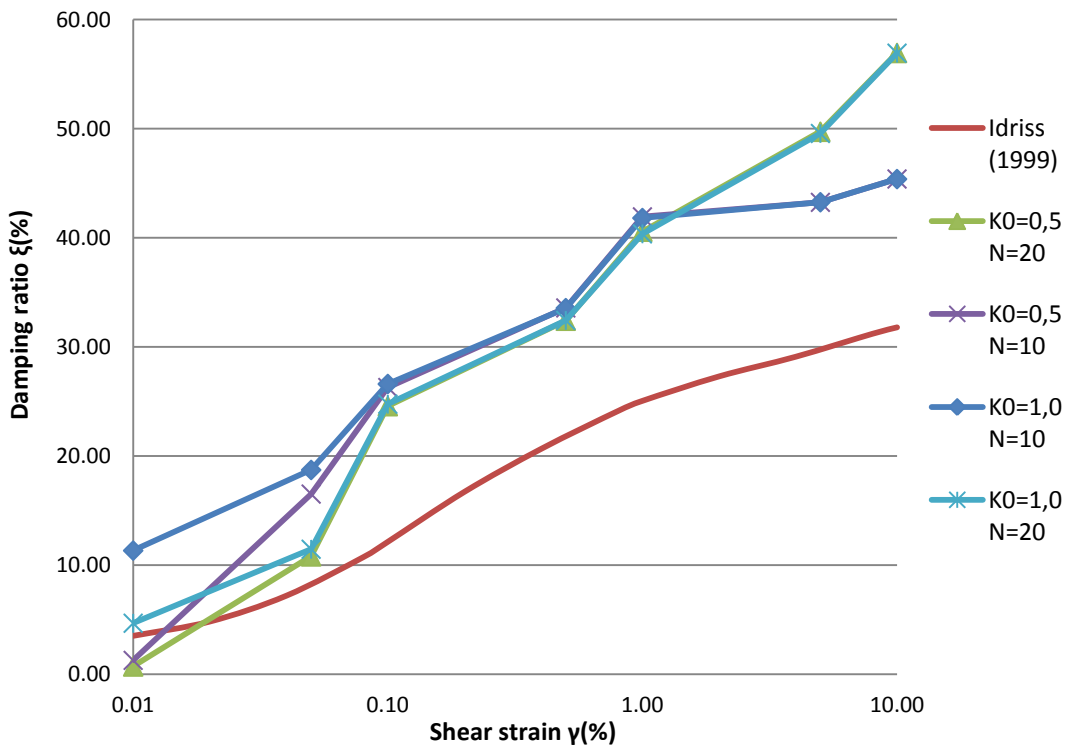


Figure 3.20: Damping ratio at different levels of shear strain from UBC3D-PLM compared to theoretical curve for sand by Idriss (1999)

### 3.5.4 Static shear stress effect

In sloping ground the initial stress conditions include a static shear stress on the horizontal plane. As it was mentioned earlier this initial static shear affects the cyclic resistance of the soil. It has been observed mainly from laboratory testing that for dense sand the increase of static shear stress ratio ( $\alpha$ ) leads to larger cyclic resistance ratio (CRR) while the opposite happens for loose sand. Seed (1983) introduced the correction factor  $K_\alpha$  to adjust CRR for the effect of static shear. Idriss and Boulanger (2003a) derived expressions, which connect  $K_\alpha$  with the state of the soil, to approximate data from simple shear tests. These relations are the following:

$$K_\alpha = a + b \exp\left(\frac{-\xi_R}{c}\right) \quad (3.12)$$

$$a = 1267 + 636\alpha^2 - 634 \exp(\alpha) - 632 \exp(-\alpha) \quad (3.13)$$

$$b = \exp(-1.11 + 12.3\alpha^2 + 1.31 \ln(\alpha + 0.0001)) \quad (3.14)$$

$$c = 0.138 + 0.126\alpha + 2.52\alpha^3 \quad (3.15)$$

where  $\alpha$  is the static shear stress ratio and  $\xi_R$  is the relative state index which was introduced by Idriss and Boulanger as a simplified state parameter and can be derived from SPT tests according to the following equation:

$$\xi_R = \frac{1}{Q - \ln\left(\frac{100(1 + 2K_0)\sigma'_{vc}}{3Pa}\right)} - \sqrt{\frac{(N_1)_{60}}{46}} \quad (3.16)$$

where Q is a parameter depending on the fabric of sand and for quartz and feldspar sands such as Fraser River Sand Q takes a value of 10.

To determine the effect of static shear in UBC3D-PLM for the given calibration of parameters cyclic DSS tests with initial static shear will be simulated in the soil test facility of PLAXIS. These tests will be used to determine the value of  $K_\alpha$  at different values of static stress ratio and to reproduce DSS tests with static shear performed in UBC.

In Figure 3.21 and Figure 3.22 the values of  $K_\alpha$  at different static shear stress levels are presented at  $K_0$  values of 1,0 and 0,45 respectively. It is obvious from the plots that UBC3D-PLM underestimates significantly the cyclic resistance ratio of the soil as static shear stresses increase. It becomes apparent that the current calibration of UBC3D-PLM cannot capture the

increasing CRR of medium to dense sands as the static shear stress ratio increases. In this case also liquefaction was defined as an increase in the pore pressure ratio up to 85%.

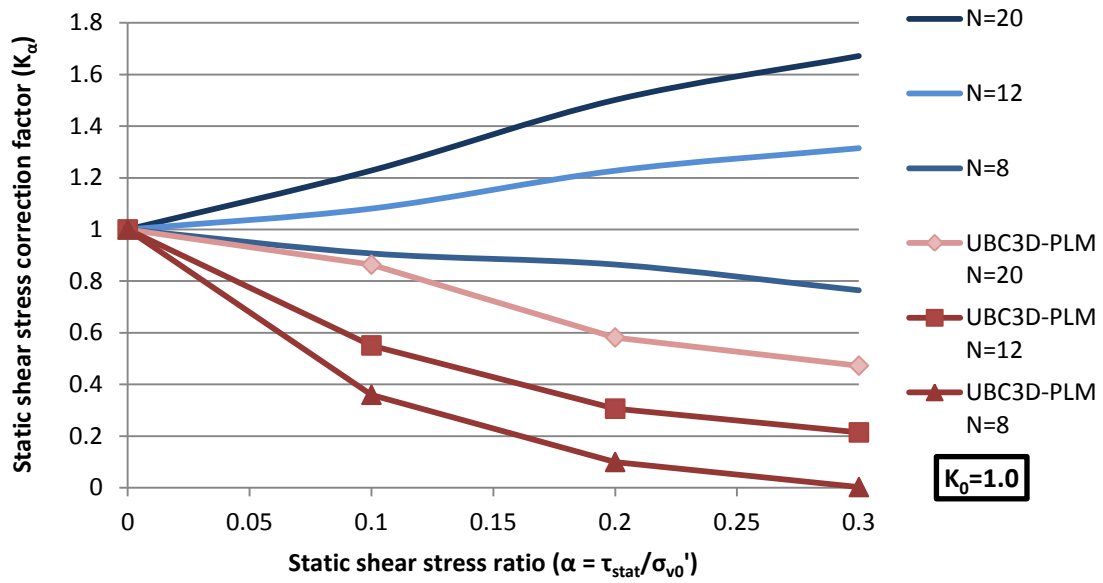


Figure 3.21: Static shear correction factor at different levels of static shear stress ratio with  $K_0=1,0$  from UBC3D-PLM in comparison with Idriss and Boulanger (2003a)

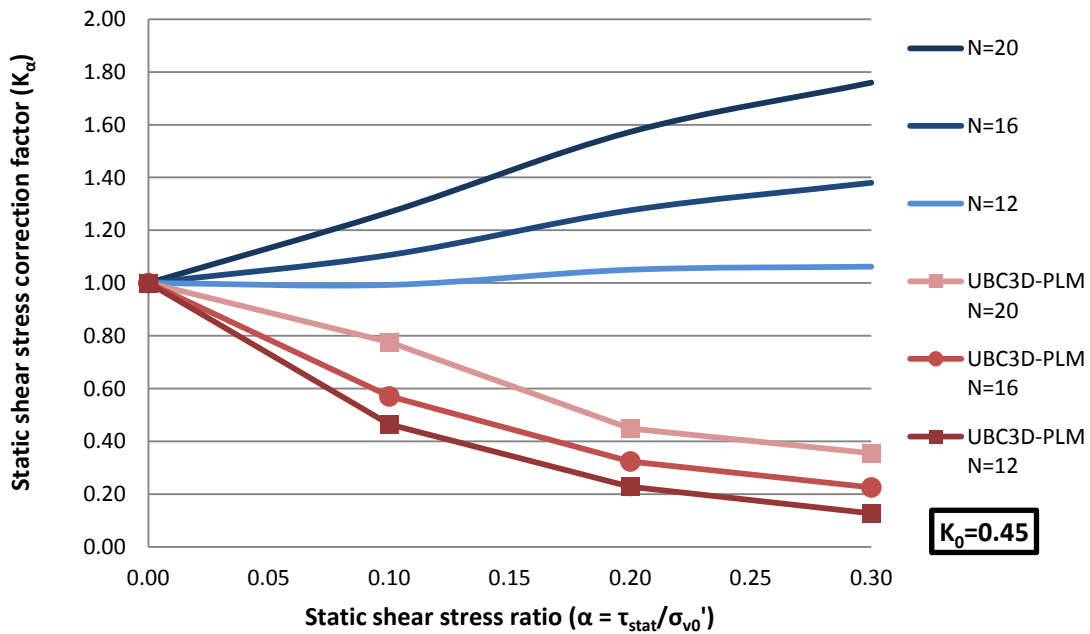
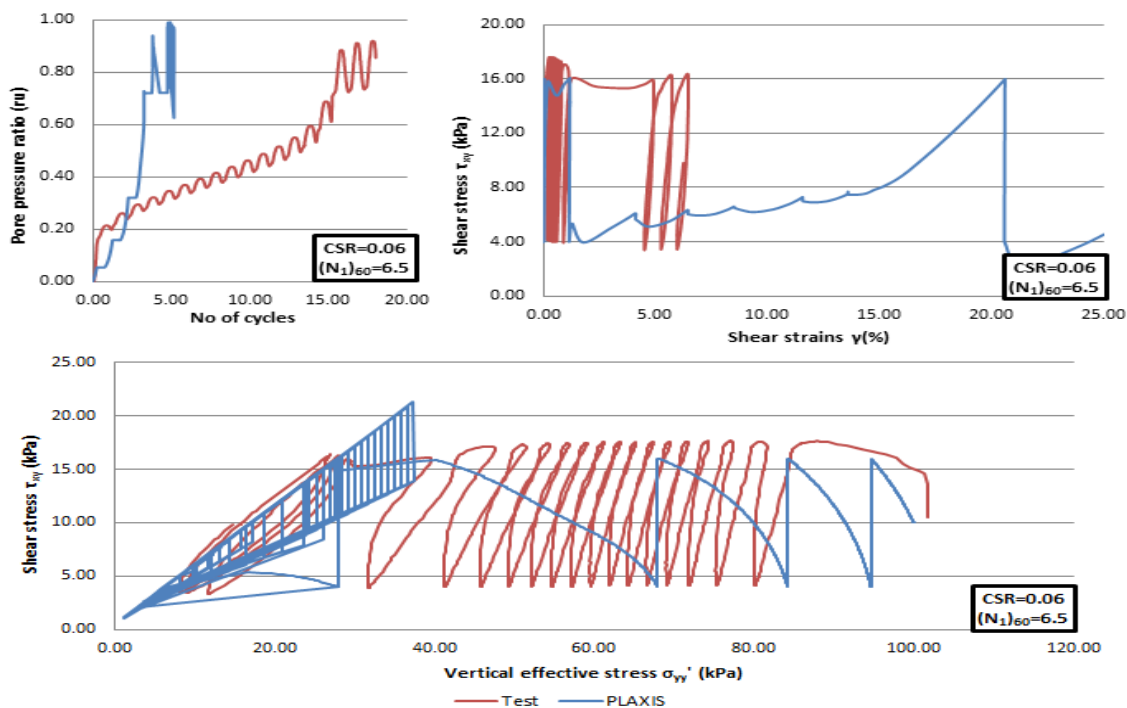


Figure 3.22: Static shear correction factor at different levels of static shear stress ratio with  $K_0=0,45$  from UBC3D-PLM in comparison with Idriss and Boulanger (2003a)

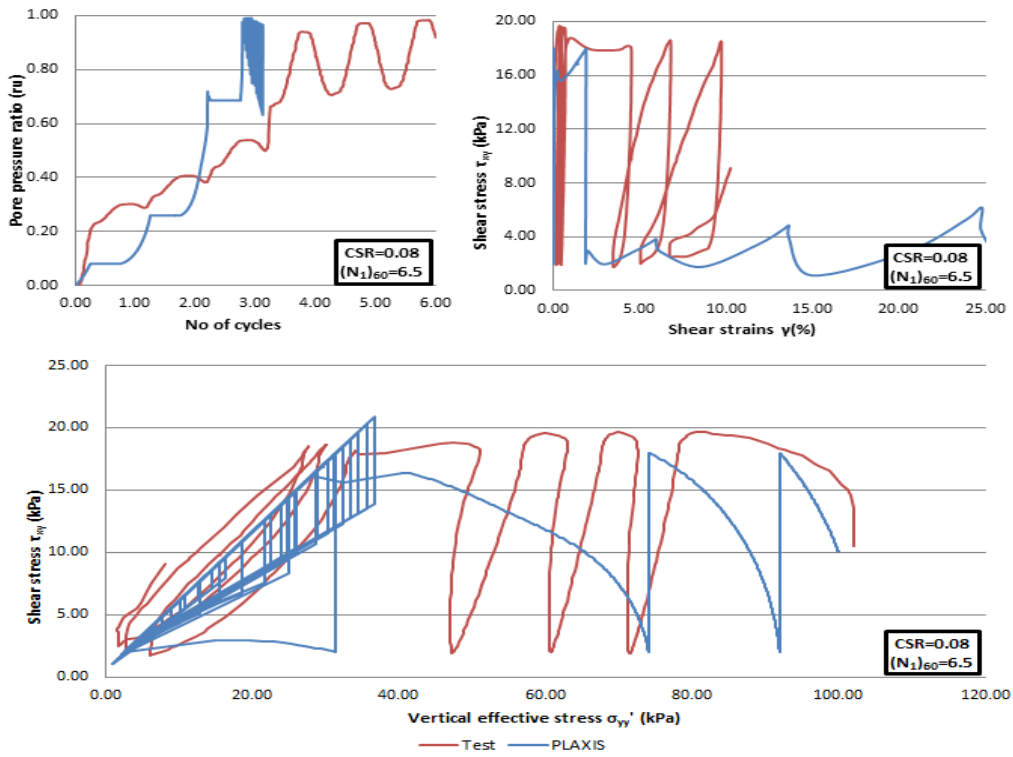
Generally, in the case there is an initial static shear the behaviour of the soil changes significantly, since now liquefaction does not manifest as cyclic mobility but causes what has been described earlier (section 2.7) as flow failure. Liquefaction under such conditions does not lead to zero effective stress since failure occurs earlier by the decrease of shear strength up to the point that the static shear exceeds it. This type of liquefaction leads to much larger shear strains which can be observed in the tests in Figure 3.23. In this figure it can be seen that the UBC3D-PLM leads to even larger strains than the ones produced by the laboratory tests and that liquefaction occurs earlier than in the tests, except for the case of  $CSR=0.10$  where the laboratory specimen liquefies earlier. This was expected considering that the model is not capable of reproducing the theoretical values of  $K_{\alpha}$ . Also, contrary to what happens with cyclic mobility in the model, in this case although the pore pressures stop increasing at a certain point (minimum G), the shear strains keep increasing at every cycle.

Moreover, from the same Figure 3.23 it can be observed that, especially for lower CSR compared to the initial static shear, during the stiffness degradation after the peak yield surface is reached certain numerical problems occur which lead to this irregular shape of the stress path and the pore pressure generation plots.

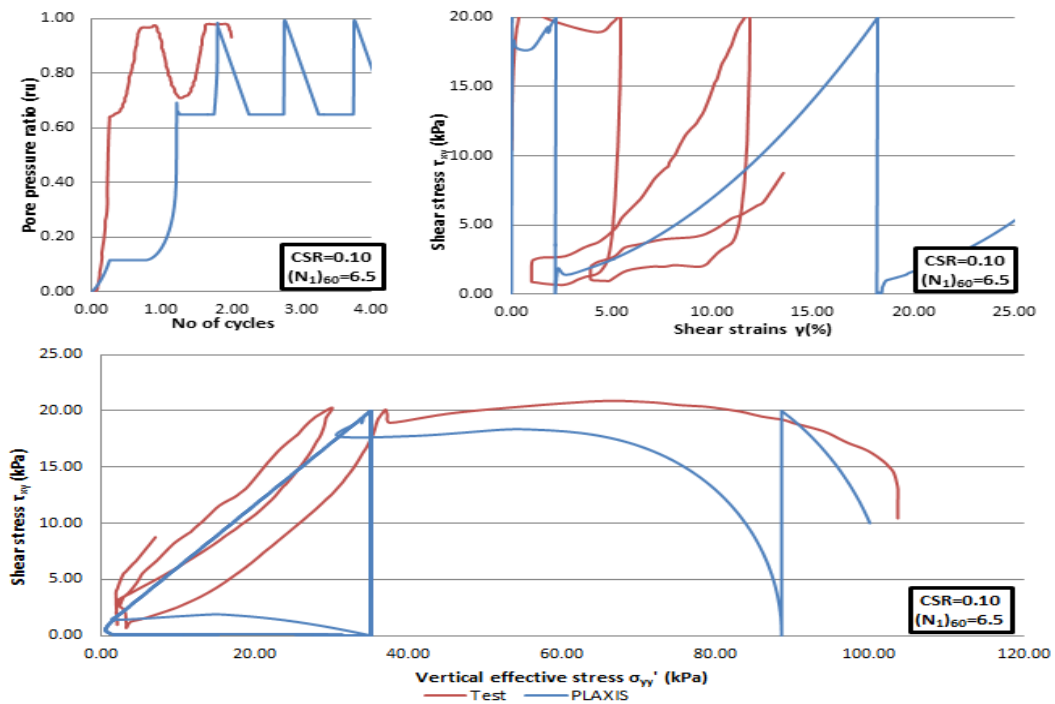
Since for the stability of slopes and embankments the effect of static shear is very significant, an effort to compensate for this unrealistic reduction of the strength was made, through changes in the calibration. Initially an attempt to select a different calibration for the shear modulus and the densification factor for all densities as made. However, since the decrease in strength is so significant and the number of available tests is small, it proved difficult to achieve a general calibration. This was mainly due to the fact that the plastic shear modulus number and/or the densification factor had to be increased very much (sometimes by 300%).



a) DSS test at  $\alpha=0.10$  and  $CSR=0.06$



b) DSS test at  $\alpha=0.10$  and CSR=0.08



c) DSS test at  $\alpha=0.10$  and CSR=0.10

Figure 3.23: Rate of pore pressure generation, stress strain behavior and stress paths from cyclic DSS tests and PLAXIS at  $\alpha=0.1$ , CSR=0.06, 0.08, 0.10

Nonetheless, by increasing only the densification factor to 1.0 a reasonable agreement with the DSS tests can be achieved. In addition to the change in the densification factor, to avoid the aforementioned numerical problems the post liquefaction factor was also set to 1.0. Since, the soil at hand is loose ( $Dr=40\%$ ) and there is an initial static shear it is expected that the increase in the pore pressure ratio before the peak surface is reached is enough to cause flow failure without any further stiffness degradation. For this reason the increase in the  $fac_{post}$  is considered reasonable. The rest of the parameters, that were used, are the same that were optimized previously to fit the DSS tests without static shear (section 3.4). The rate of pore pressure generation and the stress paths of the new simulations of DSS tests in PLAXIS are presented in Figure 3.24 and Figure 3.25, compared to the corresponding laboratory tests.

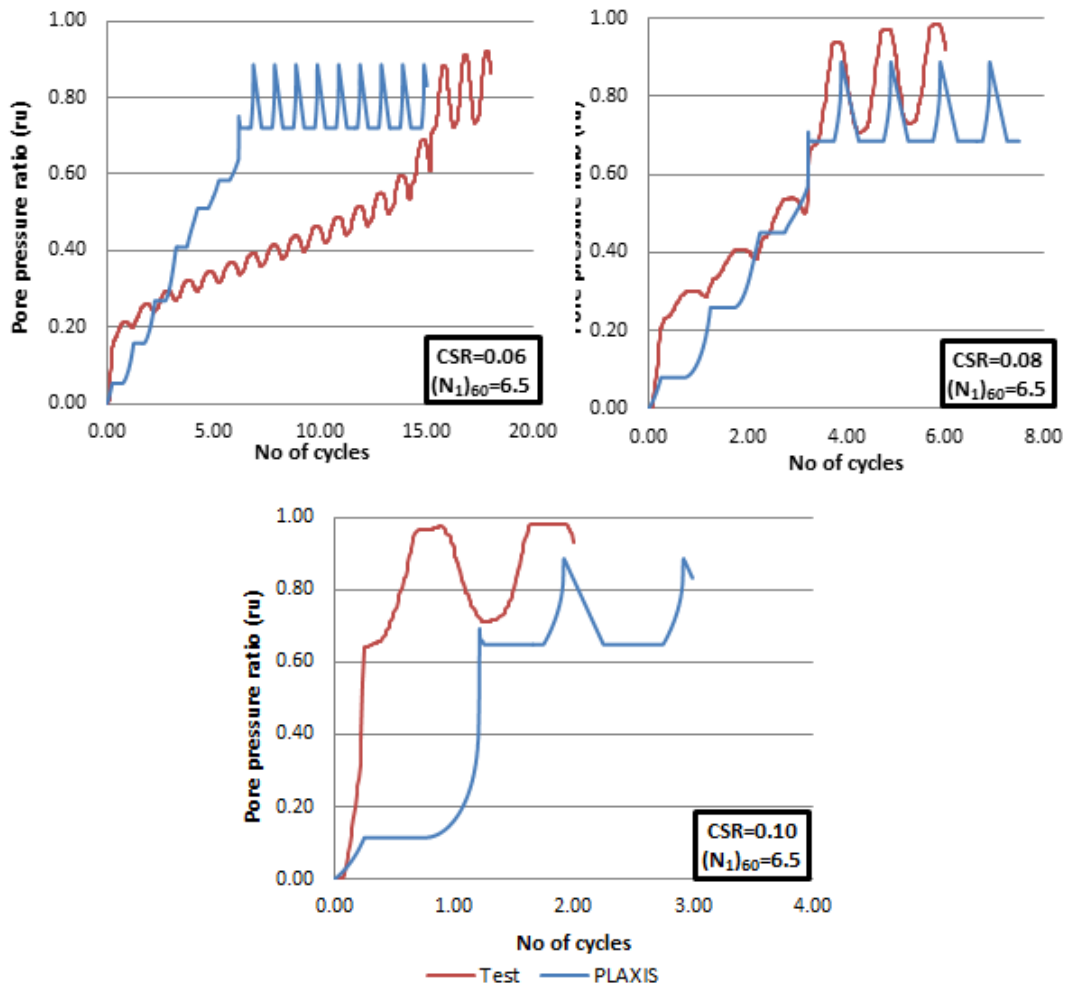


Figure 3.24: Rate of pore pressure generation from cyclic DSS tests and PLAXIS at  $\alpha=0.1$ , CSR=0.06, 0.08 0.10 and  $fac_{hard}=1.0$ ,  $fac_{post}=1.0$

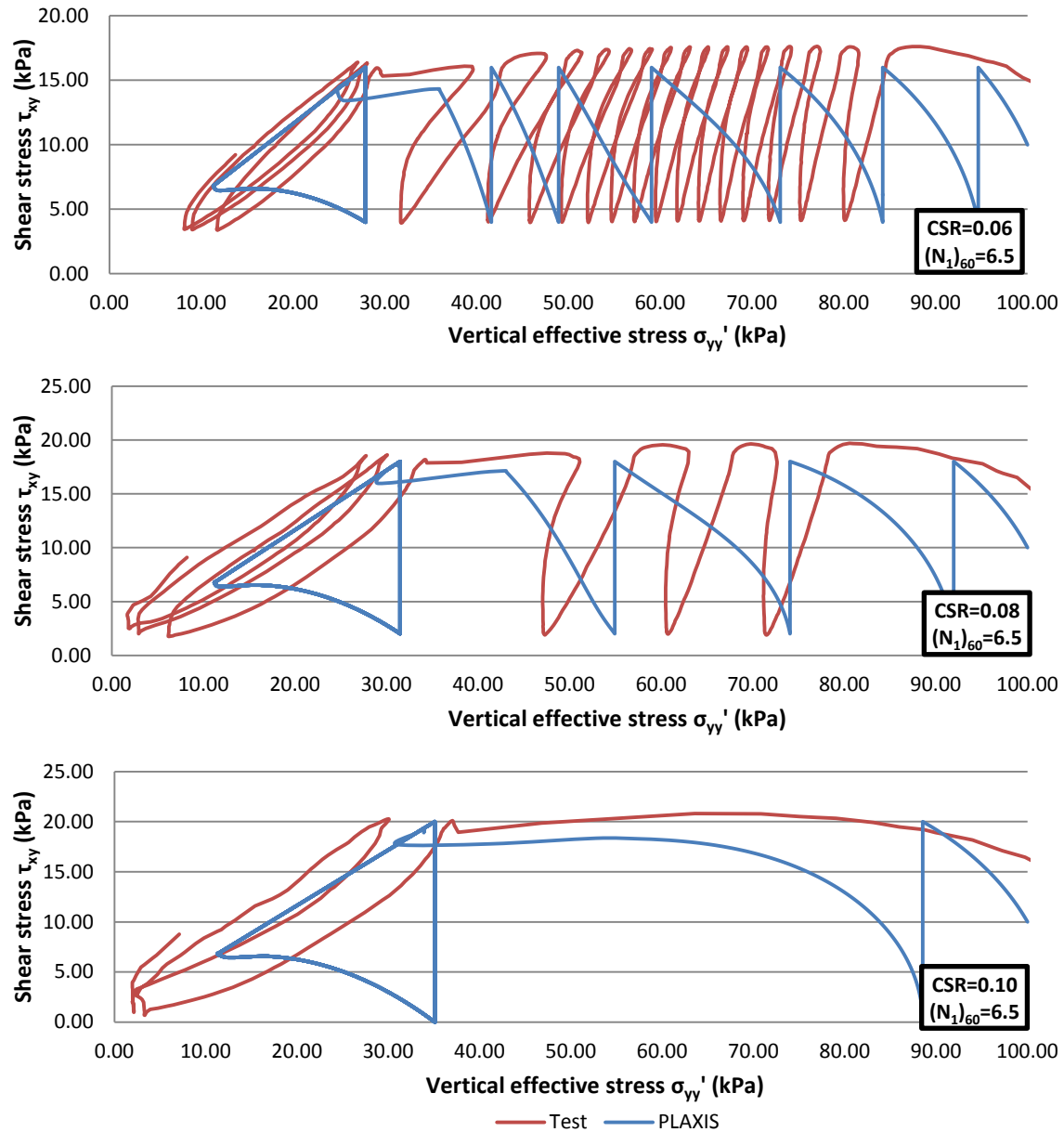


Figure 3.25: Stress paths from cyclic DSS tests and PLAXIS at  $\alpha=0.1$ ,  $CSR=0.06, 0.08, 0.10$  and  $fac_{hard}=1.0, fac_{post}=1.0$ .

### 3.6 Summary and conclusions

In this chapter an attempt was made to suggest an appropriate calibration of the model parameters for use in dynamic analysis of embankment dams. The correlations that were suggested for the parameters of UBCSAND have been used. The only parameters that were changed are the densification factor ( $fac_{hard}$ ) and the post liquefaction factor ( $fac_{post}$ ). With this calibration a good approximation of the empirical cyclic strength curve was achieved which suggests that the use of the model for predicting the onset of liquefaction at least for flat or lightly sloping ground is feasible.

It needs to be noted that this curve is empirical and it has been observed that it can vary significantly for different types of sand and percentages of fines content. For this reason, this calibration is valid as a general guideline but if there are available data it is advisable to revise it for the specific type and grading of sand.

Despite the good prediction of the cyclic resistance, the strains that are produced from the model after liquefaction occurs are limited. This is because the model cannot capture the post liquefaction behaviour of the soil.

Concerning the effect of the critical parameters, an evaluation of the performance of this calibration for the effects of the state of the soil, the lateral earth pressure coefficient at rest, the damping ratio and the static shear was made.

The effect of state is described by the relative density and the overburden stress. It has been shown that the model approximates well the effect of relative density on liquefaction resistance. While, for overburden stress different than the reference, to achieve a better fit it is possible to increase the densification factor accordingly.

Concerning the effect of  $K_0$  the model presents a different behaviour than expected from the empirical observations, since for loose soils it presents a larger CRR at lower confining stress under the same overburden stress.

Moreover, given this calibration to be able to simulate the undrained cyclic behaviour of the soil a very low Poisson's ratio has been used. For this reason it is preferable to avoid using the model for static calculations.

Since unloading is elastic in UBC3D-PLM, as it was expected the damping ratio in the model exceeds the empirical solution.

It has also been observed that initial static shear can lead to unrealistic decrease in the cyclic resistance of the model and also to certain numerical instabilities. Also, the shear strains that are generated are larger than in the laboratory. However it is possible to reduce this effect by increasing the densification and the post liquefaction factors to 1.0.

Despite these differences, a satisfactory match of the laboratory tests with the model prediction is achieved, especially for the determination of the onset of liquefaction through the generated pore pressures. Moreover, since now the certain limitations of the model have been observed a better interpretation of its results in a large scale problem can be done.

In the following chapter an evaluation of the performance of the model on sloping ground conditions will be done through the simulation of a centrifuge test.

## 4 CENTRIFUGE TESTS ON SLOPING GROUND

### 4.1 Centrifuge tests: scaling, geometry and boundary conditions

Centrifuge modelling allows soil structures to be subjected to simulated earthquake motion under highly controlled conditions. In the centrifuge, the high stresses that exist in the field are achieved by subjecting the soil structure to a high acceleration field. This means that field conditions can be reproduced in the centrifuge in models scaled down several times compared to the prototype. Special care needs to be given to the scaling laws that are used, since the acceleration field affects all the soil parameters and not only the dimensions, such as the grain size, drainage and consolidation time. In Table 4-1 the scaling laws that affect the experiment that is described below are presented. In this table  $a_c$  is the acceleration of the centrifuge,  $g$  is the acceleration of gravity, the parameters that have a subscript  $m$  correspond to the model scale and the ones with  $p$  correspond to the prototype. The difference that exists between the scaling of time for static and dynamic conditions can be overcome by increasing the viscosity of the fluid by  $N$ . An acceleration time history can be applied in the basis of the soil model while “in flight” to simulate the earthquake.

Scaling factor	$N=a_c/g$
Linear dimensions	$L_m=1/N L_p$
Acceleration	$\alpha_m=1/N \alpha_p$
Time (static)	$t_{sm}=1/N^2 t_{sp}$
Time (dynamic)	$t_{dm}=1/N t_{dp}$

**Table 4-1: Scaling laws of centrifuge model for earthquake loading**

The centrifuge test that will be simulated with UBC3D-PLM in PLAXIS has been performed in the centrifuge of C-CORE for the aforementioned project “Earthquake Induced Damage Mitigation from Soil Liquefaction”. The test as performed with an acceleration of 70g. The sand that was used is Fraser River sand whose properties were described in the previous chapter. The fluid used for saturation as Hydroxypropyl Methylcellulose, which has similar density, unit weight surface tension, compressibility and Newtonian behaviour as water, but its viscosity is 35 times the viscosity of water, this means that the permeability in the model will be twice the permeability of the prototype. The geometry of the test in prototype scale is shown in Figure 4.1, where P are the pore pressure transducers, A are the accelerometers and L are the linear variable differential transformers (LVDT) that measure the vertical displacements.

The model was constructed by air pluviation. Due to the spin up of the centrifuge and the increase of stresses, the soil will densify. For this reason the loose sand layer is placed at a relative density of 32% and is assumed to densify to a density of  $Dr=40\%$  at the reference stress

level (100kPa). After Park and Byrne (2004) for this centrifuge test it was assumed that only the loose layer is densifying according to equation (4.1) for Fraser River Sand.

$$D_r = D_{r0} + 0,0503 \sqrt{\left(\frac{\sigma_{v0}'}{Pa}\right)} \quad (4.1)$$

The free water level is set to 1,0m above the higher elevation of the soil.

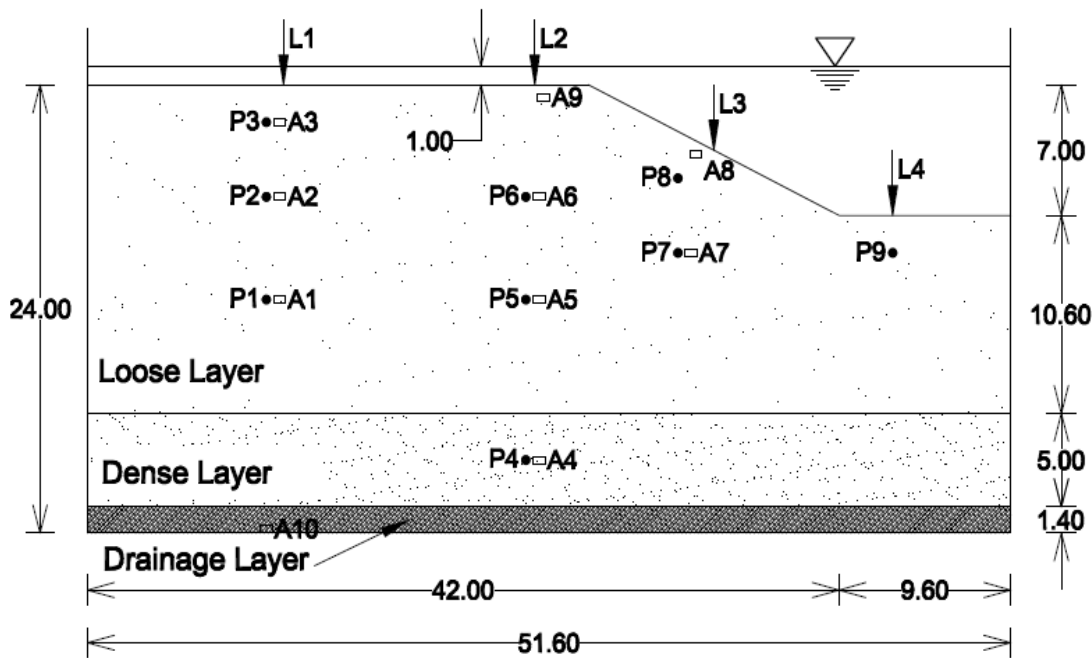


Figure 4.1: Geometry and instrumentation of centrifuge model in Prototype scale (all dimensions in m)

## 4.2 Input ground motion

The ground motion that was selected for the centrifuge test was proposed for Vancouver area and corresponds to 10% probability of occurrence in a 50-year period. This corresponds to a 475 year event and will be referred to as A475. Certain corrections and filtering of the frequencies has been done to the initial ground motion by Dr Seid-Karbasi (2003) to acquire the final acceleration time history that was used in the centrifuge. To scale the input motion for use in the centrifuge at an acceleration field of 70g, the time scale was reduced by 70 and the accelerations were increased by 70. The acceleration time history in prototype scale is shown in Figure 4.2. The peak acceleration is 0.12g and the input motion is applied in the positive direction (downslope).

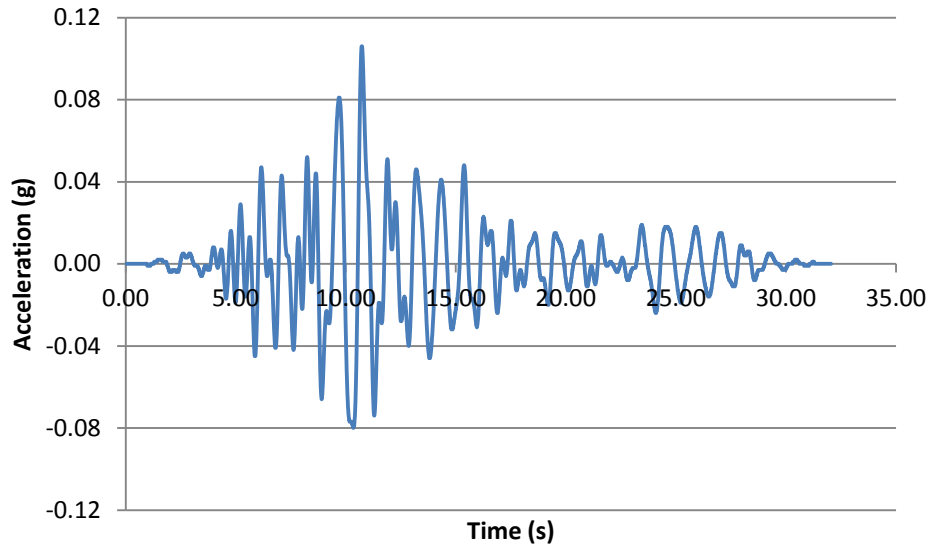


Figure 4.2: Acceleration record of A475 earthquake in prototype scale (Seid-Karbasi, 2003)

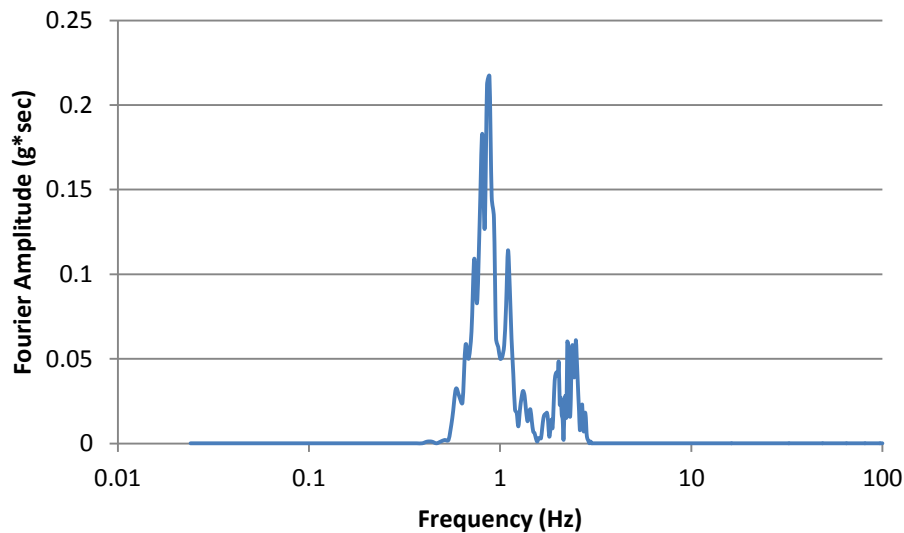


Figure 4.3: Frequency content for A475 event, Fourier Acceleration Spectrum (Seid-Karbasi, 2003)

### 4.3 Numerical modelling of centrifuge tests

For the numerical modelling of the centrifuge the constitutive model UBC3D-PLM in the finite element computer code PLAXIS was used, assuming fully undrained behaviour. This assumption is necessary since in PLAXIS it is not possible to perform a fully coupled analysis in dynamic loading conditions. For simplification reasons it is assumed that the soil layers are fully saturated ( $S_r=100\%$ ), although that does not correspond to the actual conditions of the tests where the expected degree of saturation is between 98.5 and 99.0%.

The centrifuge test is done using a rigid box. To take into account the rigidity of the box, for the static calculation the boundary conditions that are assumed are fixed displacements in both directions at the bottom boundary and on the x-direction on the left and on the right. The dynamic analysis is done assuming prescribed displacements in all the boundaries. The prescribed displacements in the x-direction are implemented in the form of the given acceleration time history and at the bottom boundary the material is not allowed to deform in the y-direction while on the lateral boundaries it is allowed to deform freely on the y-direction. The boundary conditions and the undeformed mesh are shown in

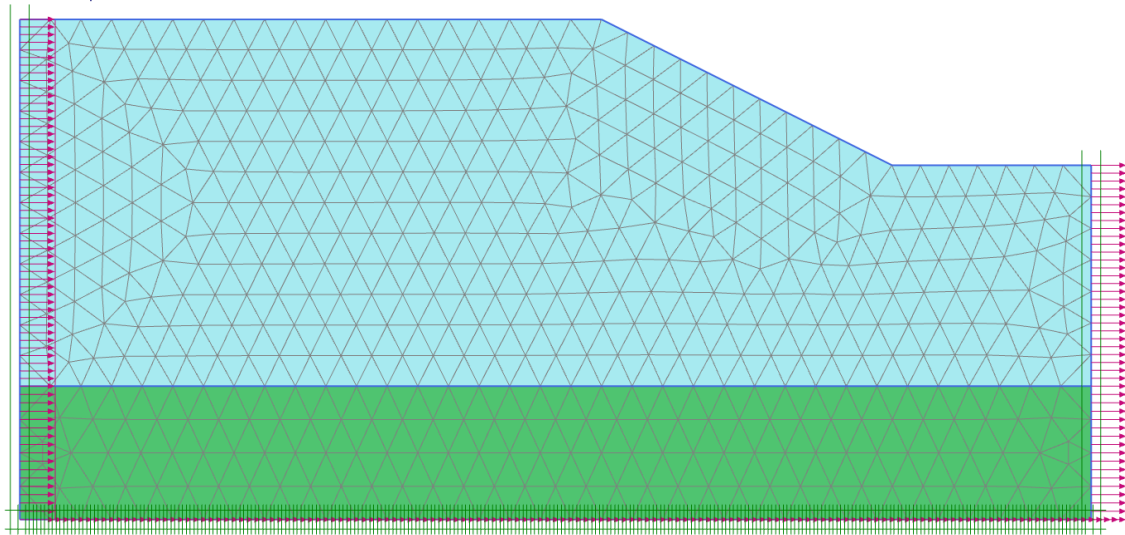


Figure 4.4.

The mesh was chosen after performing a certain number of tests with different mesh densities and comparing the variation of the results considering also the number of elements and their effect on the calculation time. Given the large shear moduli used in these dynamic analyses and considering a maximum frequency of 3Hz from the input motion spectrum, the demand for an element size significantly lower than the wave length of the propagating wave is met in any case.

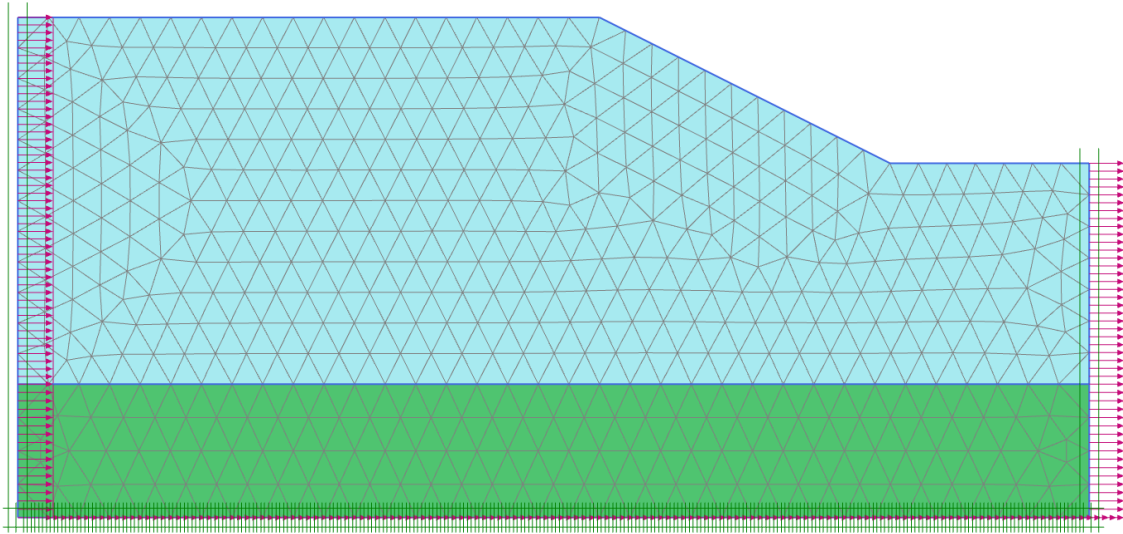


Figure 4.4: Mesh and boundary conditions for static and dynamic calculations

#### 4.4 Parameter selection

The centrifuge tests were performed using the same Fraser River Sand for which the calibration of the Direct Simple Shear tests was done in Chapter 3. For the selection of suitable parameters for UBC3D-PLM the calibration that was presented in that chapter is used taking also into consideration the specific loading conditions of the centrifuge model.

To account for the densification of the looser layer that occurs during the “spin up” of the centrifuge the initial relative density that is assumed before the earthquake is 40%, which is the mean value of the relative density of the layer according to the densification rule expressed by equation (4.1).

According to the material properties derived from laboratory tests in the University of British Columbia, the drainage layer has the same dry density and stiffness with the dense sand layer. The only significant difference is its permeability, which is approximately 100 times larger than the permeability of the dense layer (Seid-Karbasi, Byrne, 2003). The role of the drainage layer is to help with the saturation of the soil during the preparation of the model for the soil test. For this reason for the numerical modelling of the test the drainage layer is assumed to be the same with the dense sand layer.

The calculation of the initial conditions was done using both Mohr-Coulomb and UBC3D-PLM but no significant differences exist between the results of the two models. This is due to the fact that in this case the static calculation consists only by calculating the initial stress conditions and reaching the initial equilibrium, in which the main factor is the unit weight of the model and not the constitutive model that is applied.

No correction of the densification factor ( $f_{ac,hard}$ ) due to the effect of overburden stress was done, because the variation of vertical effective stress in the loose liquefiable layer is between 0 and 170 kPa and it is assumed that the difference between this stress and the reference stress level (100kPa) is small enough not to cause any significant effect in the results.

To take into account the effect of static shear, the area around the slope in which the static shear is predominant was determined by the directions of the principal stresses in the static

calculation. For this area the corrections in the model parameters that were suggested in Chapter 3 were used. The material properties that were used are presented in Table 4-2.

Model Parameters	Loose (Dr=40%)	Dense (Dr=80%)	Loose static shear (Dr=40%)
$(N_1)_{60}$	6.50	24.50	6.50
$\phi_{cv}$ (°)	33.00	33.00	33.00
$\phi_p$ (°)	33.65	37.35	33.65
$k_G^e$	809.40	1259.00	809.40
$k_B^e$	566.60	881.40	566.60
$k_G^p$	202.60	2367,00	202.60
$R_f$	0.83	0.68	0.83
$fa_{C_{hard}}$	0.45	0.45	1.00
$fa_{C_{post}}$	0.02	0.02	1.00

**Table 4-2: Material properties used for the simulation of centrifuge test with UBC3D-PLM**

## 4.5 Finite element analysis

Given all the previously described assumptions a finite element analysis was performed in PLAXIS. The undeformed mesh is shown in Figure 4.5. The area around the slope that has a different colour is the area for which the parameters suitable for initial static shear were considered.

In Figure 4.6 the total displacement vectors are shown. From this figure it can be seen that a flow failure occurs at a defined sliding surface. Due to this failure the displacements become very large with a maximum value of 10.85m. It is also apparent that the development of the slide is disrupted by the rigid boundary of the box.

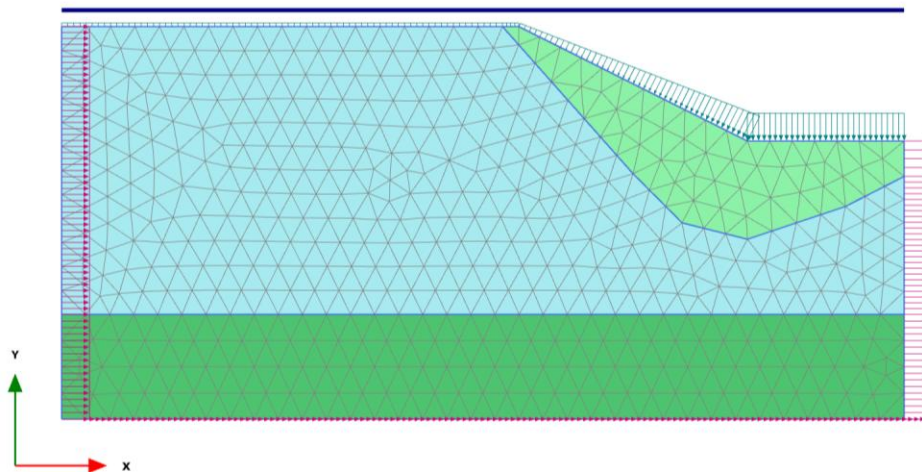


**Figure 4.5: Undeformed mesh and different materials for FE analysis**

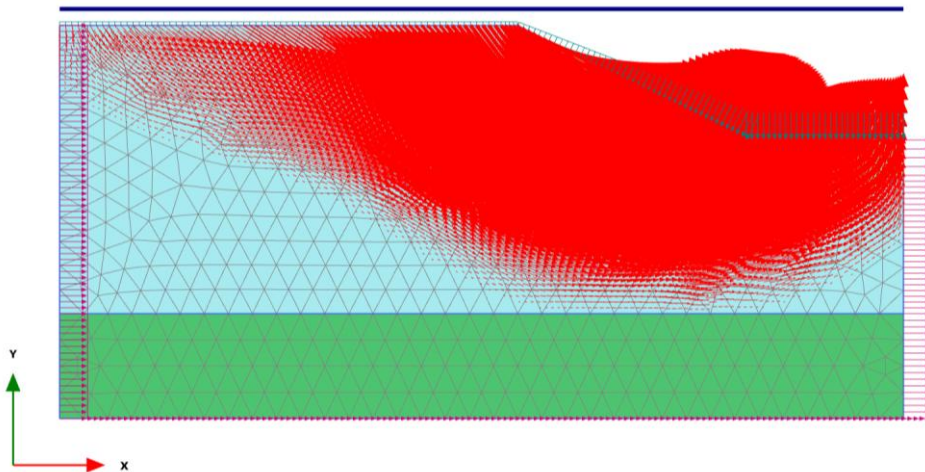


**Figure 4.6: Total displacement vectors, maximum displacement 10.85m**

The maximum pore pressure ratio at each point, which was reached at different moments during the earthquake, is shown in Figure 4.7. It is obvious from this that most of the loose sand layer liquefied during the earthquake, especially the part where the effect of static shear was considered negligible.

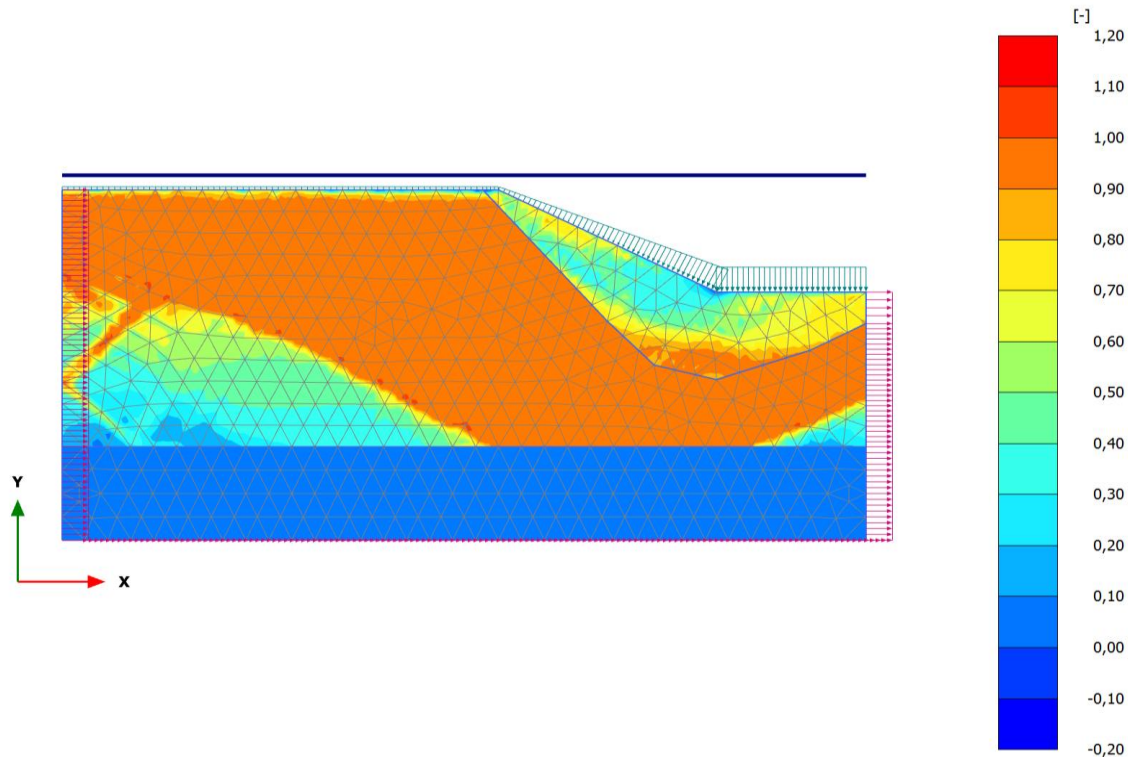


**Figure 4.7: Maximum pore pressure ratio ( $ru_{\max}$ )**

In the following figures the accelerations and the pore pressures that were measured during the centrifuge test are compared with the ones that were calculated from PLAXIS. For a better comparison three different areas were considered given the position of the sensors in the centrifuge: far from the slope, in the middle, and around the slope.

Concerning the accelerations it can be seen that far from the slope and in the middle area a good approximation of the centrifuge measurements is achieved especially before the 15<sup>th</sup> second of the earthquake motion (Figure 4.8, Figure 4.10) After that, there are certain high frequency pulses with low amplitudes which do not correspond with the measured values. This is also connected with the fact that after this time the earthquake motion is less significant and in the centrifuge there is a decrease in the excess pore pressures due to consolidation. This effect cannot be captured by the model since the analysis is fully undrained. This fact can cause these high frequencies due to volumetric locking. This numerical noise that can be observed is also enhanced by the fact that the boundaries are rigid. However it does not affect the generation of pore pressures or strains. In the middle part, the accelerations after the 15<sup>th</sup> second show behind these high frequencies also certain large period pulses which explain the shape of the excess pore pressure curves after this time. In the area near the slope, the accelerations predicted by the analysis present significant differences from the measured values. These are related to the very fast increase of the pore pressures due to the effect of static shear and to the consequent large displacements which correspond to failure of the slope. In addition it can be seen from the acceleration plots that a better fit of the measured values is obtained at larger depths below the surface.

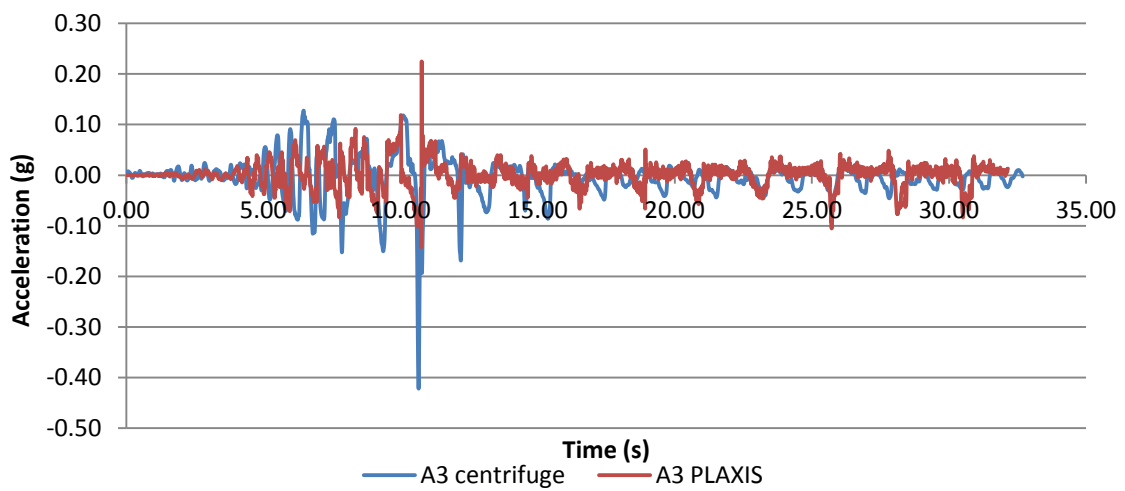
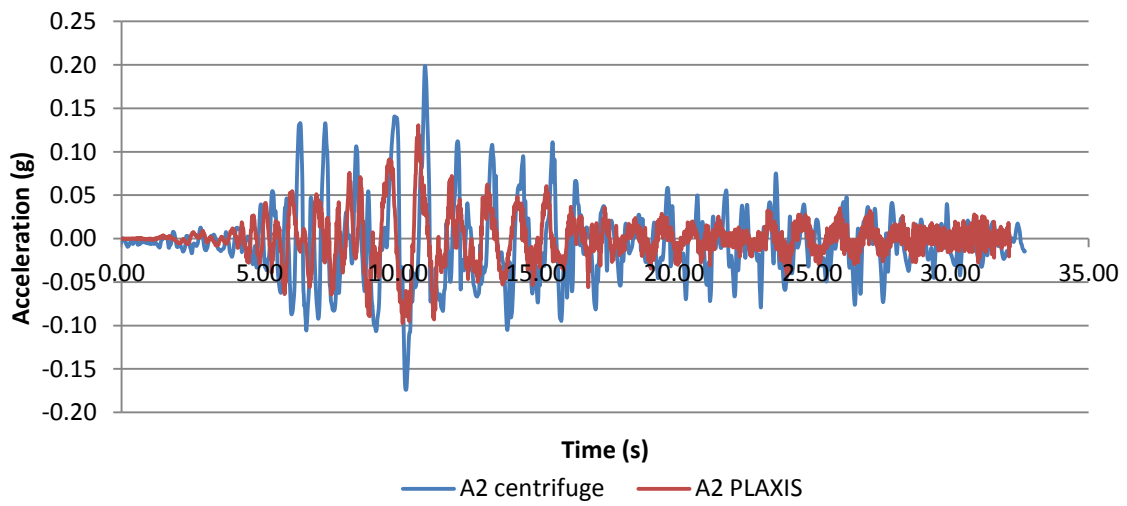
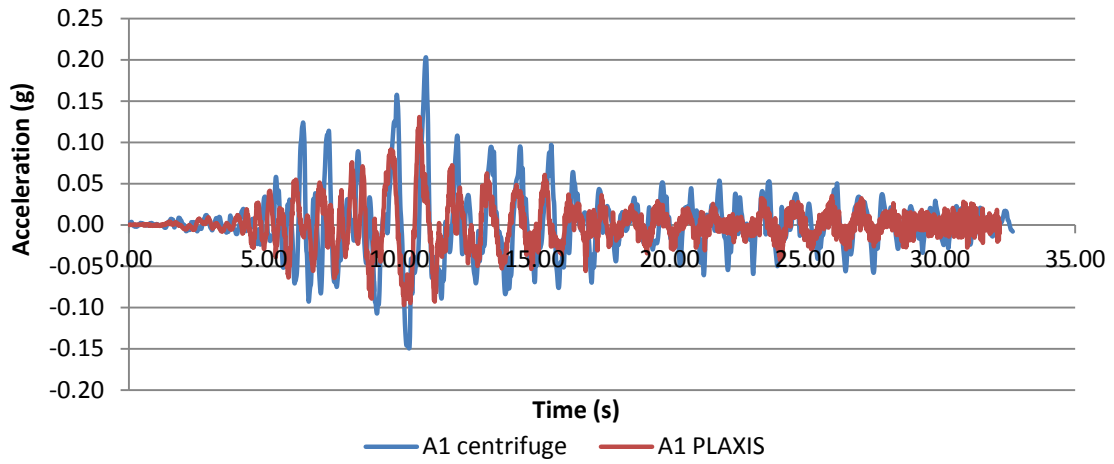
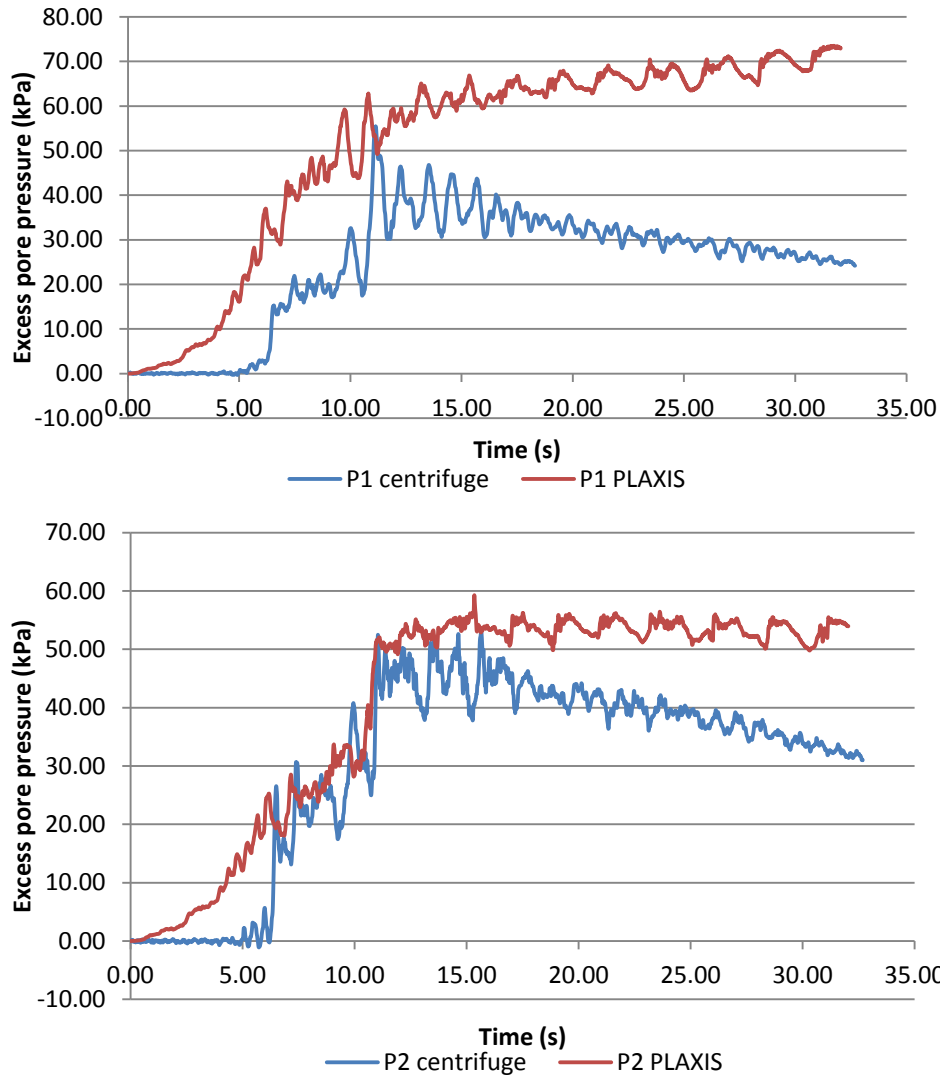


Figure 4.8: Acceleration time histories from the centrifuge and PLAXIS analysis at the area far from the slope



**Figure 4.9: Excess pore pressures from centrifuge measurements and PLAXIS analysis at the area far from the slope**

A general observation from the pore pressure plots is that in the finite element analysis there is a large pore pressure generation in the beginning of the earthquake motion which is not very realistic if it is compared with amplitude of the earthquake at the same time and position. This is even more obvious in the area around the slope (Figure 4.13) where the pore pressure increases practically instantly at 6kPa. Despite this rapid increase, in the areas not close to the slope, the analysis offers a good approximation of the pore pressure generation until the time (around 10 to 15sec depending on the point that is considered) when most of the slope has liquefied. One of the reasons why the analysis predicts higher pore pressures than the centrifuge test is that it is fully undrained. Due to the fact that the model leads the slope to flow failure very fast around the slope, the predicted pore pressure generation does not fit the measured excess pore pressures in the centrifuge.

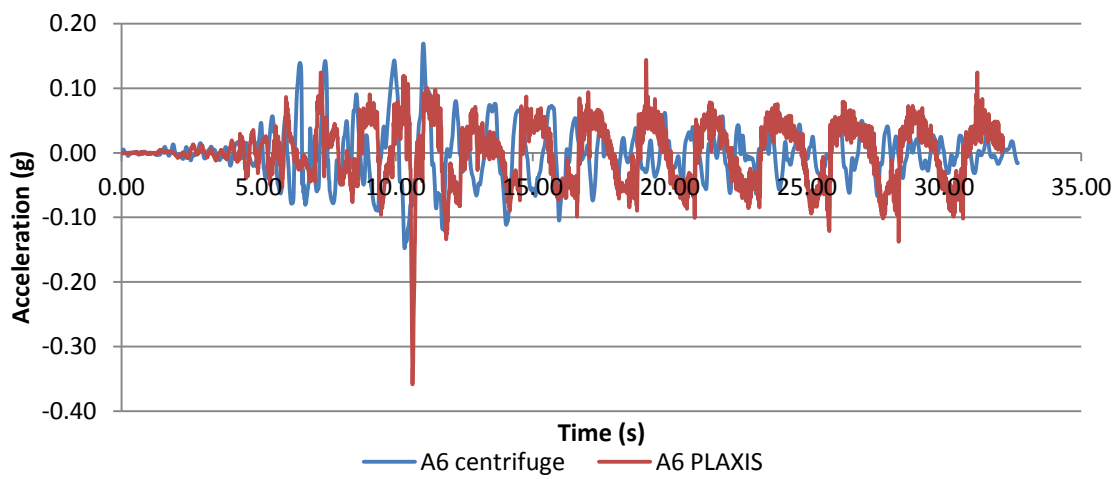
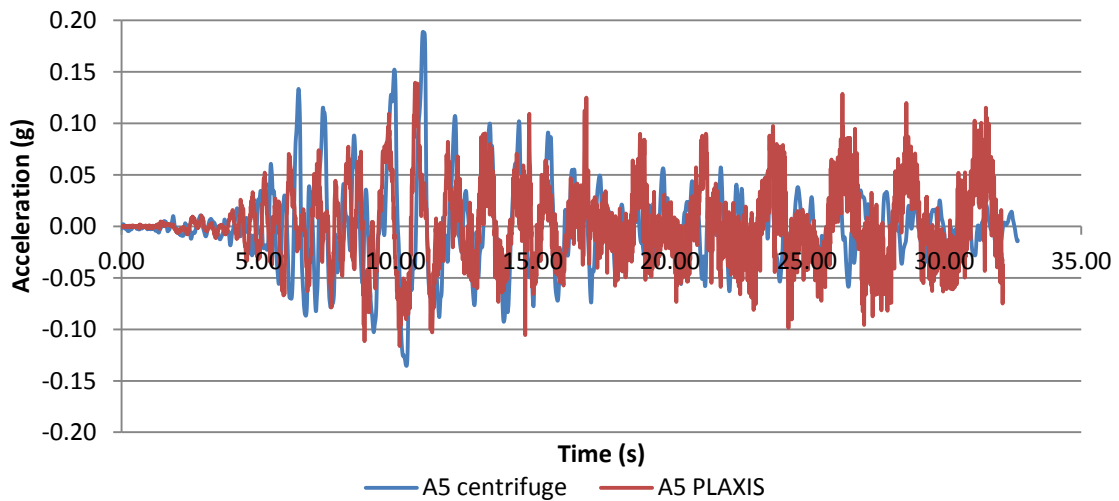
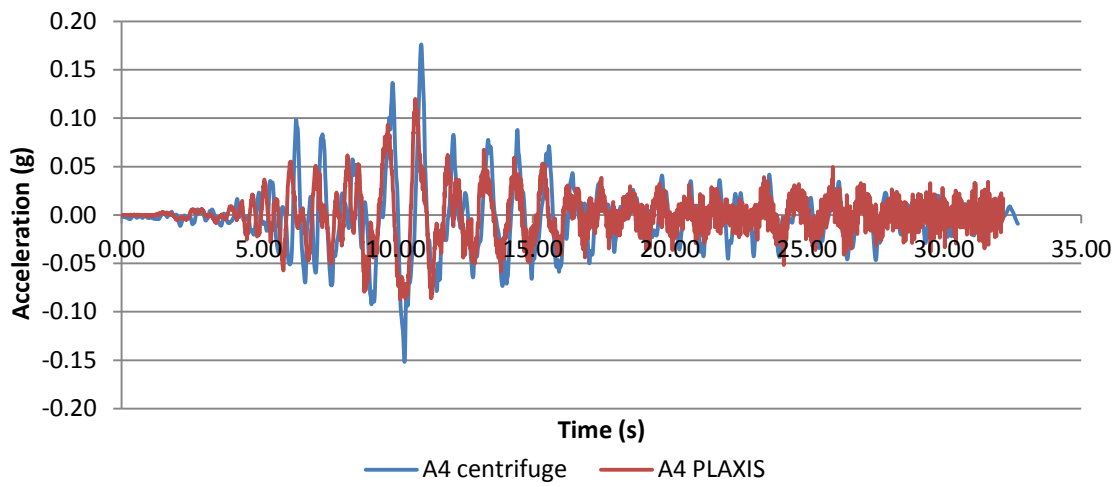


Figure 4.10: Acceleration time histories from the centrifuge and PLAXIS analysis at the middle area

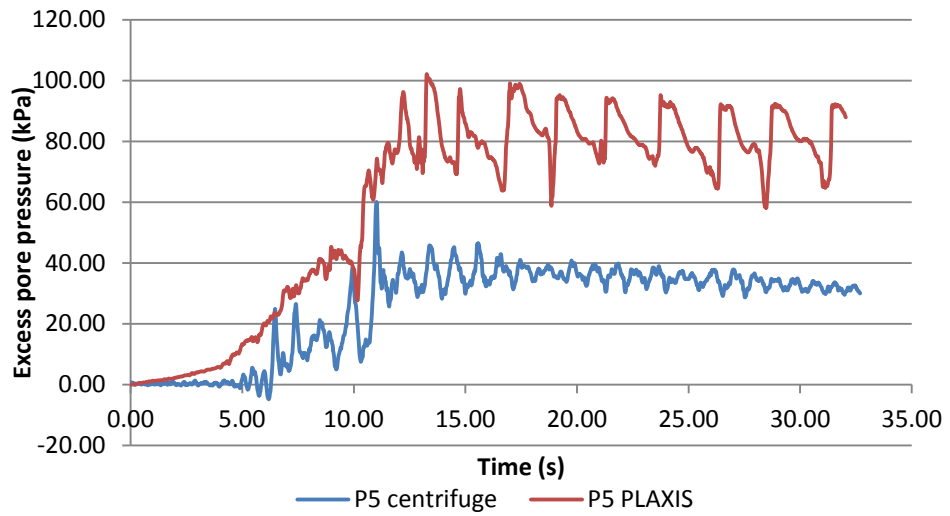
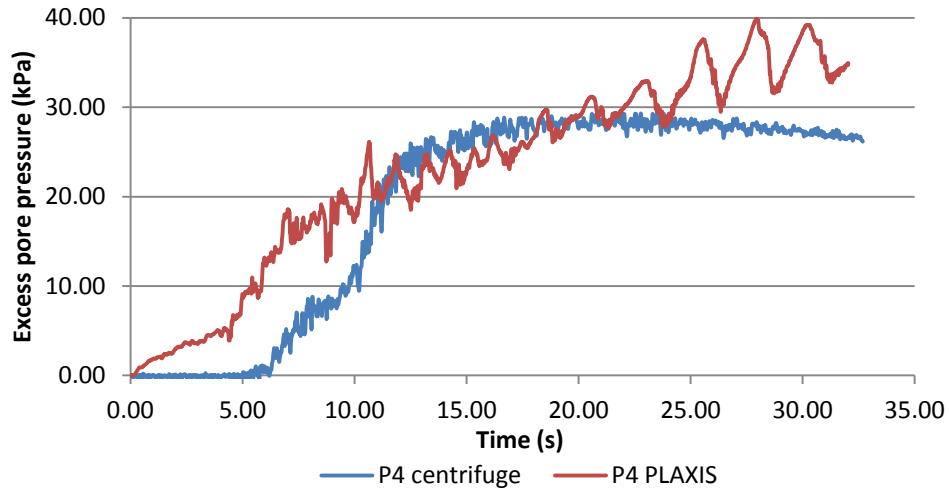
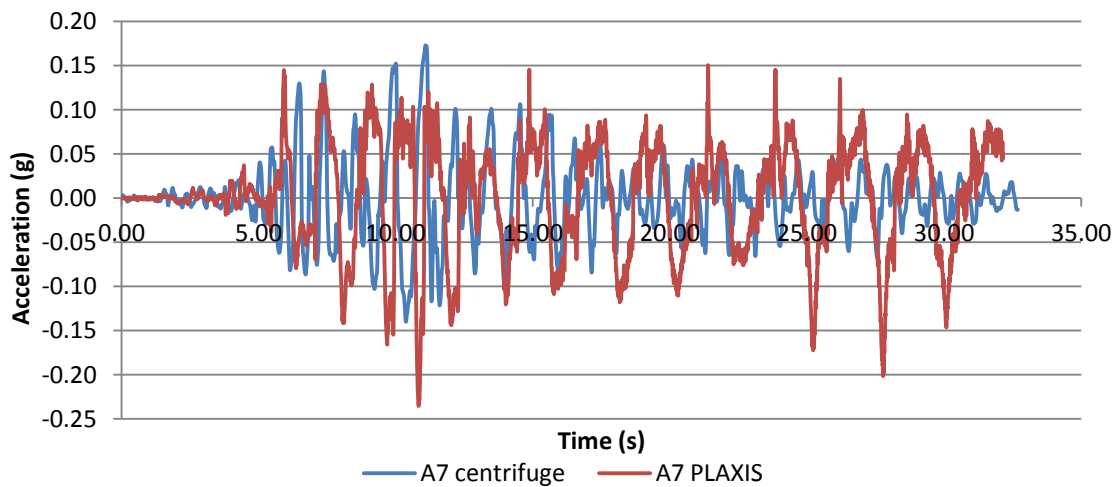


Figure 4.11: Excess pore pressures from centrifuge measurements and PLAXIS analysis at the middle area



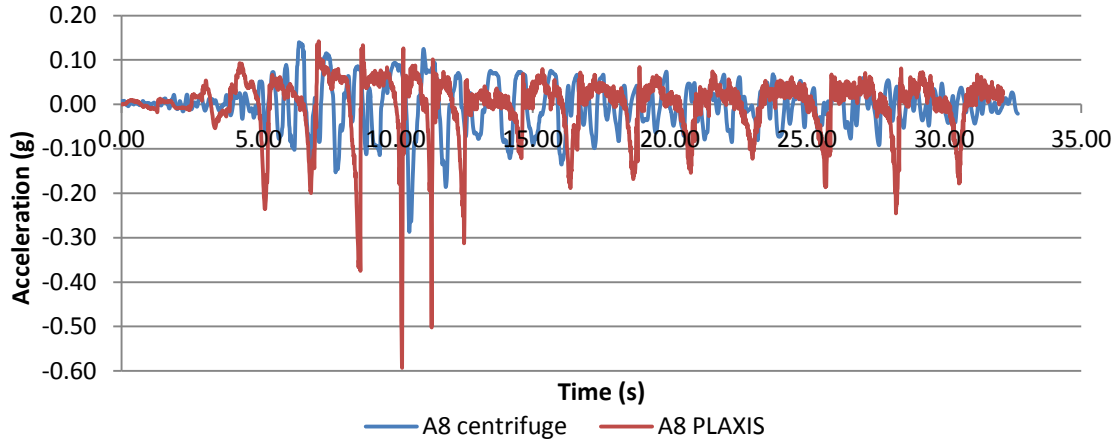


Figure 4.12: Acceleration time histories from the centrifuge and PLAXIS analysis around the slope.

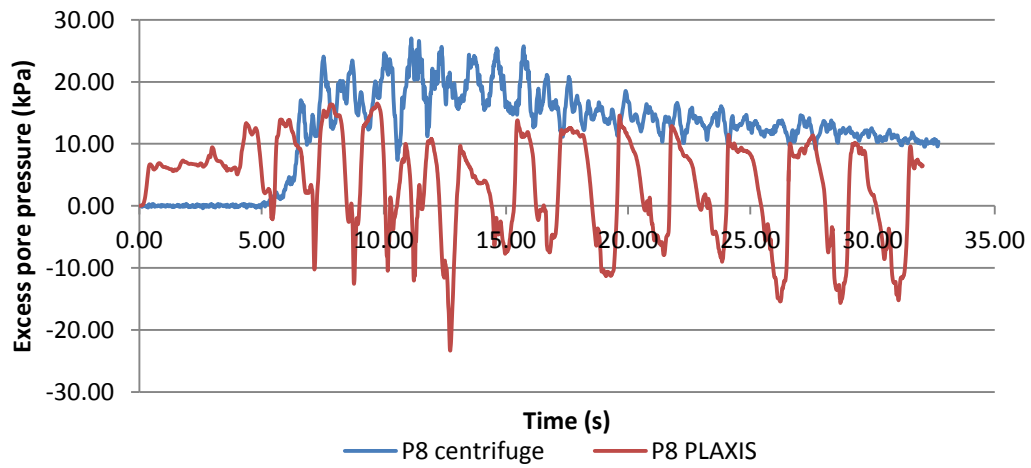
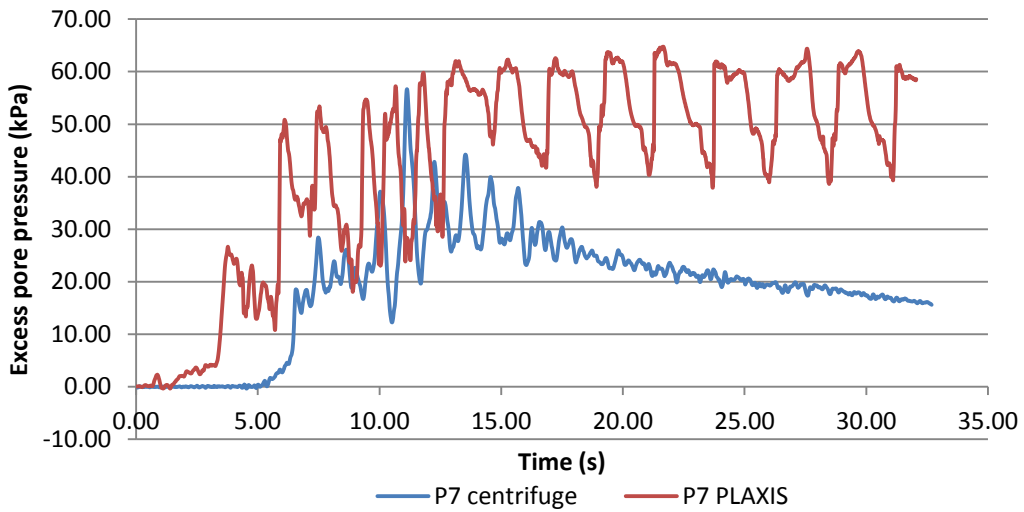


Figure 4.13: Excess pore pressures from centrifuge measurements and PLAXIS analysis around the slope

Taking a closer look at the development of the pore pressure ratio and displacements over time, it is apparent that the flow failure begins on the slope and progresses gradually to the inner part of the model.

Already 2 seconds after the earthquake begins, the pore pressure ratio on the slope has reached a value of around 40% (Figure 4.14). At 4.5 seconds liquefaction has progressed to the area assumed not to be affected by static shear with the pore pressure ratio ( $r_u$ ) reaching values of 100% (Figure 4.15) and the displacements becoming increasingly large reaching a maximum of 18cm. Since the slope is moving outward no further increase of the pore pressures occurs on it but in the rest of the loose layer the  $r_u$  keeps increasing. At 15 seconds most of the loose sand has fully liquefied ( $r_u=100\%$ , Figure 4.16) and the maximum displacement is already 4,8m.

This behaviour is not similar to what has been observed in the centrifuge test, in which the slope does not fail. To determine the reason for this difference the initial assumptions need to be revisited. It is certain that an overestimation of the pore pressure generation is due to the fully undrained analysis, but it cannot explain the complete failure of the slope that is observed. Another reason is the rapid increase of pore pressures near the slope due to static shear and the over prediction of strains connected with this type of loading that has already been observed in the DSS tests simulations (Chapter 3).

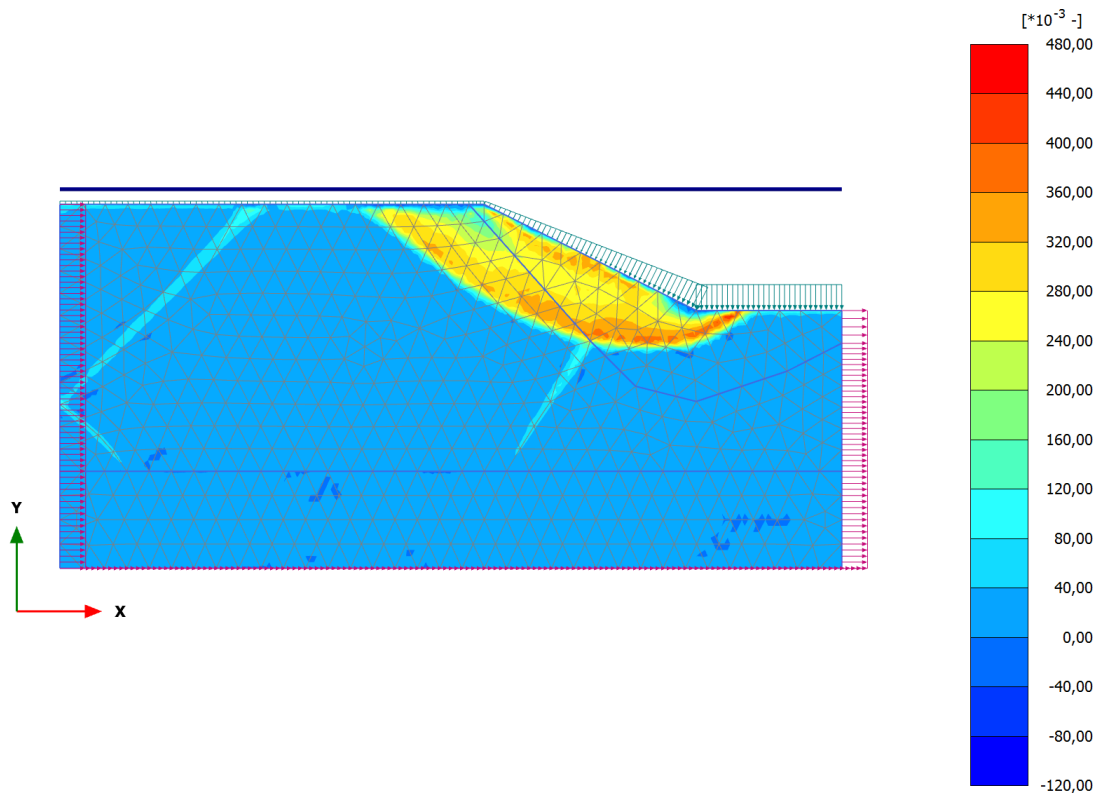


Figure 4.14: Pore pressure ratio at 2sec

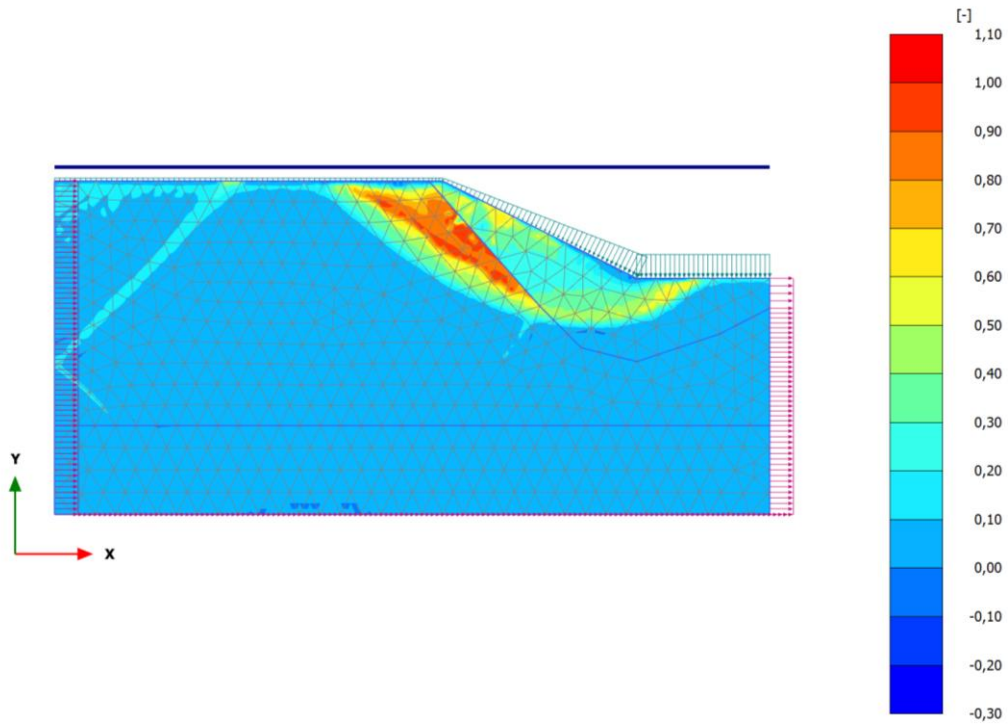


Figure 4.15: Pore pressure ratio at 4,5sec

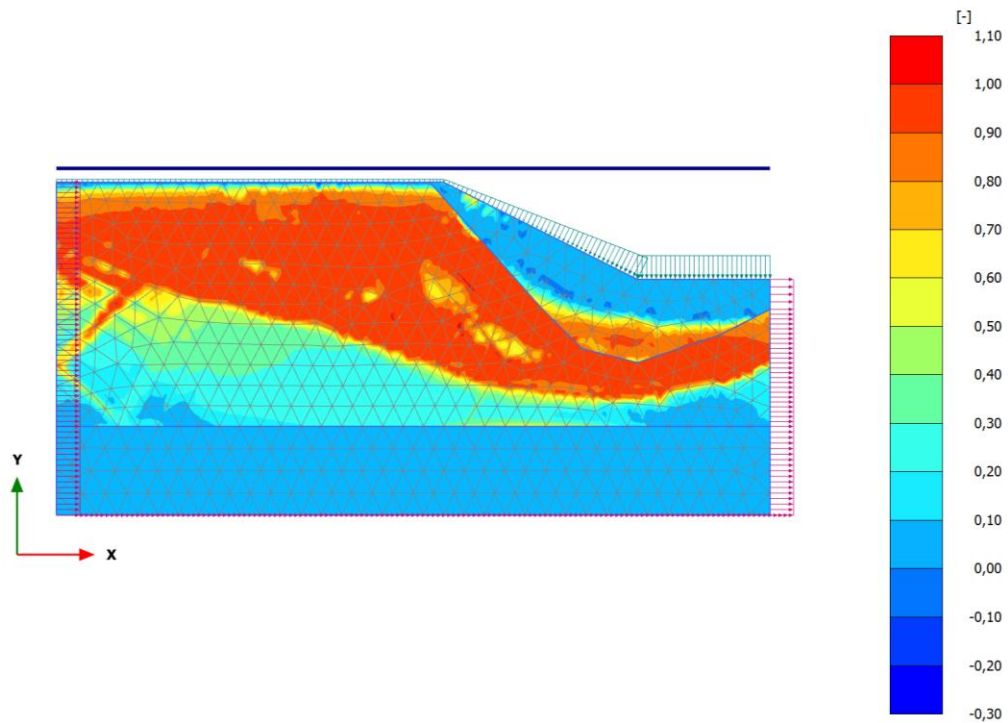


Figure 4.16: Pore pressure ratio at 15 sec

In **Error! Not a valid bookmark self-reference.** the stress strain behaviour of the model at certain positions inside the slope (point (P2 and P5, Figure 4.1) is plotted. The initial assumption was that in these areas the effect of static shear would be negligible however it is obvious from the plots that this behaviour can be described as flow liquefaction and not as cyclic mobility. For this reason it is considered that the initial assumption of static shear only near the slope needs to be revised and the corrections made to minimize its effect ( $fa_{c_{hard}}=1.0$  and  $fa_{c_{post}}=1.0$ ) should be applied on the whole loose sand layer. Given this observation, another finite element analysis was performed and the results are presented in the following section.

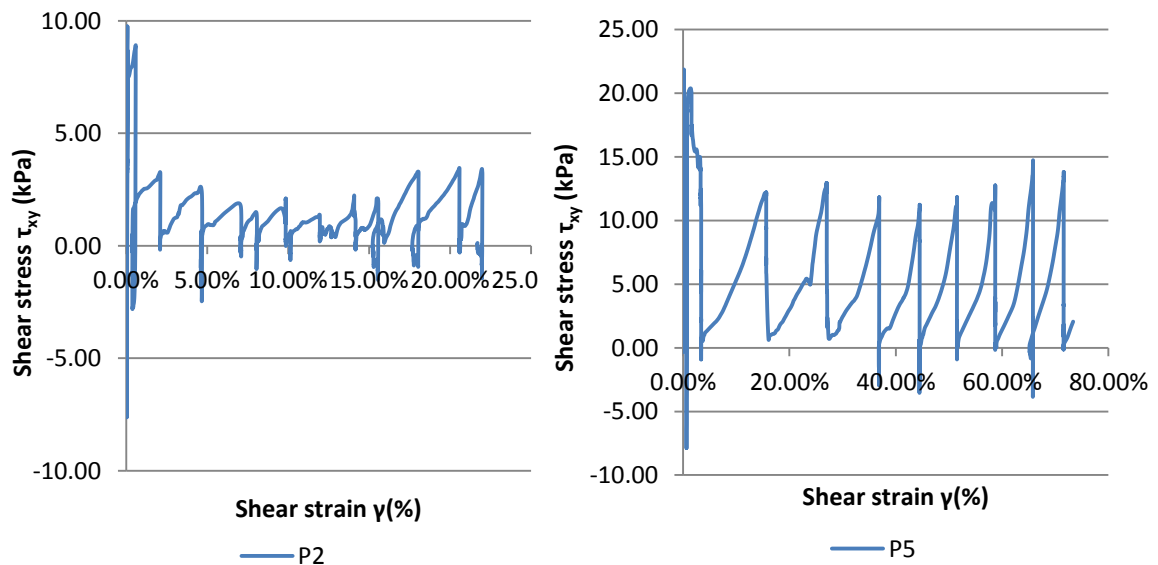


Figure 4.17: Shear stress over shear strain at two positions far from the slope (a) and in the middle area (b)

#### 4.6 Finite element analysis assuming the initial static shear affects all the loose layer

This analysis was performed using the same assumptions and boundary conditions with the previous one with the only difference that the densification factor and the post liquefaction factor were considered equal to 1.0 for the entire loose sand layer. In Figure 4.18 the total displacement vectors at the end of the earthquake are shown and in Figure 4.19 the maximum pore pressure ratios that occurred due to the earthquake. The displacements are still large leading to failure but compared to the previous analysis the failure is localized around the slope and a significantly smaller part of the loose layer liquefies.

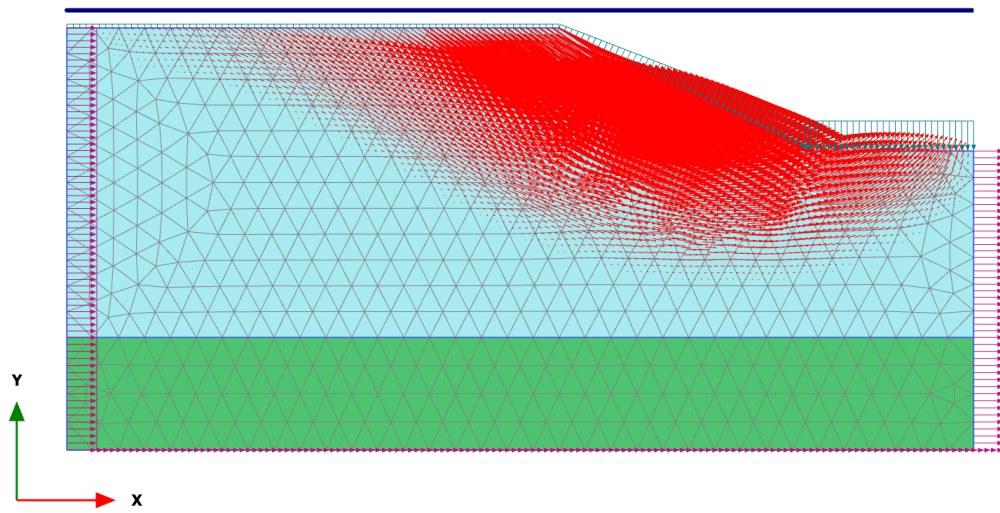


Figure 4.18: Total displacements, maximum displacement 4.4m

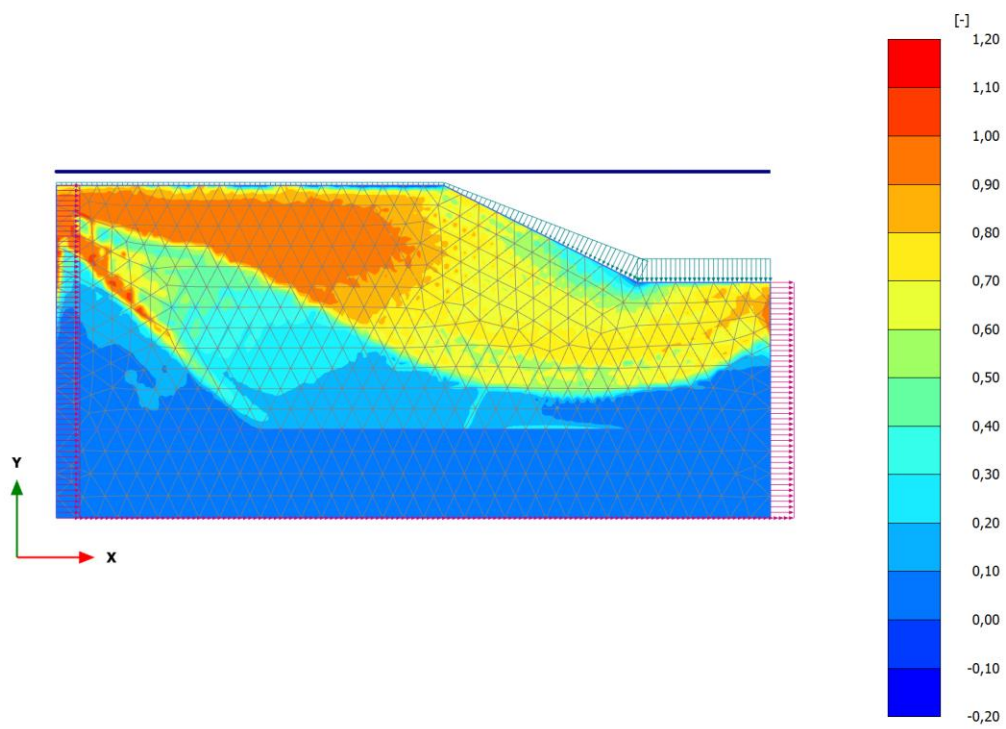


Figure 4.19 Maximum pore pressure ratio ( $ru_{max}$ )

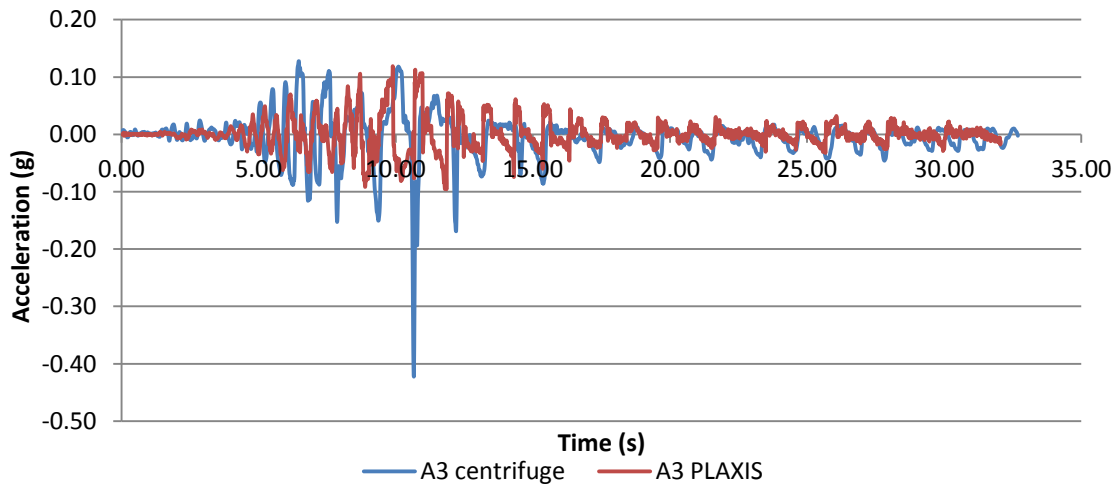
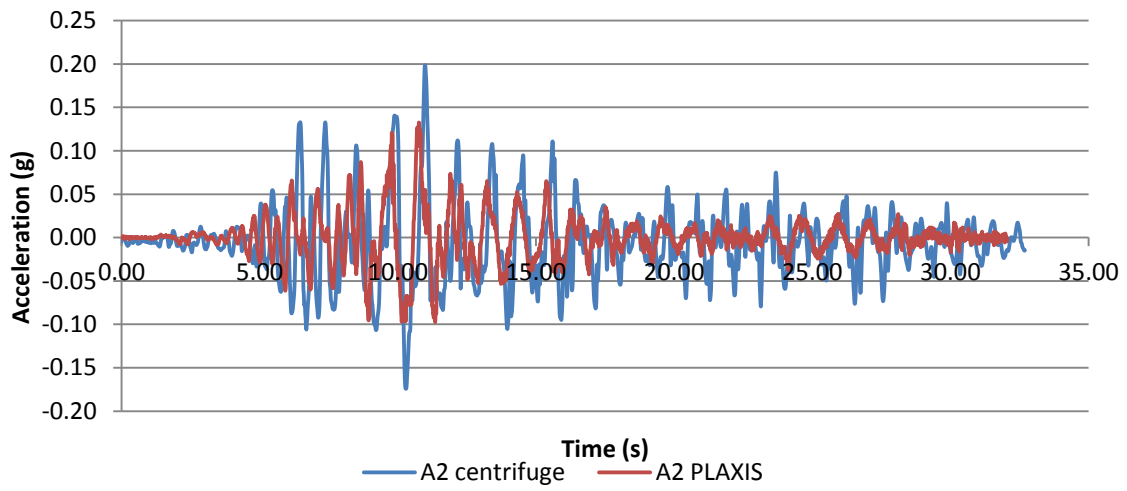
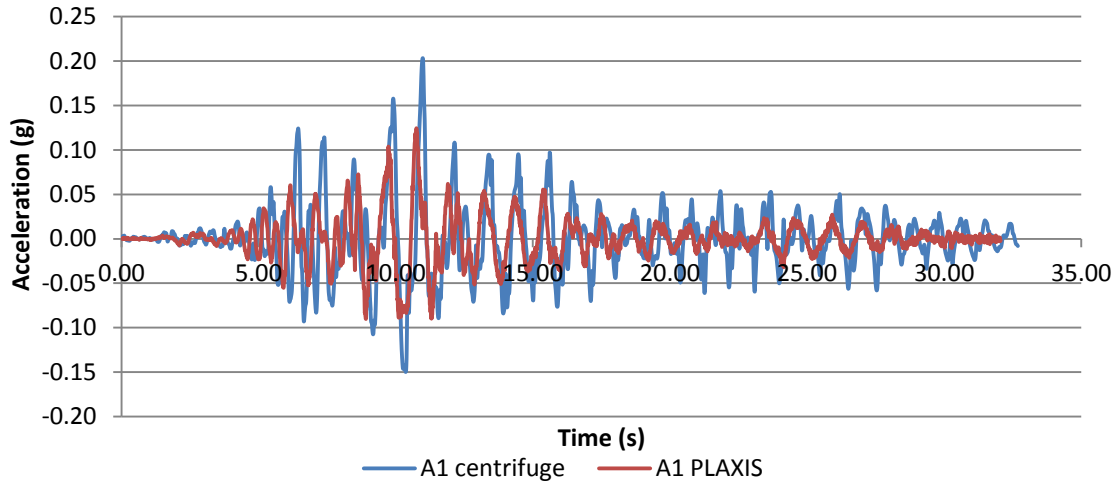
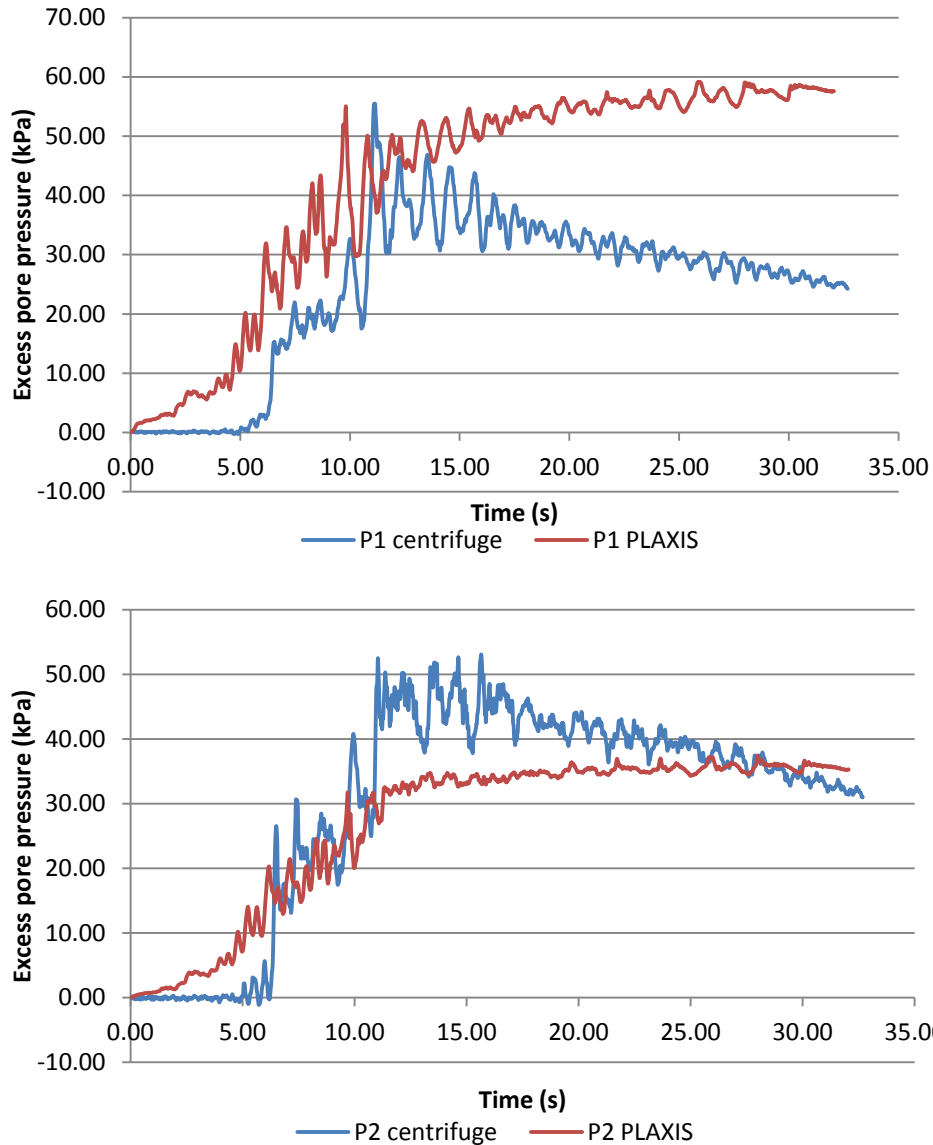


Figure 4.20: Acceleration time histories from the centrifuge and PLAXIS analysis at the area far from the slope



**Figure 4.21: Excess pore pressures from centrifuge measurements and PLAXIS analysis in the area far from the slope**

In Figures 4.20 to 4.25 a comparison of the accelerations and the excess pore pressures measured in the centrifuge and produced by the PLAXIS calculation is presented. Concerning the accelerations this analysis gives a very good approximation of the measured values in the centrifuge. The noise that was observed in the previous analysis does not exist in this case and only in the area around the slope (including point A6) these large period pulses appear after around the 15<sup>th</sup> second of the earthquake motion. This can be attributed to the lack of softening since the post liquefaction factor is set to one.

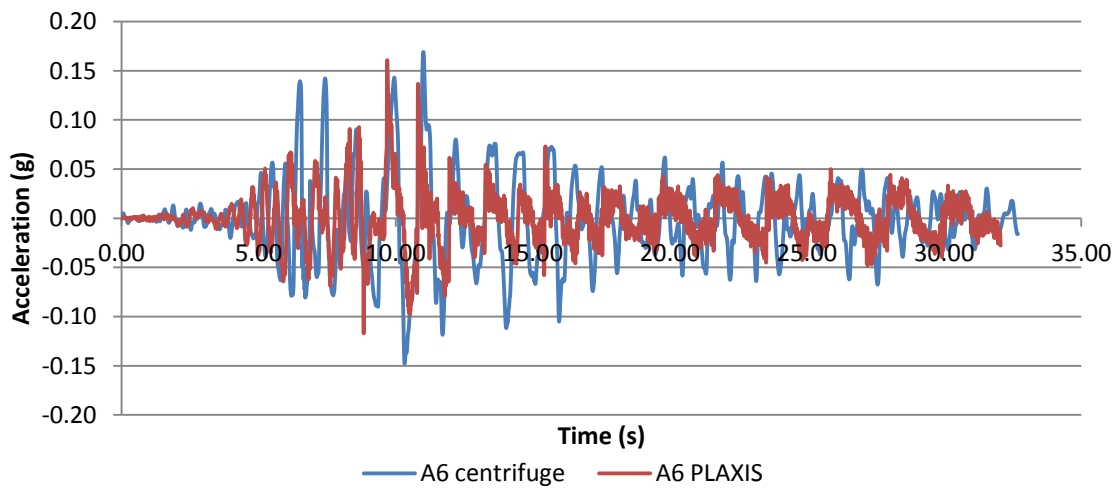
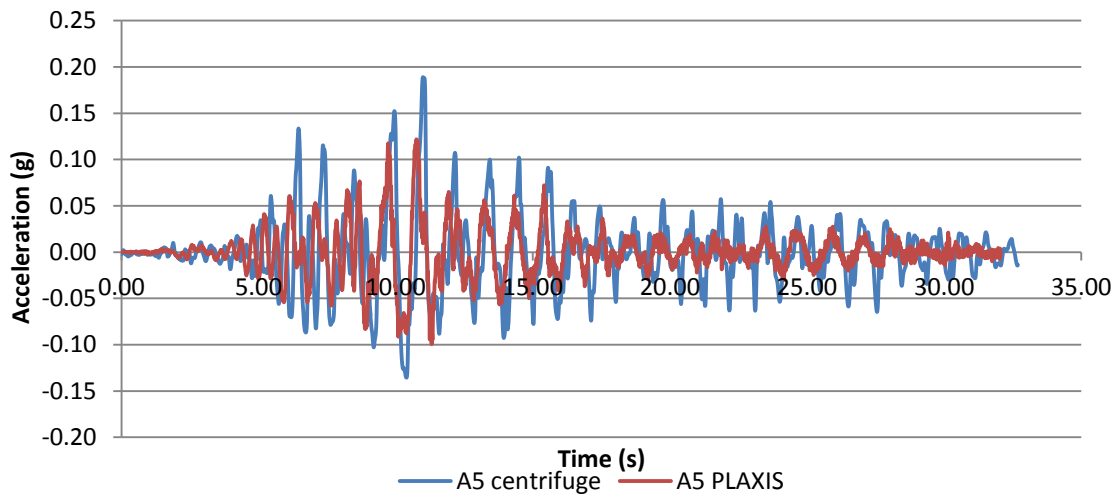
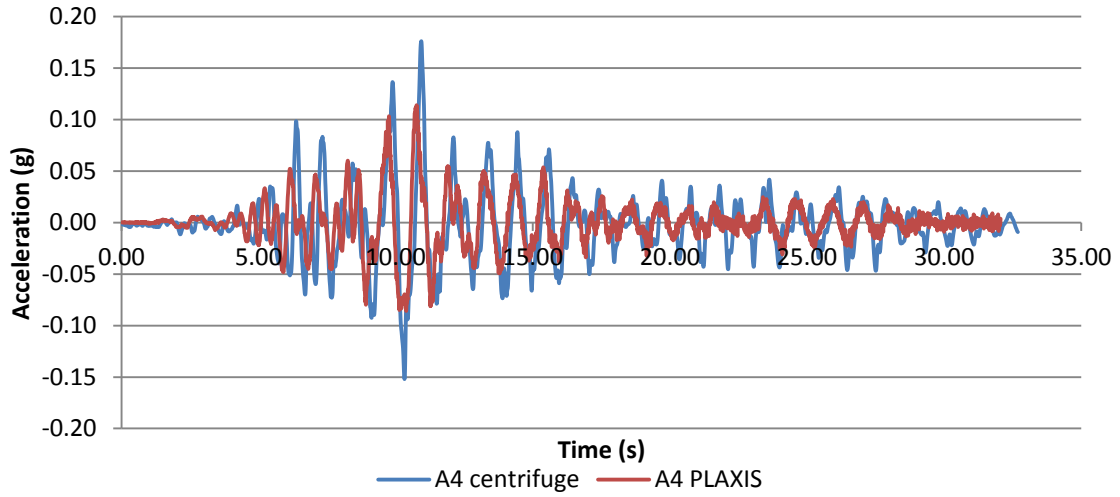
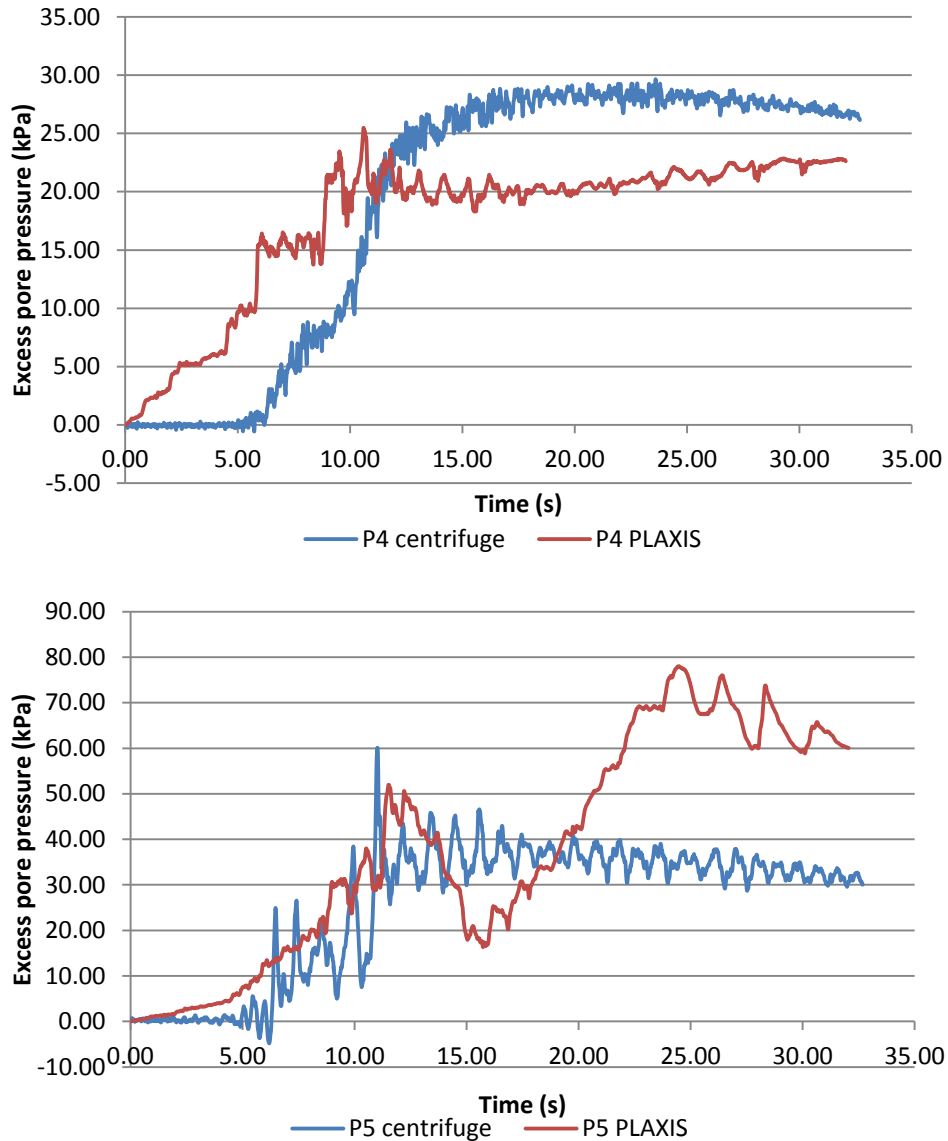


Figure 4.22: Acceleration time histories from the centrifuge and PLAXIS analysis at the middle area



**Figure 4.23: Excess pore pressures from centrifuge measurements and PLAXIS analysis at the middle area**

In terms of pore pressures again a rapid increase in the beginning of the dynamic calculation is shown, especially near the slope. However, a much better fit with the measured data is achieved, making it possible to predict with reasonable accuracy the onset of liquefaction. The lack of flow during the dynamic calculation does not allow simulating the decrease in pore pressures that is observed in the centrifuge, which contributes to the stability of the slope. Only in point P5 a sudden increase in the pore pressures is observed after 15 seconds which does not correspond to the measured values and was not expected.

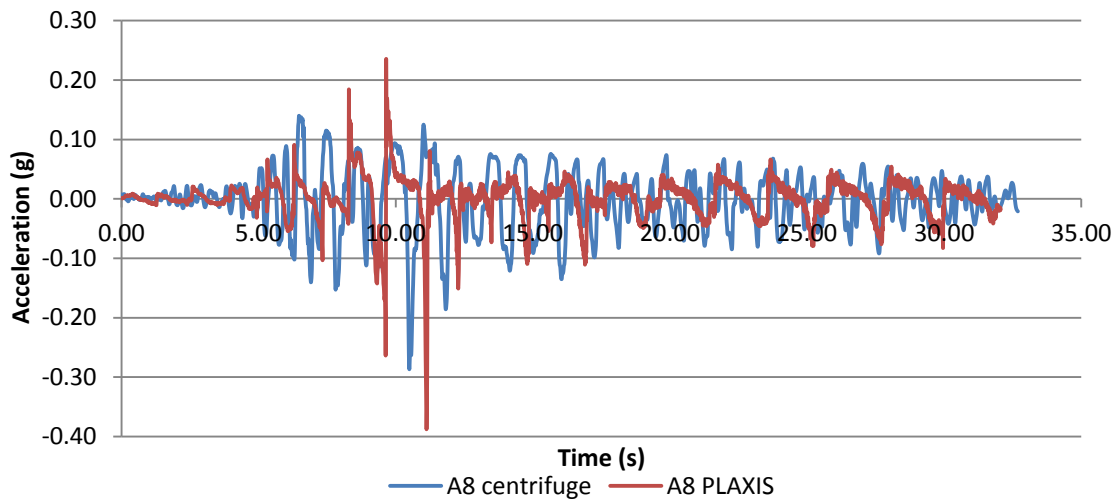
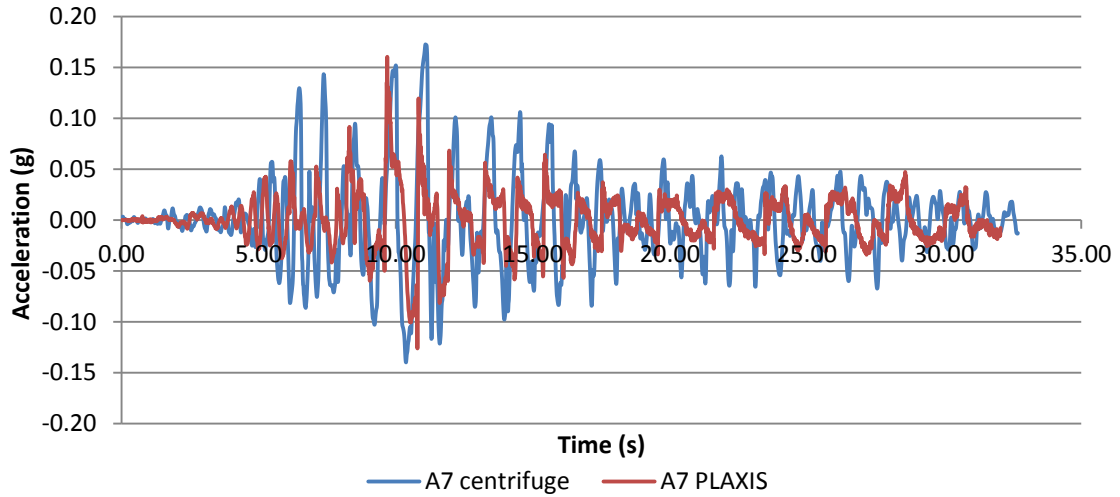


Figure 4.24: Acceleration time histories from the centrifuge and PLAXIS analysis in the area around the slope

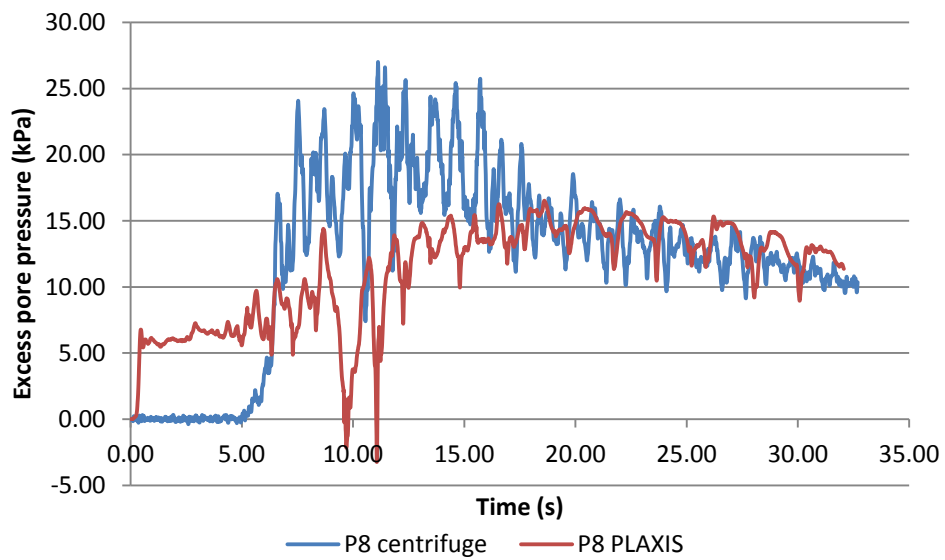
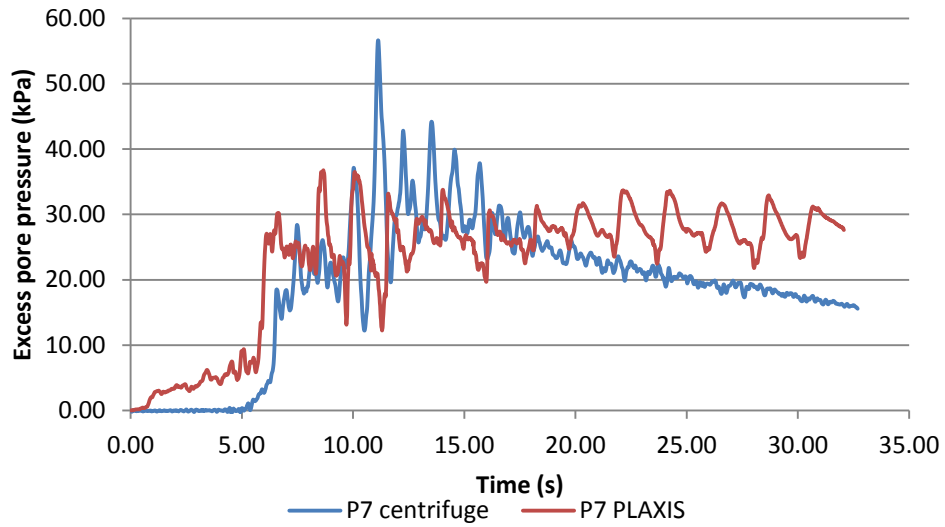
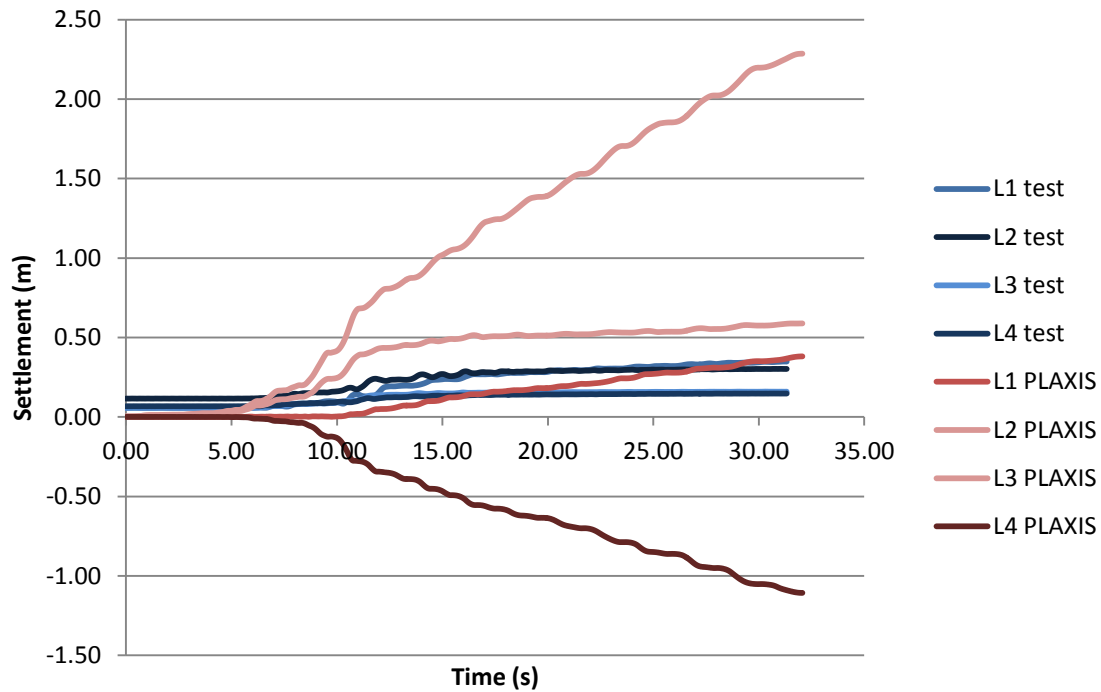


Figure 4.25: Excess pore pressures from centrifuge measurements and PLAXIS analysis in the area around the slope



**Figure 4.26: Settlements of the surface measured in the centrifuge and calculated by PLAXIS**

In Figure 4.26 the predicted settlements from the finite element analysis are shown against the measured settlements in the centrifuge. The analysis over predicts significantly the settlements compared to the measured ones. This was expected given the previous conclusions about flow liquefaction in UBC3D-PLM.

## 4.7 Summary and Conclusions

In this chapter UBC3D-PLM was used to simulate a dynamic centrifuge test. Two different analyses were performed one assuming that the effect of static shear is limited around the slope and one considering that it affects the entire loose sand layer. From the results of the analyses it has been shown that the second case provides a much better approximation of the physical model behaviour.

It has been shown that a very good approximation of the measured accelerations was possible, especially in the second analysis.

The pore pressure generation predicted by the model gives a satisfactory estimate of the actual test conditions, despite the limitation of undrained behaviour and the initial assumption of fully saturated soil. The prediction is much better for the areas away from the slope while near the slope where the effect of static shear is predominant this prediction deteriorates.

Both in terms of pore pressures and displacements, the underestimation of the cyclic resistance of the soil when there is an initial static shear loading, which was observed already from the laboratory tests, leads to unrealistic results. However, significant improvement is achieved with proper calibration.

A good prediction of the displacements that were measured in the centrifuge was not obtained. This is due to the over prediction of displacements done by the constitutive model in the case of flow liquefaction. In addition because of the undrained conditions and the aforementioned problems connected with static shear, in the finite element analysis the presence of liquefaction is much more extended compared to the test. Given this fact it can be said that post-liquefaction behaviour cannot be predicted by the model. It is preferable for such cases to define liquefaction in terms of pore pressures and not strains.

Another significant observation, by comparing the results of the two PLAXIS analyses, is that the selection of a low post liquefaction factor for loose soils and especially in the case of sloping ground can lead to a certain amount of numerical noise in the calculated accelerations and also to instabilities and unrealistic behaviour in the generated pore pressures. It is suggested that in such cases it is preferable to not include stiffness degradation at all. This assumption is reasonable given also that under these loading conditions failure occurs before the pore pressure ratio becomes 100%.

Now that certain limitations of the model have been observed in a simple geometry and it has been shown that the model can predict the onset of liquefaction satisfactorily despite them, in the following chapter the model will be applied in the case history of the Upper San Fernando Dam as a final validation of its applicability for predicting the earthquake response of embankment dams.

## 5 CASE STUDY: UPPER SAN FERNANDO DAM

Up to this point it was shown that despite its limitations, with a proper calibration, UBC3D-PLM is able to provide a very useful tool to predict the onset of dynamic liquefaction, when the simulation concerns laboratory tests under controlled conditions. However, the conditions in situ are not controlled and the unknown variables are many and usually very difficult to determine. To evaluate the performance of UBC3D-PLM for embankments it is important to see how the model can predict the response of an actual embankment dam given all the limitations and uncertainties that arise when the variability and complexity of field conditions are involved. This will be done by analysing with UBC3D-PLM the response of the Upper San Fernando dam under the 1971 San Fernando earthquake.

### 5.1 Upper San Fernando Dam

The Upper San Fernando Dam (or Upper Van Norman Dam) is part of the Van Norman Lake Complex which includes dams, reservoirs, dikes and storm and diversion structures (Figure 5.1). It is situated 30km to the north of Los Angeles. Before the 1971 San Fernando Earthquake, the complex used to be the main water distribution centre for the surrounding area.

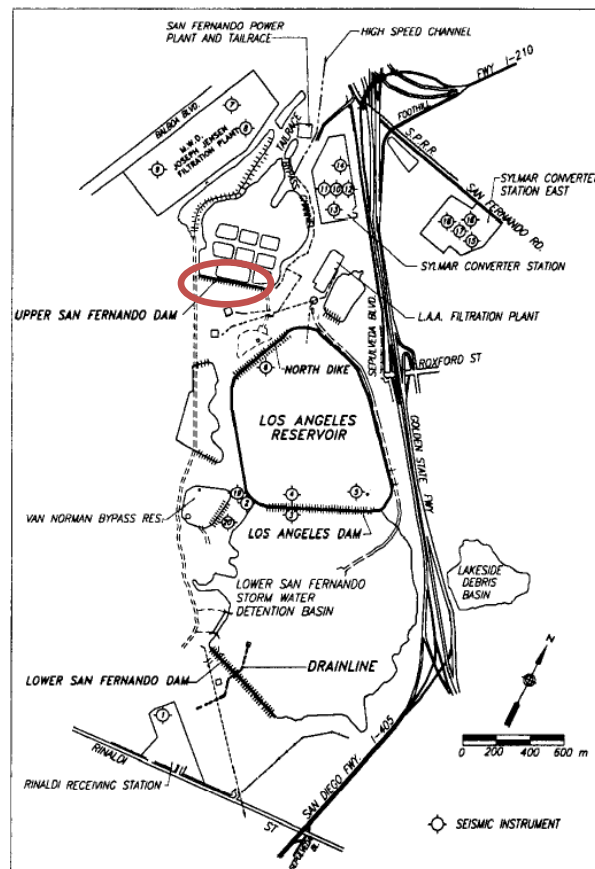
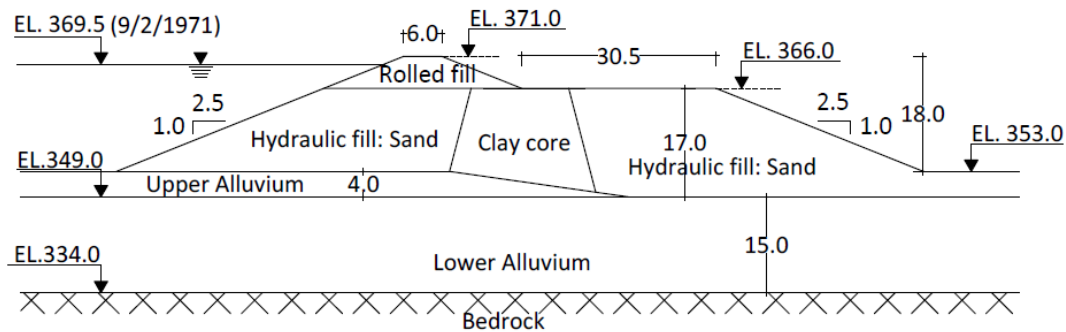


Figure 5.1: The Upper San Fernando Dam in the Van Norman Lake Complex (Bardet and Davis, 1996)

The construction of the dam started in 1921 and finished in 1922 using the method of “semi-hydraulic” fill. This method can be summarized in the following processes: the construction material is transported from the borrow area to the upstream and downstream beaches of the dam site and then it is spread by hydraulic jetting. With this process, the coarser material is deposited closer to the place of deposition and thus forming the dam shells and the finer material is deposited in the core of the dam. This way the hydraulic fill consists of two main zones: the permeable coarse grained shells and the impermeable fine grained core. The dam was founded on alluvium consisting of alternating layers of stiff clays and clayey gravels. The bedrock under the alluvium is poorly cemented conglomeritic sandstone and coarse-grained sandstone. This construction method presents several disadvantages, the most important of which is that there is no control over the exact grain size distribution of the zones of the dam and also the compaction of the fill is considered inadequate according to modern regulations. The hydraulic fill reaches an elevation of 366m and above that a section of rolled fill was constructed up to 371m. The Upper San Fernando dam is an approximately 550m long embankment with a total height around 22m. The capacity of the dam reservoir is 2.3 million cubic meters. A simplified cross section of the dam is shown in Figure 5.2 and the water level in the lake is shown at the elevation in which it was on the day of the earthquake.



**Figure 5.2: Typical cross section of Upper San Fernando Dam (Seed et al, 1973)**  
(Dimensions in meters)

### 5.1.1 Response to the 1971 San Fernando Earthquake

The San Fernando Earthquake occurred on February 9, 1971 and had a magnitude of 6.6 on the Richter scale. The epicentre of the earthquake was approximately 10km northeast from the Van Norman Complex.

The deformations caused by the earthquake were characterized by a general downstream movement of the dam body. The settlement of the crest was around 1.0m and the downstream movement 1.5m. Several longitudinal cracks were observed on the upstream face, running the full length of the dam. The movement of the dam body seemed to be general since a unique slip surface was not observed.

The occurrence of liquefaction was suggested by the water overflow that was observed on the dam's standpipe piezometers (

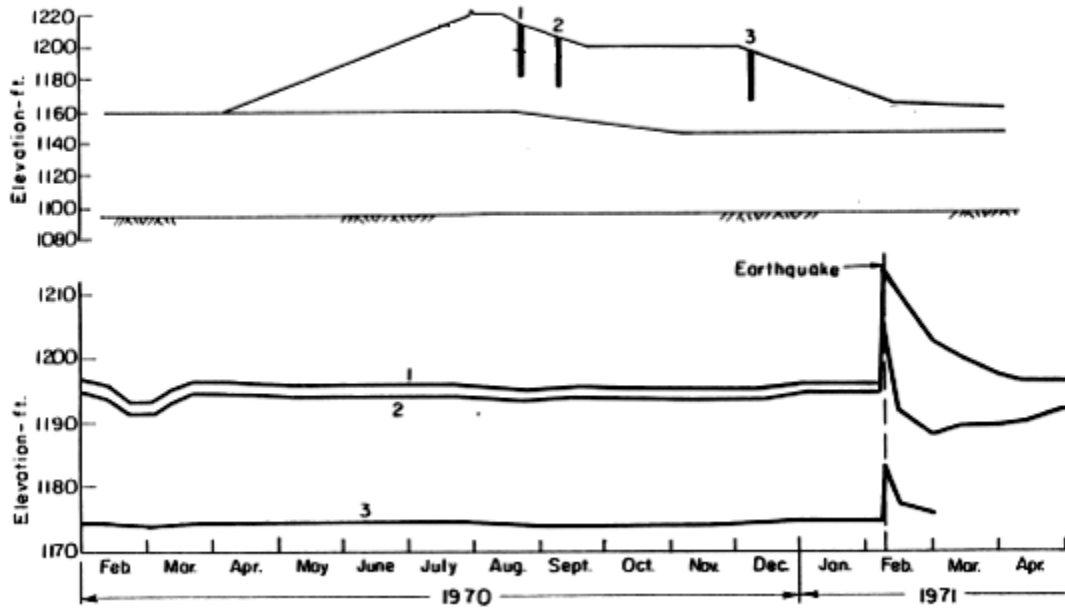
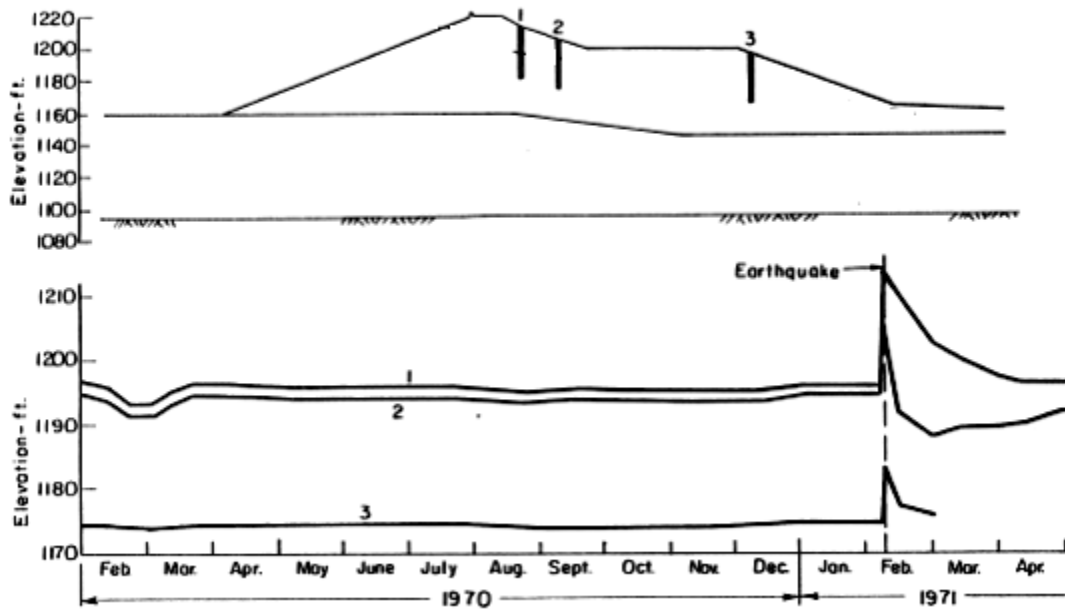


Figure 5.3) and by the sand boils that were formed below the downstream toe.



**Figure 5.3: Position of piezometers in the dam body (a) and changes in water level in the piezometers (b) before and during the earthquake (Seed et al 1976).**

### 5.1.2 Site investigation

After the earthquake, an extensive site investigation followed by laboratory testing was performed for both the Lower and the Upper San Fernando Dams by the California Department of Water Resources. The field investigation consisted of trenches, borings and seismic surveys and was performed in April and May 1971. In Figure 5.4 the positions of the trenches and the drillings on the Upper Dam is shown.

Standard penetration tests were performed in the boreholes. As it was discussed earlier, the liquefaction resistance has been correlated to the corrected SPT blow-count  $(N_1)_{60}$ . This value represents the one that would be obtained in a soil under a level ground overburden pressure of 100kPa using a standardized SPT hammer. In this case the corrections to arrive at the  $(N_1)_{60}$  value included corrections for the used equipment and also for the loading conditions taking into account the increased lateral stress that is due to the sloping ground on which most drillings were made.

However, these values are not representative of the conditions existing in the hydraulic fill before the earthquake, since due to liquefaction and displacements of the dam body, the hydraulic fill is more compacted in its post-earthquake situation. It has been estimated by Harder et al (1989) that the change in relative density before and after the earthquake is about 12% which corresponds to a decrease of the corrected SPT  $(N_1)_{60}$  values of 4-5 blows per foot (0.305m). This correction is based on the volumetric strains that have been computed based on the measured settlements of the cohesionless shell zones of the hydraulic fill.

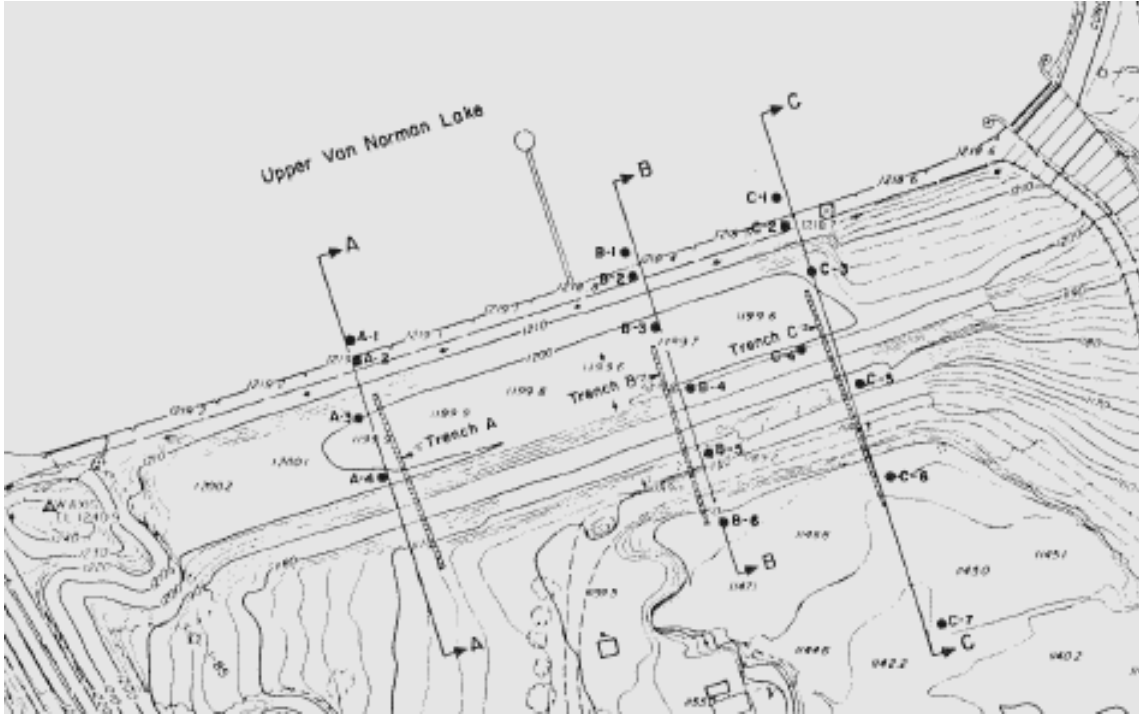


**Figure 5.4: Plan view of the Upper San Fernando Dam including the field investigation done after the 1971 earthquake (Seed et al, 1973)**

These pre-earthquake  $(N_1)_{60}$  have been modified by Beaty and Byrne (2011) with the assumption that a portion of the measured settlements were attributed to the movement of the soil mass rather than densification. Both the corrected SPT blowcounts suggested by Harder et al and Beaty and Byrne are presented in Table 5.1.

Zone	Depth below crest	$(N_1)_{60}$ Harder et al 1989	$(N_1)_{60}$ Beaty and Byrne 2011
Hydraulic Fill (upper)	7-14.5	9.0	10.0
Hydraulic Fill (mid)	14.5-18.5	13.0	14.5
Hydraulic Fill (lower)	18.5-21.0	13.0	13.0

**Table 5.1: Corrected average pre-earthquake SPT blow-counts**

## 5.2 Numerical modelling

### 5.2.1 Input ground motion

The only earthquake recordings near the dam site consist of seismoscope traces at the crest and the abutment of the lower dam which is not adequate to produce the acceleration time history of the earthquake. From the data Seed et al (1973) were able to estimate the peak acceleration of the rock outcrop (PGA) at 0.55-0.60g. Seed et al were able to modify the acceleration time history recorded on the Pacoima Dam abutment to fit the estimated accelerations and produce a reasonable approximation of the earthquake at the dam site.

This acceleration time history has a duration of 20.46 seconds and is shown in Figure 5.5 and its Fourier spectrum in Figure 5.6. This time history is commonly used in back analyses of the San Fernando Dams (Seed et al 1973 and 1976, Wu 2001, Beaty and Byrne 2011). So, this is the input motion that will be used for the dynamic analysis of the Upper San Fernando dam with UBC3D-PLM.

In general it has been shown by several researchers that the vertical component of the earthquake motion is not significant for the response analysis compared to the horizontal one (Hall and Chopra,1982). For this reason, it is considered negligible and it is ignored in most cases of dynamic response analysis.

From the spectrum it can be seen that there is not one predominant frequency but the largest amplitudes correspond to frequencies between 0.5 and 5.0Hz.

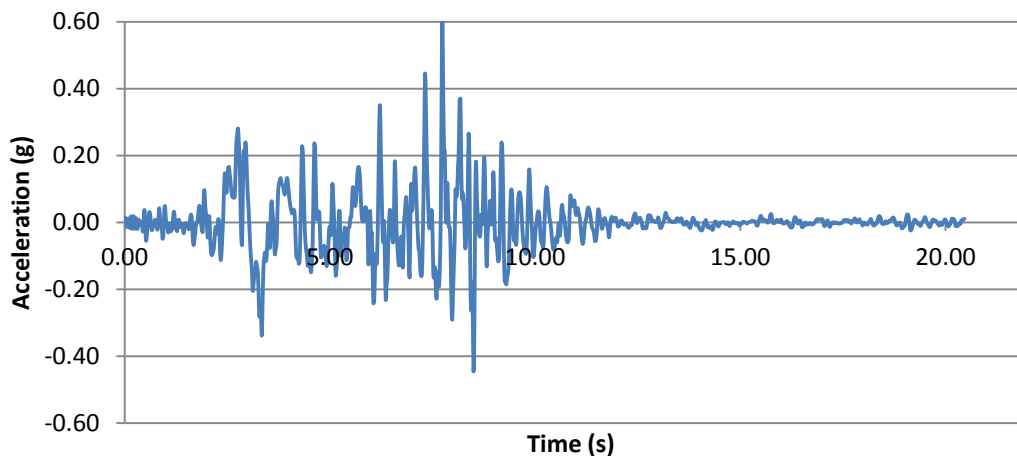
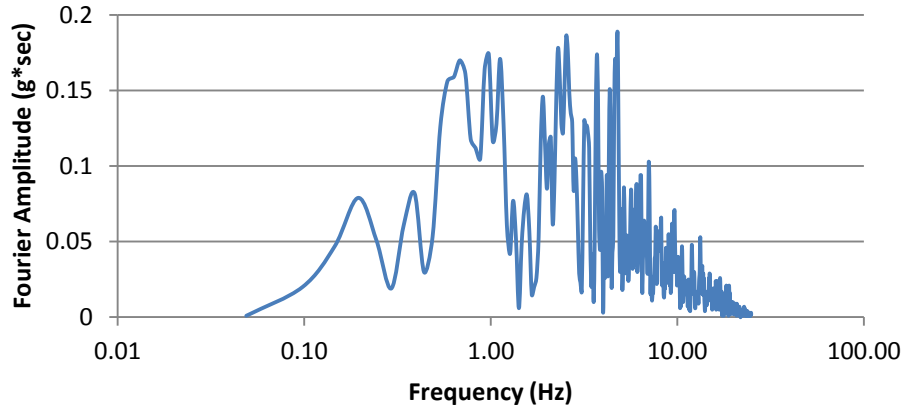


Figure 5.5: Pacoima Acceleration Time History as modified by Seed et al 1973.



**Figure 5.6: Frequency content of the modified Pacoima acceleration time history, Fourier amplitude spectrum (from SeismoSignal)**

### 5.2.2 Material models

As it has been mentioned in section 2.9 the dynamic response analysis of embankment dams usually includes a number of constitutive models for the different zones of soil that constitute the embankment but also the foundation layers etc. Moreover, it has been proven that dynamic loading creates different conditions in the soil than static and thus the static soil properties differ from the dynamic ones even if the same constitutive model is used for the analysis.

#### For the static analysis

Linear elastic model: This is a very simple model which relates the stress increments to the strain increments according to Hooke's law. This model was used to simulate the behaviour of the bedrock material since it is much stronger and stiffer than the foundation layers and the dam materials and it is not expected to sustain plastic straining. To describe this material behaviour it is only necessary to determine the stiffness in terms of Young's modulus ( $E$ ) and the Poisson's ratio ( $\nu$ ), all the other stiffness parameters are computed according to the theory of elasticity.

Hardening soil model (HS): The main characteristics of this model are the following:

- Stress-dependent stiffness behaviour according to a power law;
- Hyperbolic stress-strain relation in axial compression;
- Plastic strain due to primary deviatoric loading (shear hardening);
- Plastic strain due to primary compression (compaction hardening);
- Failure according to the Mohr-Coulomb failure criterion;
- Elastic unloading and reloading;

The model parameters are shown in Table 5.2 and the yield contour in Figure 5.7.

<b>Failure parameters according to Mohr Coulomb failure criterion</b>	
c (kPa)	Effective cohesion
$\phi$ (°)	Effective angle of internal friction
$\psi$ (°)	Angle of dilatancy
<b>Stiffness parameters</b>	
$E_{50}^{ref}$ (kPa)	Secant stiffness in standard drained triaxial test
$E_{oed}^{ref}$ (kPa)	Tangent stiffness for primary oedometer loading
$E_{ur}^{ref}$ (kPa)	Unloading/reloading stiffness
m	Exponent for stress level dependency of stiffness
<b>Advanced parameters</b>	
$\nu_{ur}$	Poisson's ratio for unloading and reloading
$p^{ref}$ (kPa)	Reference stress for stiffnesses
$K_0^{nc}$	Lateral earth pressure coefficient for normally consolidated soil
$R_f$	Failure ratio

**Table 5.2: Parameters for the Hardening Soil Model.**

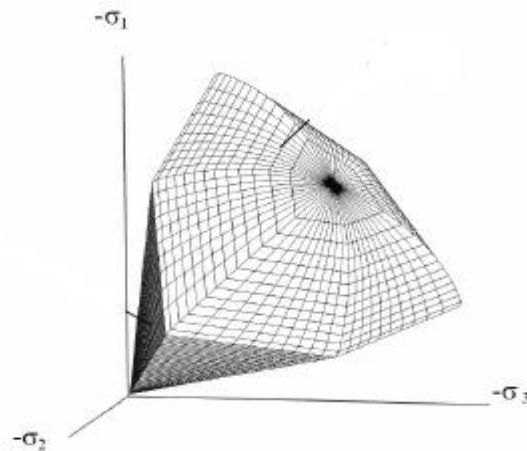


**Figure 5.7: Representation of the yield contour of the HS-model in the principal stress space**

### For the dynamic analysis

Again linear elastic model was used for the rock.

Hardening soil small model (HS-small): The difference of this model compared to the Hardening Soil Model is that it takes into account the small strain stiffness and its non-linear degradation with increasing strain. This is a very significant feature when it comes to dynamic loading conditions because small strains are of significant importance and also during unloading and reloading hysteretic behaviour is implemented. This way a certain amount of material damping is included during dynamic loading. The small strain stiffness and its degradation is implemented in the Hardening soil small model by the addition of two more parameters compared to the HS model:

- $G_0$ , which is the initial or very small strain shear modulus
- $\gamma_{0.7}$ , which is the shear strain level at which the secant shear modulus  $G_s$  has decreased to about 70% of  $G_0$

This model was used to all the layers and zones that are not susceptible to liquefaction, namely the clay core, the rolled fill and the upper and lower alluvium.

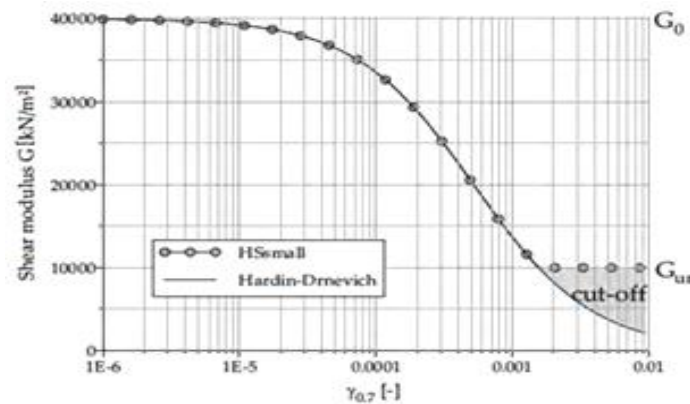


Figure 5.8: Stiffness degradation curve from the HS-small model (PLAXIS Material Models Manual, 2011)

UBC3D-PLM: This model has been described and validated in large extent in the previous chapters and it has been used for the modelling of the liquefiable zones of the hydraulic fill.

### 5.2.3 Material Properties

The selection of suitable material properties for the numerical modelling of the Upper San Fernando Dam can be very difficult given the fact that the construction of the dam was done in the 1920s and there is no proper documentation for the materials and the processes that have been used. For this reason all the available data used in the analyses done after the failure are based on the site investigation and laboratory testing done after the earthquake, as described before. It has been observed that there is a large scatter in the acquired data from the different locations of the dam and especially for the upstream slope the existing investigation was restricted by the fact that the reservoir level was still high.

In general different researchers suggest significantly different soil parameters depending also on the approach that they use and on their initial assumptions. However, it seems that most of the

analyses are based on the initial analysis done by Seed et al in 1973 and by Lee et al in 1975, so these were considered to be the most reliable sources to derive suitable parameters for modelling.

For the static analysis the parameters that have been used are presented in Table 5.3 and are a direct translation of Seed's suggested parameters for the needs of the used material models.

<b>Parameters for static calculation</b>					
	Rolled Fill	Hydraulic fill	Clay core	Upper Alluvium	Lower Alluvium
$\gamma_{\text{unsat}}$ (kN/m <sup>3</sup> )	21.1	18.9	18.9	18.9	19.0
$\gamma_{\text{sat}}$ (kN/m <sup>3</sup> )	22.0	19.2	19.2	19.2	20.7
c (kPa)	124.5	0.0	0.0	0.0	0.0
$\phi$ (°)	25.0	37.0	37.0	37.0	37.0
$E_{50}^{\text{ref}}$ (kPa)	16570.0	25450.0	25450.0	18760.0	46900.0
$E_{\text{oed}}^{\text{ref}}$ (kPa)	16600.0	28980.0	28980.0	14950.0	37380.0
$E_{\text{ur}}^{\text{ref}}$ (kPa)	49710.0	76350.0	76350.0	56280.0	140700.0
m	0.8	0.5	0.5	0.5	0.5
$\nu_{\text{ur}}$	0.2	0.2	0.2	0.2	0.2
$K_0^{\text{nc}}$	0.6	0.4	0.4	0.4	0.4
$R_f$	0.9	0.8	0.8	0.8	0.7

**Table 5.3: Material properties used in the static analysis**

For the dynamic analysis for all the materials except for the liquefiable hydraulic fill zones, the exact same parameters used for the static calculation have been used with the additional characteristic that the small strain stiffness was taken into account as it was determined by seismic surveys done in situ. Another difference is that the Poisson's ratio was decreased to 0.1 which is more suitable for dynamic calculations. These parameters are shown in Table 5.4.

For the hydraulic fill in the dynamic analysis the UBC3D-PLM constitutive model has been used with the correlations that were presented in Chapter 2 and considering that the effect of static shear will be present in the whole liquefiable zone. The corrected SPT blowcounts  $(N_1)_{60}$  that were used to derive the model parameters were the ones suggested by Beaty and Byrne (2011) (Table 5.1). The parameters that occurred from this calibration are shown in Table 5.5.

Parameters for dynamic analysis				
	Rolled Fill	Clay core	Upper Alluvium	Lower Alluvium
$G_0$ (kPa)	112800.0	65100.0	86800.0	238700.0
$\gamma_{0.7}$	1.0E-04	1.0E-04	1.0E-04	2.0E-04
$v_{ur}$	0.1	0.1	0.1	0.1

**Table 5.4: Additional parameters used in the dynamic analysis of the non-liquefiable materials**

Given the vertical effective stresses after the static analysis shown in Figure 5.10 which in the liquefiable zones of the hydraulic fill range between 0 and 200kPa, it was assumed that there is no need to make any correction in the densification factor due to the overburden stress, especially since it has been already increased to 1.0 to account for the effect of static shear.

UBC3D-PLM parameters			
	7-14.5m below crest	14.5-18.5m below crest	18.5-21.0m below crest
$(N_1)_{60}$	10.0	14.5	13.0
$\phi_{cv}$ (°)	35.5	35.5	35.5
$\phi_p$ (°)	36.5	36.9	36.8
$k_G^e$	934.3	1057.0	1020.0
$k_B^e$	654.0	740.2	713.7
$k_G^p$	380.3	766.9	616.9
$R_f$	0.8	0.7	0.8
$fa_{c_{hard}}$	1.0	1.0	1.0
$fa_{c_{post}}$	1.0	1.0	1.0

**Table 5.5: UBC3D-PLM model parameters used in the dynamic analysis for the liquefiable materials**

#### 5.2.4 Geometry and Mesh

The geometry of the simplified cross-section of dam which was used for the analysis is shown in Figure 5.2. This cross-section was created by Seed et al (1973) as a representative cross-section of the dam and has been used by several researchers over the years for the analysis of this case study (Seed et al 1976, Wu 2000, Beaty and Byrne 2011). For this reason, it was considered as a reasonable simplification for the scope of this analysis.

For the selection of the mesh the minimum expected wave length of the input motion was estimated using the following equations:

$$V_s = \sqrt{\frac{G}{\rho}} \quad (5.1)$$

$$\lambda = \frac{V_s}{f} \quad (5.2)$$

where  $\lambda$  is the wavelength,  $V_s$  is the shear wave velocity,  $G$  is the small strain shear modulus,  $f$  is the frequency,  $\rho$  is the soil density. To calculate the minimum wavelength the minimum small strain shear modulus of all the materials was used and the frequency was considered equal to 5Hz which is the maximum frequency with significant amplitude as shown in Figure 5.6.

It is a rule of thumb in dynamic analyses that the mesh elements need to be at smaller than  $\lambda/6$ - $\lambda/10$ . In this case the minimum wave length is  $\lambda_{\min}=3.6\text{m}$  and the average element size used in the analyses was around 2.5m and on the dam where the liquefiable material is the mesh was made denser.

#### 5.2.5 Boundary Conditions

For the static calculation standard fixities were assumed, meaning horizontal fixities on the lateral boundaries and horizontal and vertical fixities on the base.

In general in dynamic analyses the effect of the boundary conditions is stronger in comparison to static analyses, due to the reflection/absorption (depending on the type of boundary) of seismic waves on the boundary. Thus for this calculation the lateral boundaries were placed so that their distance from the dam is equal to two times the length of the dam, which was considered adequate to minimize their effect on the calculation.

In this case two different analyses were performed with different boundary conditions. These were tied degrees of freedom and free field boundaries.

Tied degrees of freedom are a boundary condition based on the assumption that the left and right lateral boundaries have almost the same displacements. To apply this, the nodes of the finite element mesh which are at the same elevation on the lateral boundaries are tied to each other. This condition works perfectly in the case of one-dimensional wave propagation but it is unable to absorb the waves reflected from within the model (structures or excavations). Because the tied degrees of freedom are applied from the static calculation already, the model has to be fully symmetric in terms of geometry and loads. For this reason, the model was mirrored.

Free field boundaries were created as an attempt to simulate the response that the earthquake would produce at the location of the boundary if the structure did not exist. So, the input

earthquake motion is transformed from the free field boundary by applying equivalent forces to the main domain and at the same time a viscous boundary is applied to absorb the waves reflected from internal sources.

In both cases the input motion is applied at the bottom of the mesh in the form of prescribed accelerations. Since a part of the bedrock was also modelled the most suitable type of boundary is to assume a compliant base. This is due to the fact that the input wave propagates from the bedrock existing beyond the model base to the bedrock inside the model, so there is no change in the dynamic impedance.

### 5.2.6 Static analysis

The static analysis of the dam was performed as a staged construction in which the dam was built in layers. The level of the water inside the dam body was determined directly by defining the phreatic level, based on the measurements of the piezometers that existed on the dam and on the seepage analysis performed by Beaty and Byrne (2011).

The active water pressures, vertical effective stresses and shear inside the dam before the earthquake are shown on Figure 5.9, Figure 5.10 and Figure 5.11 respectively.

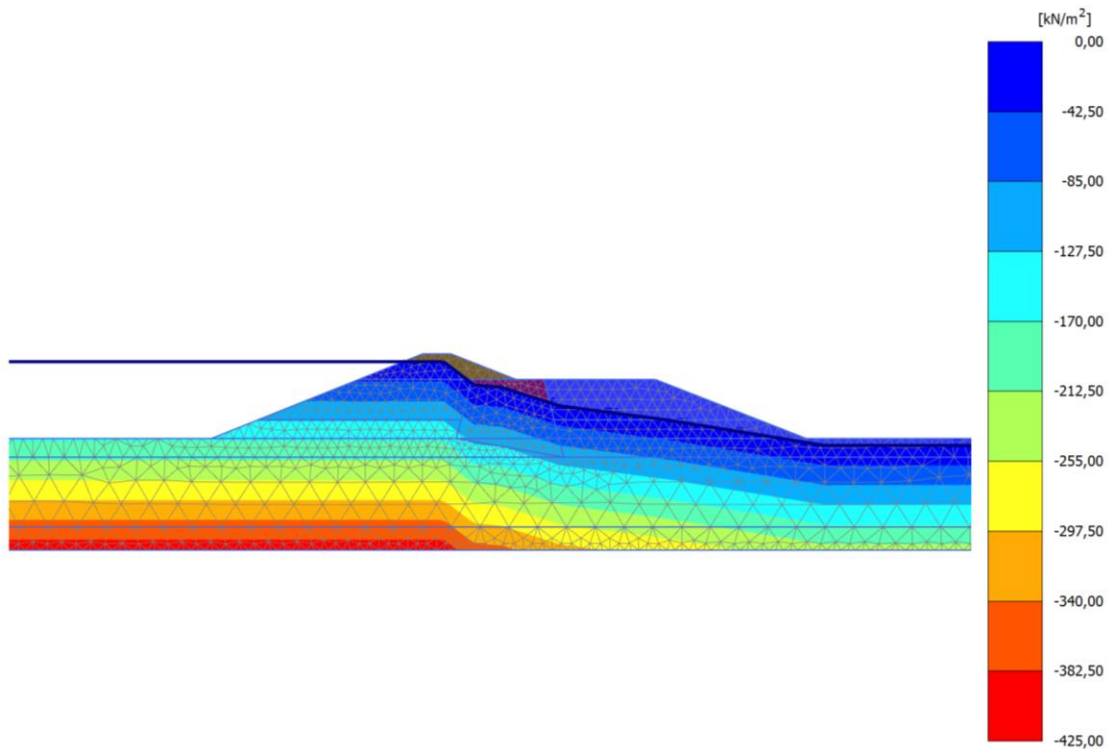


Figure 5.9: Active pore pressures in the dam body before the earthquake

The results of the static analysis were the same in both analyses with free field boundaries and tied degrees of freedom although the models have a different geometry since for tied degrees of freedom the model is twice as large because to achieve symmetry the dam has been mirrored.

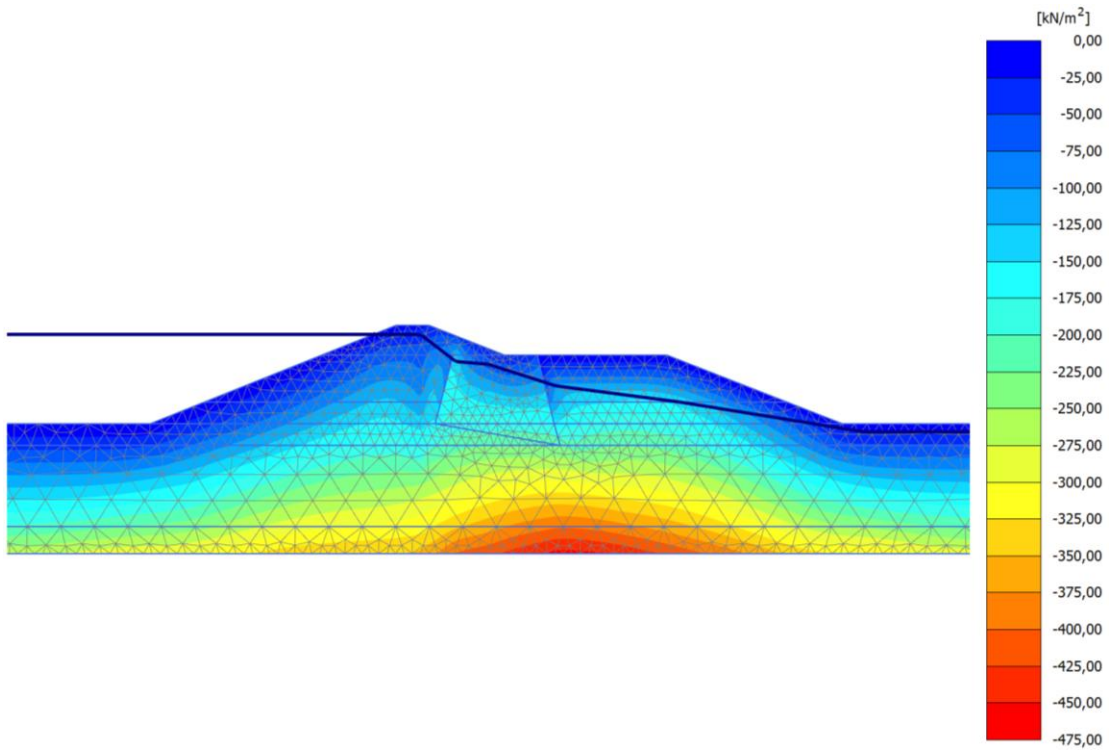


Figure 5.10: Vertical effective stresses ( $\sigma'_{v0}$ ) before the earthquake

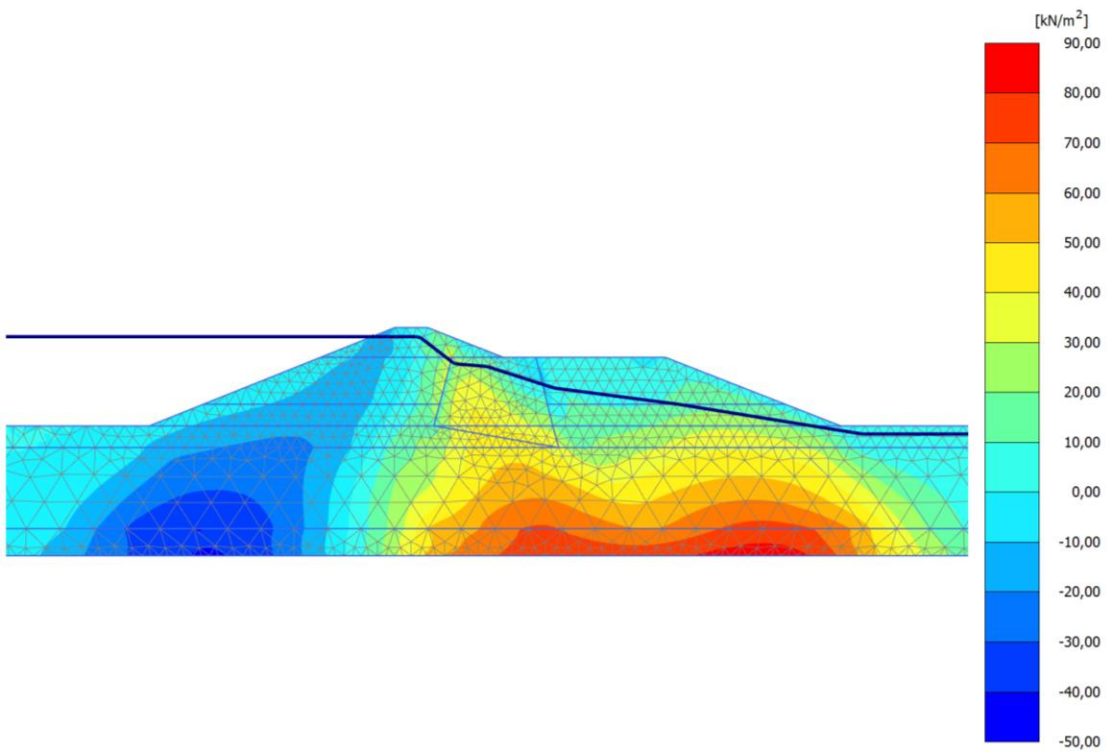


Figure 5.11: Shear stresses on the horizontal plane ( $\tau_{xy}$ ) before the earthquake

### 5.2.7 Dynamic analysis

The dynamic analysis was done with the previously described input motion and properties. Given that in the hysteretic loops of the HS-small model do not provide sufficient material damping, for these materials an additional amount of  $\xi=2\%$  of Rayleigh damping was added. The input motion was applied as prescribed accelerations on the bedrock. The calculation is fully undrained. Concerning the hydrodynamic loads, it has been shown by Hall and Chopra (1982) that on embankments under earthquake loading their effect is insignificant, thus they were ignored. This assumption is used in the vast majority of seismic response analyses of embankments.

The exact same material properties and initial assumptions (damping, hydrodynamic loading, input motion) were used in both analyses with the different boundary conditions.

It has to be noted that the pore pressure ratio in UBC3D-PLM is defined as the change in vertical effective stress over the initial vertical effective stress ( $ru = 1 - \frac{\sigma'_{v}}{\sigma'_{v0}}$ ) instead of the excess pore pressure over the initial vertical effective stress ( $ru = \frac{u-u_0}{\sigma'_{v0}}$ ). This is due to the fact that when the pore pressure ratio is determined in terms of excess pore pressure it has been observed (Beatty and Byrne, 2011) that large fluctuations occur which are not connected with liquefaction and have to do mostly with the redistribution of stresses. This could lead to unrealistically large pore pressure ratios (significantly larger than 100%). For this reason the determination of pore pressure ratio is done through the change in effective stress. However this definition leads to the disadvantage that even in places where there is no change in the pore pressures the effective stresses change when the soil deforms. So a value of  $ru$  different than zero occurs above the phreatic level where liquefaction cannot occur (see Figure 5.13, Figure 5.14, Figure 5.18, Figure 5.19). In general the value of pore pressure ratio above the phreatic level since in sand the unsaturated zone is insignificant, can be ignored without any consequence to the evaluation of the results.

### 5.2.8 Free field boundaries

The free field boundaries present certain limitations when in contact with undrained material data sets and especially with UBC3D-PLM. For this reason near the boundary the material was replaced by the same material that is used for the rest of the calculation but drained. Moreover extra care needs to be taken when determining the suitable number of sub-steps for the dynamic calculation because if the load that is applied on one step is relatively large the model might have difficulties converging.

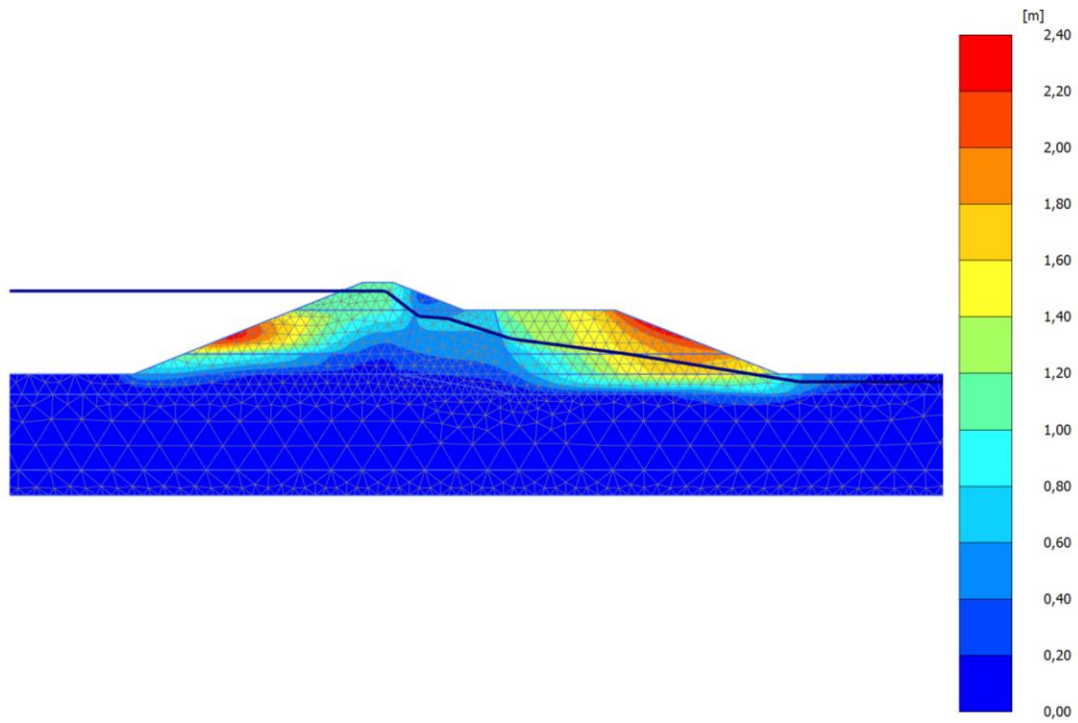


Figure 5.12: Total displacements at the end of the earthquake with free field boundaries (maximum displacement 2.34m)

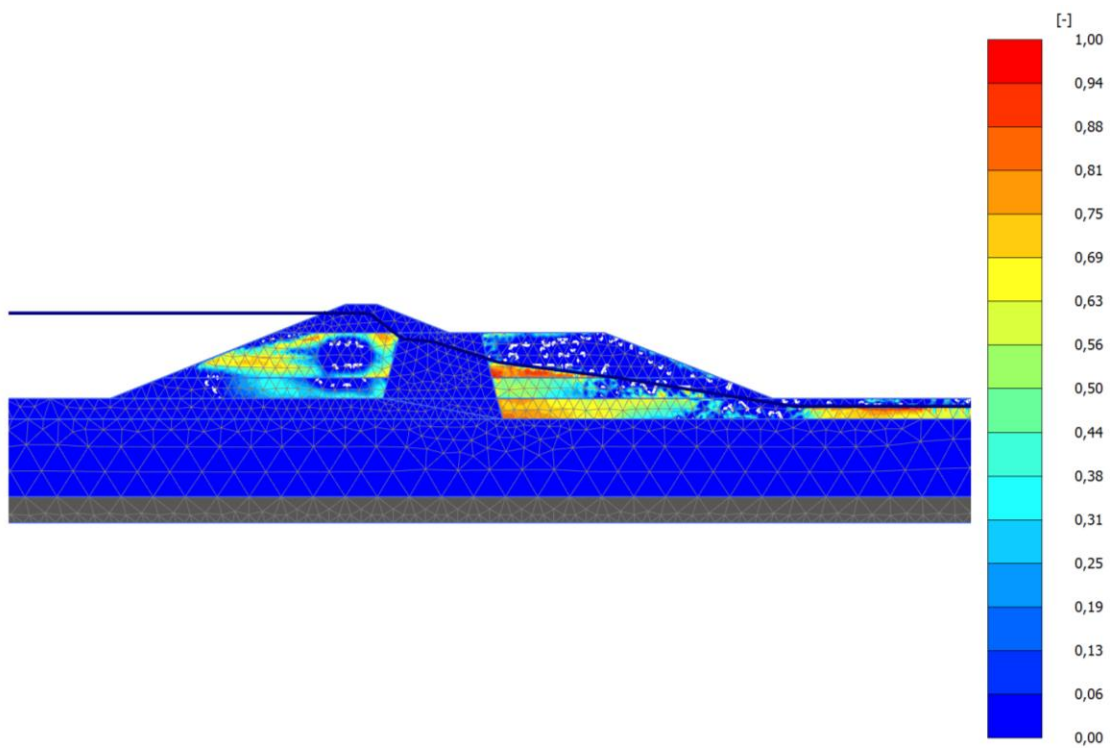


Figure 5.13: Pore pressure ratio  $ru$  at 6 seconds after the beginning of the earthquake for free field boundaries

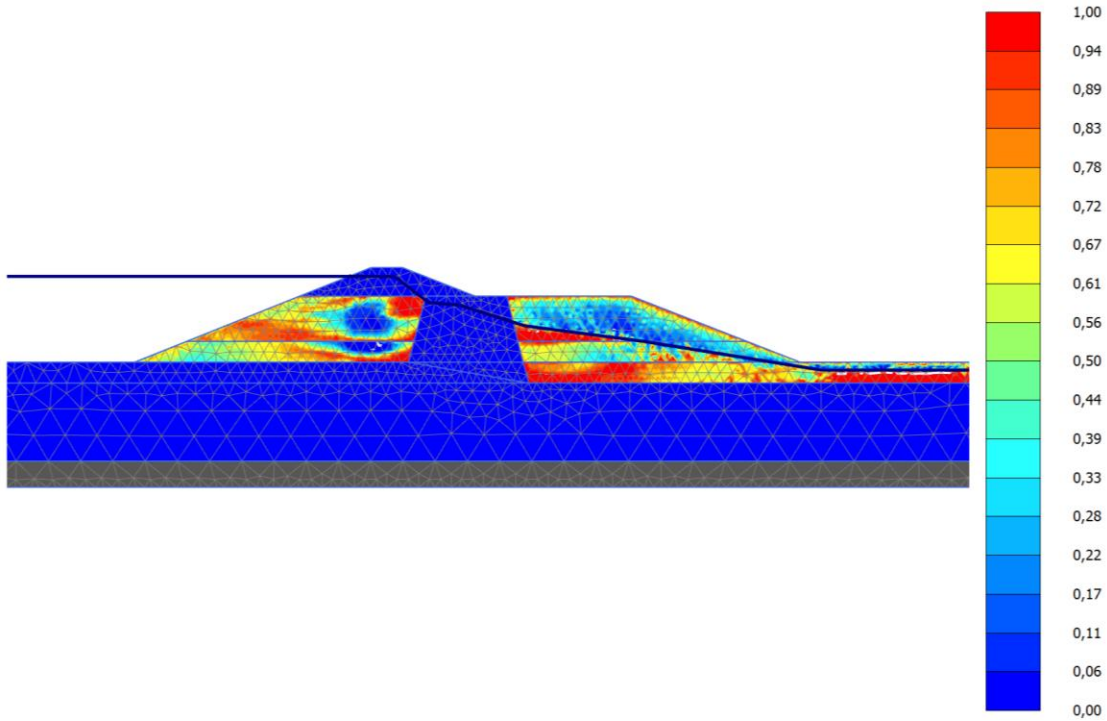


Figure 5.14: Pore pressure ratio  $ru$  at the end of the earthquake loading with free field boundaries.

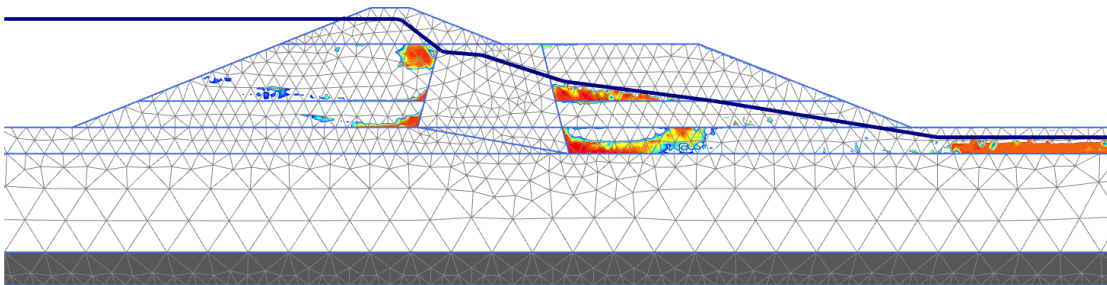


Figure 5.15: Liquefied areas of the embankment corresponding to  $ru > 0.90$  with free field boundaries.

### 5.2.9 Tied degrees of freedom

As mentioned earlier to apply the tied degrees of freedom boundary condition the model needs to be mirrored as shown in Figure 5.16. Given that the lateral boundaries are generally placed far from the dam, the choice of mirroring the model to the left hand side is not expected to affect the results. The direction of the earthquake with respect to the dam cross-section is expected to affect the dynamic response, so the embankment on the left will be taken into

consideration for the analysis of the result. This is done so that the acceleration is positive towards the downstream side of the dam, which is compatible with the analysis of the input motion done by Seed et al (1973) and with the analyses of the Upper San Fernando Dam performed by Seed et al (1976) Wu... and Beaty and Byrne (2011).



Figure 5.16: Geometry of the model for analysis with tied degrees of freedom.

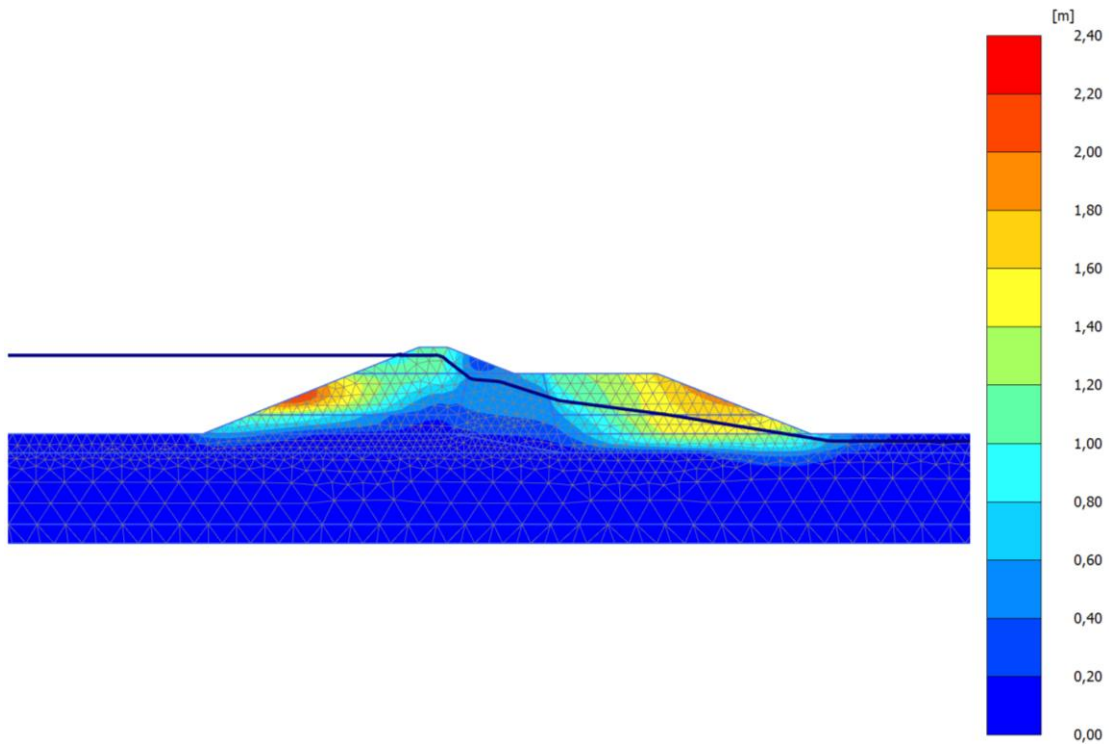


Figure 5.17: Total displacements at the end of the earthquake with tied degrees of freedom.

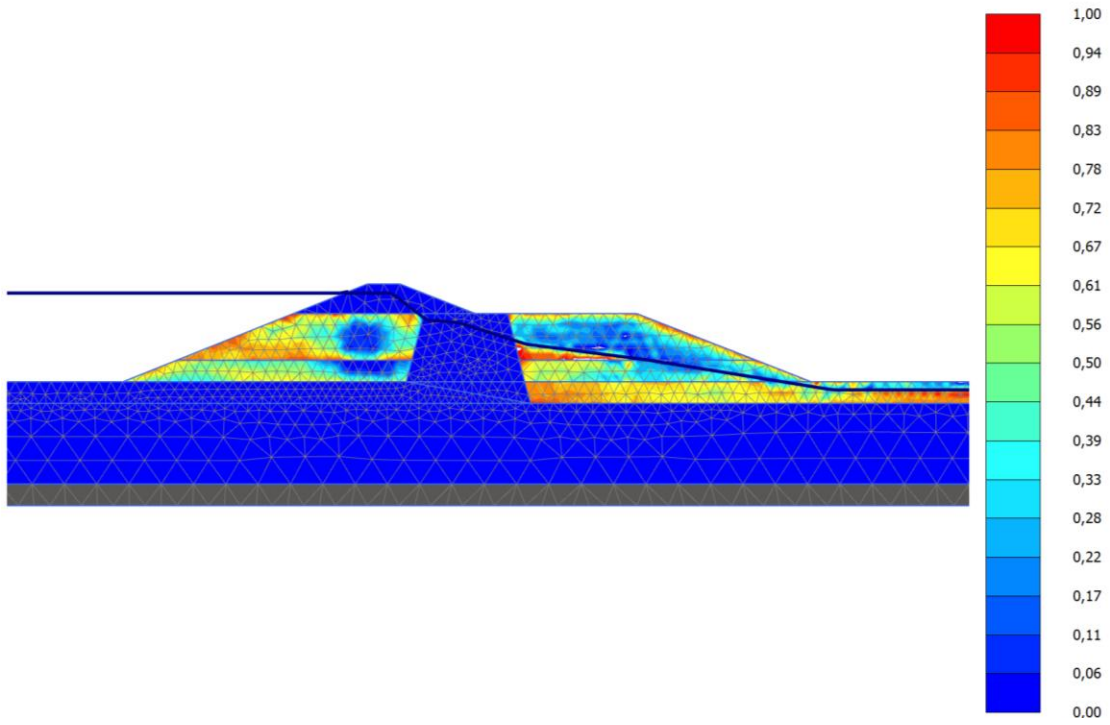


Figure 5.18: Pore pressure ratio  $ru$  after 6 seconds after the beginning of the earthquake with tied degrees of freedom.

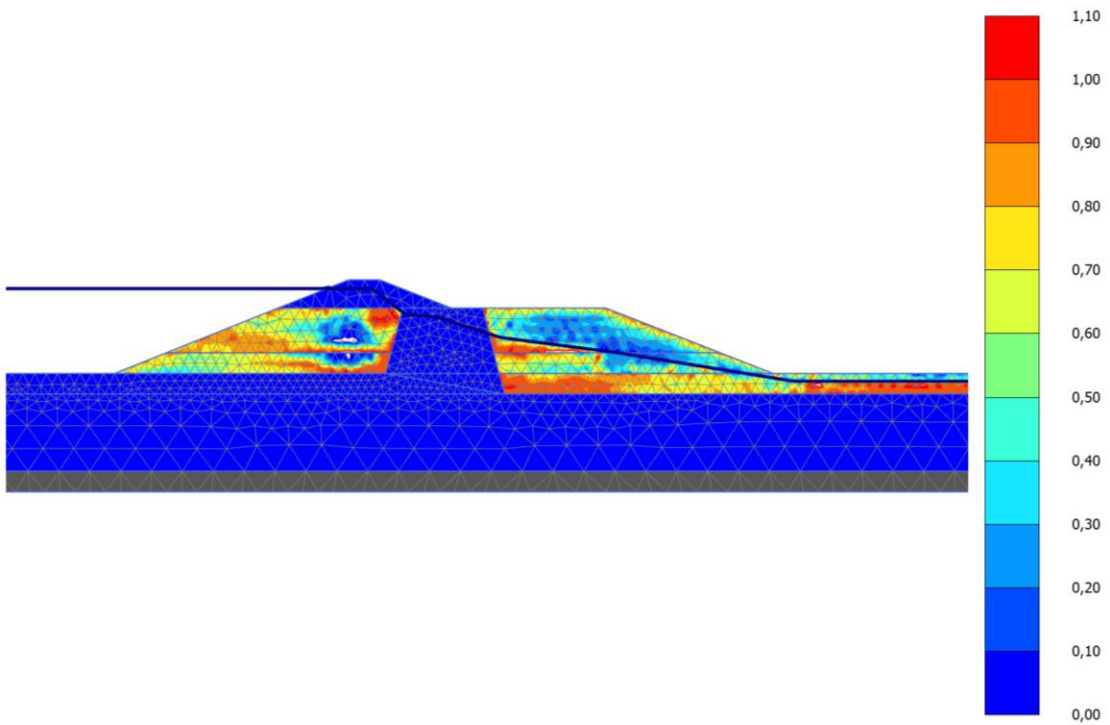


Figure 5.19: Pore pressure ratio at the end of the earthquake with tied degrees of freedom.

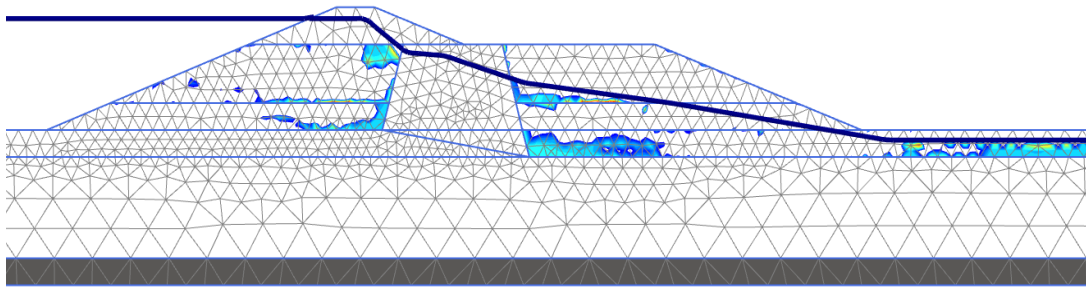


Figure 5.20: Liquefied areas of the embankment corresponding to  $ru > 0.95$  with tied degrees of freedom.

### 5.3 Comparison between the two analyses and the measured displacements of the dam

It is obvious from the two previous sections that the differences in the dynamic response of the Upper San Fernando Dam between the two different boundary conditions are not significant. In general the liquefiable areas have more or less the same extend and are located at the same places on the cross-section.

In terms of pore pressure generation the only difference is that in the case of free field boundaries at 6 seconds from the beginning of the earthquake certain spots can be seen where there is a certain amount of suction (white spots). While in the tied degrees of freedom there are some areas where the pore pressure ratio exceeds 100%.

In terms of displacements the results are again very similar between the two analyses although the tied degrees of freedom lead to slightly smaller deformations. As it was mentioned earlier in the tied degrees of freedom boundary there is no absorption of the reflected wave and thus one would expect larger deformations compared to the free filed boundaries. However, it seems that the mode of deformation of the embankment affects the acquired results. Because in the tied degrees of freedom the lateral boundaries are tied to each other, they do not allow the dam to deform freely in both directions. This could explain these slightly smaller displacements observed in the tied degrees of freedom model.

When compared to the actual displacements measured on the dam, it can be seen in Figure 5.21 that the magnitudes of the predicted displacements are close to the measured ones. The biggest differences appear on the crest of the dam where the measured horizontal displacement is 1.5m towards the downstream side and the predicted ones are 0.3m and 0.2m (free field and tied degrees of freedom respectively) towards the upstream side. This can be explained by the fact that in both PLAXIS analyses the upstream shell of the hydraulic fill presents high pore pressure ratios near the slope (Figure 5.14 and Figure 5.19), reaching values of 0.8. This can be related to the limitation concerning the effect of static shear that has been observed in the previous chapters. This movement towards the upstream side causes also the difference in the horizontal displacement on the point on the berm right below the rolled fill. Another smaller difference exists on the downstream toe which settled 0.1m in reality while the computed displacements are 0.3m upward.

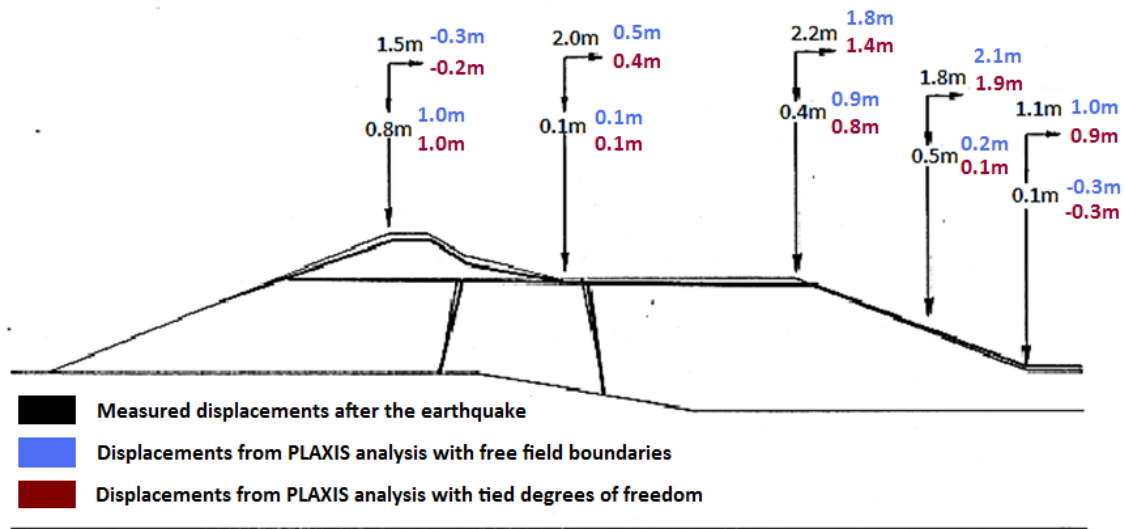


Figure 5.21: Measured displacements after the earthquake in comparison with the displacements computed from the finite element analyses in PLAXIS 2D with free field boundaries and tied degrees of freedom.

#### 5.4 Comparison with other finite element analyses of the case history of the Upper San Fernando Dam

The Upper San Fernando Dam is one of the very well known case studies, which has been the reason for several advancements in the geotechnical community's knowledge concerning dynamic liquefaction. For this reason there are several analyses that have been published over the years about the response of the dam and the pore pressure generation in the hydraulic fill.

The first analyses were performed by Seed et al in 1973 and again in 1976. In these analyses Seed tried to predict the cyclic stresses inside the hydraulic fill caused by the earthquake and compare them to the cyclic resistance of the soil to the same loading which was estimated by cyclic tests in the laboratory. In Figure 5.22 the areas of the hydraulic fill which would fail due to liquefaction are shown according to Seed et al, 1973.

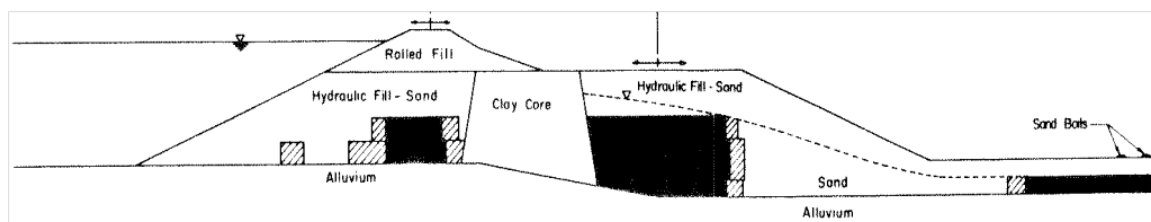


Figure 5.22: Liquefied areas according to the analysis of Seed et al (1973) after 6 seconds (black) and 15 seconds (grey) of the earthquake motion.

Although a direct comparison with the acquired results from the UBC3D-PLM analyses is not possible since the calculation processes are very different it can be observed that the areas where failure is predicted by Seed et al correspond well to the areas where high pore pressure ratios

are predicted by PLAXIS 2D. Except for the area near the upstream slope where the most possible scenario is that UBC3D-PLM over predicts the excess pore pressures.

Of course Seed's analysis is just an initial effort to interpret the dynamic response of the Upper San Fernando Dam and since the understanding of liquefaction phenomena has evolved significantly.

Another researcher who did an effective stress analysis of the Upper San Fernando Dam is Wu in 2001. Wu modified and used the Martin-Finn-Seed pore pressure model which relates drained volumetric strains to pore pressures in the undrained condition. Using this model and assuming that liquefaction occurs at a pore pressure ratio of 95%, Wu produced the results presented in Figure 5.23. In this case, a more direct comparison with UBC3D-PLM is possible. It can be seen by comparing Figure 5.15, Figure 5.20 and Figure 5.23 that the extend of the liquefied areas in the models is similar but their distribution in the hydraulic fill differs, since Wu predicts on the upstream fill and at larger elevation liquefaction near the slope while UBC3D-PLM predicts liquefaction near the clay core. And on the downstream side Wu predicts a more continuous liquefaction zone, while in PLAXIS the liquefied areas are a little more extensive and progress also to higher elevations.

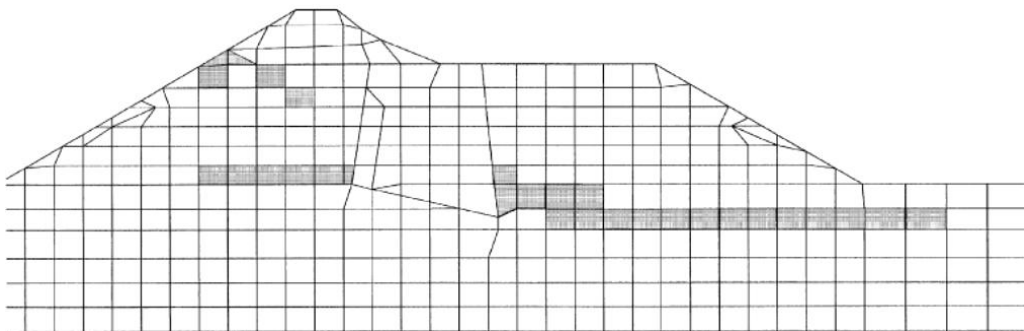


**Figure 5.23: Liquefied areas (grey) ( $r_u > 0.95$ ) with according to the analysis of Wu (2001) using the modified Martin –Finn-Seed pore- pressure model.**

## 5.5 Summary and conclusions

In this chapter the performance of UBC3D-PLM in simulating field conditions was evaluated through the case study of the Upper San Fernando Dam. This attempt was based on several assumptions and simplifications, due to the several uncertainties connected with the actual conditions existing in the field.

In general the acquired results give a satisfactory approximation of what has been observed in reality, although they are conservative in the prediction of liquefaction on the upstream slope.

Again in this case the inability of the model to simulate realistically the effect of static shear affects significantly the accuracy of the results leading to more liquefaction and larger displacements, especially on the upstream slope because on the downstream the face of the slope is not saturated.

Given this disadvantage, a good prediction of the displacements was achieved. However, this result is not very reliable, considering that the model is not capable of simulating the post liquefaction behaviour of the soil. To achieve a better approximation of this behaviour, it is suggested that after the earthquake an additional analysis of the deformations of the dam is done using the post-liquefaction resistance of the areas where liquefaction was predicted.

It has to be noted that to obtain a more accurate and reliable analysis, it would be useful to perform several tests to determine the optimum mesh discretization for this problem.

Concerning the boundary conditions, although the two analyses with the different lateral boundaries provide similar results, their effect should be researched in more detail by placing the boundaries at different distances from the dam and also by assuming a rigid base instead of a compliant one.

In addition, because there are many uncertainties concerning the determination of the soil properties and a large variability between in the parameters selected by different researchers for this specific case history, it would be suggested to perform a certain number of parametric analyses. For example the assumption of a fully impermeable core which is followed has been contradicted by Stark based on the fact that liquefaction has been observed in piezometer no 2 which is located inside the clay core (Figure 5.3).

Also it would be preferable to perform a full seepage analysis to determine the existing water levels in the embankment right before the earthquake, because the existing water level affects significantly the occurrence of liquefaction, but the available permeability data were insufficient for that.

Despite the further investigation that could be done, the approach that was adopted in this case is based on reasonable assumptions and it is considered adequate to demonstrate the applicability of UBC3D-PLM in the prediction of liquefaction on embankment dams.

## 6 CONCLUSIONS AND DISCUSSION

---

### 6.1 Conclusions

In this project an attempt to evaluate the applicability of the UBC3D-PLM model for use in the prediction of the onset of liquefaction in embankment dams under earthquake loading was done. Initially the model was calibrated to fit undrained DSS tests and general suggestions about appropriate correlations of the model parameters with the soil's corrected SPT blowcount  $(N_1)_{60}$  were made. These correlations were able to successfully approximate the empirical cyclic resistance curve. The second step was to evaluate the effect of certain critical parameters on the behaviour of the model. These parameters were: the state of the soil (as expressed by its relative density and initial stress state), the lateral earth pressure coefficient, the material damping and the initial static shear. After that, dynamic centrifuge tests on sloping ground were simulated in PLAXIS 2D, to be able to evaluate the performance of the model in a case where the soil properties and the boundary conditions are well known. Finally, the case history of the Upper San Fernando Dam under the 1971 San Fernando Earthquake was reproduced in PLAXIS 2D, using UBC3D-PLM to simulate the liquefiable material of the hydraulic fill.

Some general conclusions can be drawn from the results acquired in this process concerning the possibilities and limitations of UBC3D-PLM.

It has been shown, initially from the simulation of laboratory tests, that the model can predict well the onset of liquefaction in terms of pore pressure generation, since with the suggested calibration a good approximation of the cyclic strength curve is achieved (Figure 3.11). This result has been validated further by the centrifuge tests and the case study. Although especially in the centrifuge a certain over prediction of the excess pore pressure is observed at the beginning of the earthquake.

For the predicted displacements, it has been observed that in the case of cyclic mobility UBC3D-PLM underestimates the strains because after a certain loading cycle (depending on the post liquefaction factor that is used) the strains are locked at a certain level and do not increase further, which is not the case in reality. While in the case of flow liquefaction, where static shear plays an important role, the strains are generally over predicted after a certain pore pressure ratio depending also on the initial loading conditions.

This over and under estimation of displacements depending on the initial loading conditions, has to do with the fact that UBC3D-PLM does not account for post-liquefaction behaviour. Although a certain amount of softening is considered, after the peak yield surface is reached, by means of the post liquefaction factor, this behaviour does not correspond to the actual post-liquefaction resistance of the soil.

Moreover, it has been shown that the effect of the relative density of the soil on the liquefaction resistance is well approximated by the model while the effect of the lateral earth pressure coefficient ( $K_0$ ) is not in very good accordance with the suggested correlations. Concerning the effect of the initial overburden stress, UBC3D-PLM tends to give a lower cyclic resistance ratio compared to the suggested by the empirical and laboratory observations (Figure 3.15). However, the effect of these parameters depends also on the calibration of the model and it has been shown that significant improvements can be achieved by calibrating the model for the specific conditions expected in the field. Also, due to the elastic unloading the hysteretic damping in the model is larger than in reality.

The effect of static shear on the horizontal plane on the cyclic resistance of the soil remains a controversial topic in liquefaction analysis in general. Special attention has been paid to this parameter because it is very critical in the case of embankment dams and because UBC3D-PLM is unable to simulate well its effect. It has been observed that the model underestimates significantly the values of the static shear correction factor ( $K_a$ ) (Figure 3.21 and Figure 3.22) as it has been determined from laboratory observations. Generally the more the initial loading conditions deviate from the isotropic axis the model's capability of predicting the soil behaviour decreases. This is also apparent when the lateral earth pressure coefficient is of concern but the effect is much stronger when static shear stress exists on the horizontal plane. An improvement in the prediction of liquefaction can be achieved with certain corrections in the model parameters. In the case of the centrifuge this limitation has a stronger effect. This limitation leads to a more conservative analysis which over-predicts the pore pressure generation on sloping ground.

Throughout this project, the importance of a proper calibration of the model for the type of sand and the specific loading conditions of the project that is being modelled has been proved very critical for the accuracy of the analysis. From the simulations of the laboratory tests and

also from the centrifuge, it is clear that the model behaviour is strongly stress path dependent and that, if the loading conditions are not taken into account during the calibration of the model, the acquired results might deviate significantly from the real soil behaviour. Especially in the centrifuge tests this became very apparent in the initial model where due to the initial assumption about the effect of static shear.

In dynamic calculations the influence of the small strain material properties is very significant despite the fact that earthquakes can ultimately lead to very large displacements. The correlations used to determine the model parameters are suitable for dynamic loading since both the initial shear modulus and Poisson's ratio refer to small strains ( $<10^{-4}$ ). Of course due to the hyperbolic stress strain relation this stiffness degrades with increasing strains. However, for static loading conditions this very larger stiffness can lead to unrealistic results. So if UBC3D-PLM is used for static analysis a new calibration is needed. Although due to the secondary yield surface which leads to plastic strains during reloading, the acquired result will probably lead to an over estimation of permanent deformations.

Finally, it has been observed that the post liquefaction factor can lead to numerical instabilities and unrealistic behaviour if it is set to very low values, while if it is higher than it should it can prevent the soil from liquefying. It has been observed that for loose sands a higher value of the factor is more suitable while for dense a lower one.

## 6.2 Recommendations and fields that require further research

For the determination of suitable parameters for the model, the simulation of laboratory tests under similar loading conditions and with the same type of sand is preferable to the use of the aforementioned correlations. Generally, different types of sand lead to significantly different cyclic resistance curves, so the applicability of the correlations has a limited range.

Moreover, it is generally advisable to avoid the use of UBC3D-PLM for static calculations since a different calibration will be needed and the acquired result will be more accurate using a different nonlinear elasto-plastic constitutive model, such as the Hardening Soil model.

The corrections made in the correlations for the effect of static shear, improve slightly the performance of the model but they are not adequate. This is a limitation of the model that cannot be completely eliminated. However, it could be improved further with a better calibration of the model, which would require a large number of cyclic DSS tests and preferably at different overburden stresses, so that the interaction of these two parameters is also determined.

Extra care needs to be taken in the determination of the post liquefaction factor, generally it should be decreased with increasing relative density. In the case of embankment dams and slopes in general, it is suggested to avoid the use of a post liquefaction factor different than 1.0, unless the soil is very dense. However, this limitation is not only a matter of calibration and it is a common disadvantage of most liquefaction models. The reasons for that have with uncertainties in the behaviour of the soil during this process of softening and loss of strength which is associated with several phenomena such as grain crushing and redistribution.

Since the model cannot predict post-liquefaction behaviour, it is suggested that UBC3D-PLM is used to determine the susceptibility of the soil to dynamic liquefaction under a specific earthquake loading and the location in the soil structure where liquefaction will occur. However, if a complete analysis of the expected deformations is needed, then in the liquefiable areas a

different analysis should be done based on the post liquefaction resistance of the soil, which is one of the most controversial topics of soil dynamics. For most engineering projects the knowledge of the occurrence or not of liquefaction is enough to define the appropriate course of action in terms of design.

Taking everything into consideration, despite its restrictions and limitations UBC3D-PLM can be a very useful tool for practical applications in embankment dams, given that the engineer is aware of the model behaviour and the specificities of the problem at hand.

## 7 REFERENCES

---

Beaty M.H. and Byrne P.M., 2011, UBCSAND constitutive model version 904aR, Itasca.

Beaty M.H., Perlea V.G., 2011, Several observations on advanced analyses with liquefiable materials, 21<sup>st</sup> Century Dam Design-Advances and Adaptations, 31<sup>st</sup> Annual USSD Conference, San Diego, California.

Been, K., Jefferies, M., 2006, Soil liquefaction: A critical state approach, Taylor and Francis, London and New York.

Byrne P.M., Cheung H., Yan L., 1987, Soil parameters for deformation analysis of sand masses, Canadian Geotechnical Journal, 24(3): 366–376.

Finn W.D., Ledbetter R.H., Marcuson W.F. III, 1995, Modern practice in the seismic response analysis of embankment dams, Scientia Iranica, Vol. 2, No 2, pp 145-164.

Gazetas G., 1987, Seismic response of earth dams: some recent developments, Soil dynamics and Earthquake engineering Vol. 6, No 1, pp.2-47.

Hall J.K., Chopra A.K., 1982, Hydrodynamic effects in earthquake response of embankment dams, Journal of Geotechnical and Geoenvironmental Engineering, ASCE, 108(4): 591-597.

Hardin B.O., 1978, The nature of stress-strain behaviour of soils, Earthquake Engineering and Soil Dynamics--Proceedings of the ASCE Geotechnical Engineering Division Specialty Conference, June 19-21, 1978, Pasadena, California, Volume I: 3-90.

ICOLD, 1989, Selecting seismic parameters for large dams, Guidelines, Bulletin 72, International Commission of Large Dams, Paris.

ICOLD, 2001, Design features of dams to resist seismic ground motion, Bulletin 120, International Commission on Large Dams, Paris.

ICOLD, 2010, ICOLD Position Paper on Dam Safety and Earthquakes, ICOLD Committee on Seismic Aspects of Dam Design, International Commission on Large Dams, Paris.

Idriss I.M., Boulanger R.W., 2008, Soil liquefaction during earthquakes, Earthquake Engineering Research Institute, USA.

Kramer S.L., 1996, Geotechnical Earthquake Engineering, Prentice Hall Inc., Upper Saddle River, USA.

Marcuson W.F. III, Hynes M.E., Franklin A.G., 2007, Seismic Design and Analysis of Embankment Dams: The State of Practice, The Donald M. Burmister Lecture, Department of Civil engineering Mechanics, Columbia University.

Novak P., Moffat A.I.B., Nalluri C., Narayanan R., 2007, Hydraulic Structures, fourth edition, Taylor and Francis, London and New York.

Olson S. M., Stark T. D., 2003, Use of laboratory data to confirm yield and liquefied strength ratio concepts, Canadian Geotechnical Journal, 40: 1164-1184.

Olson S.M., Mattson B.B., 2008, Mode of shear effects on yield and liquefied strength ratios, Canadian Geotechnical Journal, 45: 574-587.

Park S.S. and Byrne P.M., 2004, Numerical modeling of soil liquefaction at slope site, International Conference on Cyclic behaviour of soils and liquefaction, pp.571-580.

Petalas A., 2012, Validation and Verification of a Practical Constitutive Model for Soil Liquefaction in PLAXIS, Msc Thesis, TU Delft, The Netherlands.

Petalas A., Galavi V., 2012, PLAXIS Liquefaction Model: UBC3D-PLM, PLAXIS, Delft, The Netherlands.

Seid-Karbasi M., 2003, Time Histories of input motions selected for physical and numerical modelling, Research program: Earthquake Induced Damage Mitigation from Soil Liquefaction, University of British Columbia, Report No 2003/02.

Seid-Karbasi M., Byrne P.M., 2003, Numerical Modelling of Physical Model Response to Earthquake: Class A Prediction, Research program: Earthquake Induced Damage Mitigation from Soil Liquefaction, University of British Columbia.

Seed H.B., Lee K.L., Idriss I.M., Makdisi F.I., 1973, Analysis of the slides in the San Fernando Dams during the earthquake of Feb. 9, 1971, Earthquake Engineering Research Center, Report No EERC 73-2, University of California, Berkeley, California.

Seed R.B. and Harder L.F., 1990, SPT-based analysis of cyclic pore pressure generation and undrained residual strength, Proceedings H.B. Seed Memorial Symposium, Bitech Publishers, Vol. 2, pp 351-176.

Serff N., Seed H.B., Makdisi F.I., Chang C.Y., 1976, Earthquake Induced deformations of Earth Dams, Earthquake Engineering Research Center, Report No EERC 76-4, University of California, Berkeley, California.

Wijewickreme, D., Sriskandakumar, S., and Byrne, P.M., 2005, Cyclic loading response of loose air-pluviated Fraser River Sand for validation of numerical models simulating centrifuge tests, Canadian Geotechnical Journal, 42: 550-561.

Youd, T.L., Idriss, I.M., Andrus, R.D., Arango, I., Castro, G., Christian, J.T., Dobry, R., Finn, W.D.L., Harder Jr. L.F., Hynes, M.E., Ishihara, K., Koester, J.P., Liao, S.S.C., Marcuson III, W.F., Martin, G.R., Mitchell, J.K., Moriwaki, Y., Power, M.S., Robertson, R.K., Seed, H.B., and Stokoe II, K.H., 2001, Liquefaction resistance of soils: summary report from the 1996 NCEER and 1998 NCEER/NSF workshops on evaluation of liquefaction resistance of soils. Journal of Geotechnical and Geoenvironmental Engineering, ASCE, 127(10): 817–833.

Vaid Y. P., Sivathayalan S., Static and cyclic liquefaction potential of Fraser Delta sand in simple shear and triaxial tests, Canadian Geotechnical Journal, 1996, 33(2): 281-289